Consistent chiral three-nucleon interactions in nuclear structure

Master Thesis

Joachim Langhammer

Advisor	Prof. Dr. Robert Roth
Second Advisor	MSc. Sven Binder

September 2010

TECHNISCHE
UNIVERSITÄT
DARMSTADT

CONTENTS

SECTION 1

Introduction

From the point of view of low-energy nuclear structure physics, the atomic nucleus is built of protons and neutrons, the so called nucleons. Quarks and gluons, which represent the internal degrees of freedom of the nucleons, are not considered explicitly. The issue of nuclear structure physics is, on the one hand to make precise predictions for experimental observables, e.g. binding and excitation energies and nucleon densities, which can also be used as input for further investigations, e.g. in astrophysics. On the other hand, one is interested in a theoretical framework which can describe the experimental properties of nuclei based on the fundamental physics of the strong interaction.

In this thesis we pursue the strategy of solving the time-independent many-body Schrödinger equation, which is equivalent to solving the eigenvalue problem of the Hamilton operator. While the statement of the task is rather simple, two difficulties arise when we approach the eigenvalue problem. Firstly, only some basic symmetry assumptions, e.g. rotational invariance, restrict the possible operator structures in the nuclear interaction. Therefore, an appropriate interaction applicable over a wide range of nuclei is still absent. Secondly, solving the many-body problem itself is non-trivial, because it will turn out that we have to deal with large model spaces to get valuable results.

Concerning the nuclear interaction, in the 1990s one assumed two-nucleon interactions and accepted that irreducible interactions within triples of nucleons were neglected. Prominent examples of these potentials are the Argonne-V18 or CD-Bonn interactions, that reproduce nucleon-nucleon scattering data as well as deuteron properties but contain lots of phenomenology.

Using these potentials for the calculation of spectra of various nuclei, one fails to match experimental results. A well-known example for such failure is the ground

state of ^{10}B which has, as a result of a calculation with the Argonne-V18 or CD-Bonn potential, the wrong angular momentum $J = 1$ instead of the experimental value $J = 3$ [1]. To overcome these discrepancies, the two-nucleon interactions were supplemented by various three-nucleon potentials. Spectra obtained with these potentials combined with the two-nucleon potentials match experimental data much better. But it is not obvious which two-nucleon interaction should be combined with which three-nucleon interaction. Furthermore, one should aim at a more fundamental derivation of the nuclear interaction starting from Quantum Chromodynamics (QCD) as the underlying theory.

A direct derivation of a nuclear potential from QCD is problematic because of its nonperturbative character in the low-energy regime. Moreover, describing nuclei as systems of interacting quarks and gluons, is not feasible nowadays. Fortunately, this detailed description is not necessary, because we investigate an energy regime, where quarks and gluons are not resolved and, thus, we can adopt an effective theory valid for the low-energy regime of nuclear physics. A modern approach is the so-called chiral effective field theory (χEFT) which treats nucleons and pions as degrees of freedom and takes all relevant symmetries of QCD, especially the chiral symmetry, into account. In this framework a systematic expansion of the nuclear potential exists, as Weinberg showed in [2]. More details will be discussed in section 2.

It turns out that the aforementioned problems can be remedied by this procedure. Firstly, we have a more fundamental derivation of the potential, which has the nice feature that only two new parameters occur when we include three-body interactions at next-to-next-to leading order (N2LO). Secondly, it is now clear which three-nucleon interaction should be used together with the two-nucleon interaction, namely the one corresponding to the same expansion order. The first time the three-nucleon interaction shows up is at N2LO, and three-nucleon forces of higher order are not available yet. Therefore, this order is considered in this thesis, especially the three-nucleon part is investigated.

Results of first no-core shell model calculations with Lee-Suzuki-transformed chiral two-body interaction (NN) and two-plus-three-body interaction (NN+NNN) in a small model space $N_{\max} = 6$ are compared to experimental results for ^{10}B in fig. 1 [3]. Obviously, the quantum numbers of the ground state are correct if one includes the three-body interaction. The chiral two-body interaction alone, like the CD-Bonn or Argonne-V18 two-body potentials predict an incorrect ground state of ^{10}B. Moreover, the overall agreement with experiment is significantly improved with the use of the three-body interaction.

We start our investigations with the matrix elements of the chiral interaction

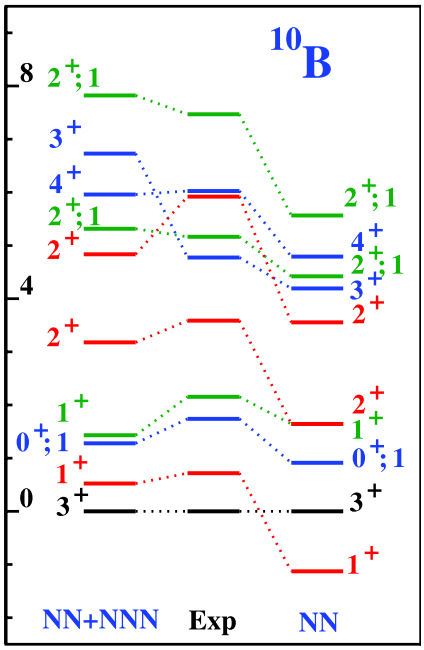

Figure 1 – *Spectrum of ^{10}B in MeV as result of Lee-Suzuki no-core shell model calculations in a $N_{max} = 6$ model space. The used harmonic-oscillator frequency is $\hbar\Omega = 14$ MeV. Results including the chiral two-body interaction (right), the chiral two-plus-three-body interaction (left) are compared to experiment (middle) [3].*

up to N3LO for two-nucleon interactions and N2LO for three-nucleon forces and extract the three-nucleon interaction matrix elements. These three-nucleon matrix elements are given with respect to fully antisymmetrized three-particle Jacobi states [4]. For nuclear structure calculations it is more convenient to work with matrix elements with respect to a Slater-determinant basis consisting of single-particle harmonic oscillator states based on Cartesian coordinates. This basis is also known as m-scheme basis. Consequently, we have to derive and implement the transformation from Jacobi to m-scheme matrix elements, which will include two harmonic oscillator brackets. It turns out that this is a non-trivial task, because it is computational demanding. Generally, we follow the strategy outlined in [5] and precompute a certain overlap coefficient to speed up the transformation code. Having the m-scheme matrix elements we are in principle able to attack the eigenvalue problem of the Hamiltonian. But the storage of m-scheme matrix elements becomes problematic even for modest model space sizes. Therefore, our strategy is to compute matrix elements with respect to states that carry a total coupled angular momentum $\mathcal{J}$ and isospin T. These matrix elements are then decoupled to m-scheme matrix elements in the many-body calculation. With this strategy it is possible for the first time to calculate matrix elements of the N2LO three-nucleon interaction up to a total three-particle harmonic oscillator energies

of at least $E_{3\text{max}} = 14$. The standard energy limit before was $E_{3\text{max}} \lesssim 9$ according to fig 1.

As already mentioned above, solving the Schrödinger equation numerically is not straight forward. The complex nuclear interaction induces strong correlations between the nucleons that result in the need of very large model spaces in order to incorporate these correlations and to obtain converged results.

Therefore, the bare interaction is not suitable to perform calculations for heavier nuclei, since the results in tractable model spaces are still not converged with respect to model space sizes. One possible way to overcome this obstacle is the use of unitarily transformed interactions. Here, we will apply the similarity renormalization group (SRG) transformation. This can be done at the level of the original fully antisymmetric three-particle Jacobi harmonic oscillator matrix elements. Then the transformation into the coupled scheme can be performed as mentioned above. Afterwards, also heavier nuclei are accessible in a reasonable way within tractable model spaces. Furthermore, we are able to distinguish between the effects of induced three-particle interactions due to the SRG transformation and the impact of the genuine three-particle interaction from χEFT.

Finally, many applications and studies of the impact of the three-body matrix elements, especially matrix elements in the framework of χEFT, are accessible. We show results of calculations in the importance-truncated no-core shell model (IT-NCSM), which allows for ab-initio nuclear structure studies beyond the domain of the full no-core shell model NCSM [6]. The principal idea is to reduce the model space in which the matrix eigenvalue problem has to be solved using an a priori importance measure that determines whether a basis state is included in the model space or not. The IT-NCSM yields eigenstates of the Hamilton operator which are the ingredient for calculations of various observables. We show results including the bare N2LO three-particle interaction for ^{4}He as well as the SRG-transformed three-body interaction for ^{4}He and ^{6}Li. Thereby, we can distinguish between the induced and genuine three-body force influences.

Moreover, we present first results of Hartree-Fock calculations with the SRG-transformed chiral interactions including the N2LO three-body force. With this method the whole nuclear chart is accessible. As example we investigate ^{4}He, ^{16}O, ^{40}Ca, ^{48}Ca and ^{90}Zr.

This thesis is organized as follows: In section 2 we give a short introduction into chiral effective field theory. For the rest of the thesis matrix elements of the chiral interactions are our input. We transform these matrix elements given in three-particle relative states into a form depending on Cartesian coordinates that is suitable for many-body calculations in section 4. However, to carry out this

transformation we need some mathematical background and tricks, presented in section 3. After the transformation of the three-body interaction matrix elements we discuss the unitary transformation of the interaction via the similarity renormalization group in section 5. An important issue in this section will be the proper separation of the three-body part of the interaction form the two-body part. In section 6 we present the results of IT-NCSM and Hartree-Fock calculations and discuss the impact of the chiral three-body forces. Finally, we give a résumé of this thesis including an outlook in section 7.

In the appendices the interested reader can find some technical remarks on our implementation of the transformation presented in section 4 and the SRG transformation in appendix A. Moreover, in appendix B one can find the formula of the two-body Talmi transformation, which is the analog transformation as in section 4 but on two-body level.

SECTION 2

Chiral effective field theory (χEFT)

Even nowadays, it is a challenging task to deduce the nuclear interaction from its underlying theory, the quantum chromodynamics (QCD). A direct derivation of the nuclear potential from QCD is not yet feasible because of the large value of the QCD coupling constant in the low-energy regime relevant for nuclear structure physics. Nevertheless, there has been great progress in developing an effective theory for low-energy QCD in the past two decades. The starting point of this so called chiral effective field theory (χEFT) is the most general Lagrangian involving the relevant degrees of freedom that is consistent with a set of basic symmetry principles. Especially the spontaneously and explicitly broken chiral symmetry of QCD is taken into account, constraining the form of each term in the Lagrangian. As we are dealing with low energies, the relevant degrees of freedom are nucleons and pions instead of quarks and gluons. The pions emerge here as Goldstone bosons due to the spontaneous breaking of chiral symmetry and acquire nonzero mass because of the explicit chiral symmetry breaking. Heavier mesons are integrated out and, thus, are absorbed in the low-energy constants (LECs) describing the short-range interactions.

It turns out that the effective Lagrangian comprises an infinite number of terms and still seems to be intractable. However, Weinberg showed that a systematic expansion of the nuclear potential in powers of $\frac{Q}{\Lambda_\chi}$ exists [2, 7, 8]. Here, Q is a generic momentum in the nuclear process at the order of the pion mass and Λ_χ is the scale of the chiral symmetry breaking at the order of the ρ-meson mass, $m_\rho = 770\,\text{MeV}$. Thus, $\frac{Q}{\Lambda_\chi}$ is small and the perturbative expansion is expected to converge. This procedure is called chiral perturbation theory (χPT). Since the number of contributing terms for a given power of $\frac{Q}{\Lambda_\chi}$ is finite, one can systematically calculate the different contributions to the nuclear interaction. The resulting terms are shown in

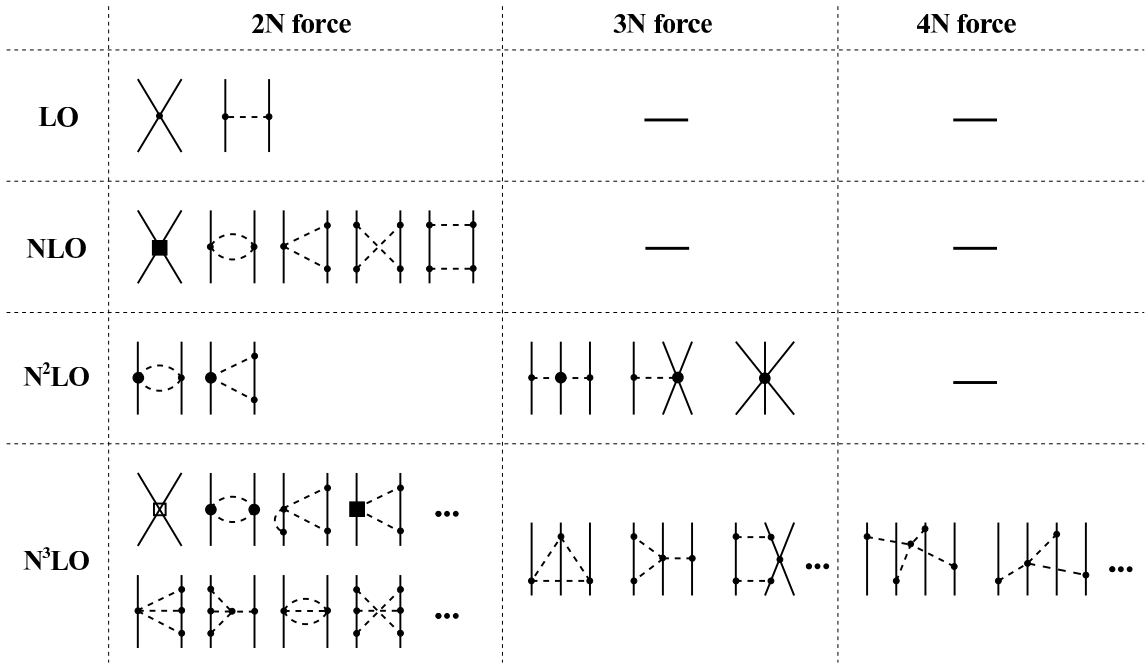

Figure 2 – *Different contributions to the nuclear potential derived in χPT using Weinberg's power counting. Different symbols for the vertices indicate different operator structures of the potential. The diagrams should not be confused with Feynman diagrams [9].*

fig. 2 diagrammatically. We observe that at leading order (LO) and next-to leading order (NLO) only a two-body interaction shows up. This is due to the fact that all diagrams that generate a three-body force up to NLO cancel each other. Three-nucleon forces start contributing at next-to-next-to leading order (N2LO), meaning $\left(\frac{Q}{\Lambda_\chi}\right)^3$, while the four-nucleon force is still absent at this order. The three-nucleon force is given by a two-pion exchange, a one-pion exchange plus two-nucleon contact and a three-nucleon contact term, as shown in fig. 2 from left to right. At next-to-next-to-next-to leading order (N3LO) the first corrections to the three-body force arise and the four-body force starts contributing. We can see that χEFT explains the hierarchy of the few-nucleon forces: two-nucleon interactions are more important than three-nucleon forces, since they arise at lower order of $\frac{Q}{\Lambda_\chi}$. The same holds for the greater importance of three-nucleon interactions compared with four-nucleon interactions. Moreover, the nuclear potential from χEFT clearly determines which three-nucleon force should be used along with the two-nucleon force, in contrast to the previous approaches using more phenomenological three-body forces whose parameters are fitted differently depending on the used two-body force.

Throughout this thesis we use the two-nucleon interaction at N3LO available from Entem and Machleidt [10]. They showed that the accuracy of this potential is

comparable to the high-precision Argonne-V18 (AV18) nucleon-nucleon potential. Its 24 LECs (for the isospin invariant version) have been fitted on nucleon-nucleon phase shifts and deuteron properties.

The operator structure for the three-nucleon interaction is available at N2LO today. Hence, this will be the three-nucleon force we investigate in this thesis. According to [11], the three contributing diagrams are given by:

two-pion exchange

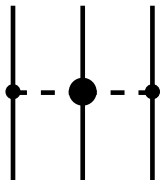

$$\mathbf{V}_{TPE} = \sum_{i\neq j\neq k} \frac{1}{2}\left(\frac{g_A}{2F_\pi}\right)^2 \frac{(\vec{\boldsymbol{\sigma}}_i\cdot\vec{q}_i)(\vec{\boldsymbol{\sigma}}_j\cdot\vec{q}_j)}{(\vec{q}_i^{\,2}+M_\pi^2)(\vec{q}_j^{\,2}+M_\pi^2)} \boldsymbol{F}_{ijk}^{\alpha\beta}\boldsymbol{\tau}_i^\alpha\boldsymbol{\tau}_j^\beta \tag{2.1}$$

$$\boldsymbol{F}_{ijk}^{\alpha\beta} = \delta^{\alpha\beta}\left[-\frac{4c_1M_\pi^2}{F_\pi^2}+\frac{2c_3}{F_\pi^2}\vec{q}_i\cdot\vec{q}_j\right]+\sum_\gamma \frac{c_4}{F_\pi^2}\epsilon^{\alpha\beta\gamma}\boldsymbol{\tau}_k^\gamma\vec{\boldsymbol{\sigma}}_k\cdot[\vec{q}_i\times\vec{q}_j]\,,$$

one-pion exchange two-nucleon contact

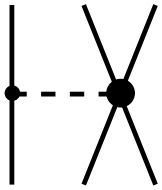

$$\mathbf{V}_{OPE} = -\sum_{i\neq j\neq k}\frac{g_A}{8F_\pi^2}\frac{c_D}{F_\pi^2\Lambda_\chi}\frac{\vec{\boldsymbol{\sigma}}_j\cdot\vec{q}_j}{\vec{q}_j^{\,2}+M_\pi^2}(\vec{\boldsymbol{\tau}}_i\cdot\vec{\boldsymbol{\tau}}_j)(\vec{\boldsymbol{\sigma}}_i\cdot\vec{q}_j)\,, \tag{2.2}$$

three-nucleon contact

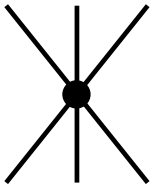

$$\mathbf{V}_{cont} = \frac{1}{2}\sum_{j\neq k}\frac{c_E}{F_\pi^4\Lambda_\chi}(\vec{\boldsymbol{\tau}}_j\cdot\vec{\boldsymbol{\tau}}_k)\,. \tag{2.3}$$

The expressions are operators with respect to spin and isospin, but matrix elements with respect to the momenta. Here, $F_\pi = 92.4$ MeV is the weak decay constant of the pion, M_π the pion mass, $g_A = 1.26$ the axial-vector coupling constant and $\vec{\boldsymbol{\sigma}}$, $\vec{\boldsymbol{\tau}}$ the Pauli matrices for spin and isospin, respectively. The momentum $\vec{\boldsymbol{q}}_i \equiv \vec{\boldsymbol{p}}_i' - \vec{\boldsymbol{p}}_i$ is the momentum transfer of particle i. It is interesting that only two new LECs, c_D and c_E, show up with the three-nucleon interaction that need to be determined by experiment. The LECs c_1, c_3 and c_4 are already present in the two-body interaction and, therefore, fully constrained by the nucleon-nucleon system.

The N3LO contributions to the three-body force are presently worked out. This seems to be a formidable task, since many new diagrams appear. In contrast, the contributions to the four-body interaction at N3LO already have been worked out

[12]. Both, the N3LO three-body contributions as well as the N3LO four-body contributions, are parameter free, meaning that no additional LECs are needed.

We stress that the derivation of the operator structure of the diagrams is not the last step towards their inclusion into nuclear structure calculations. Additionally, one has to evaluate the matrix elements of the different contributions that then enter the many-body calculations. For the N2LO three-body interaction P. Navrátil worked out the matrix elements of operators (2.1), (2.2) and (2.3) in [4]. For that he used the fact that the three-particle interaction can be written as

$$\mathbf{V}^{NNN} = \mathbf{V}_1^{NNN} + \mathbf{V}_2^{NNN} + \mathbf{V}_3^{NNN} \,, \tag{2.4}$$

where the individual parts are connected by permutations. For the evaluation of the matrix elements he used totally antisymmetrized three-particle relative states $|EJTi\rangle$. Thus, the matrix elements can be written as

$$\langle EJTi|\mathbf{V}^{NNN}|EJTi\rangle = 3\,\langle EJTi|\mathbf{V}_1^{NNN}|EJTi\rangle \,. \tag{2.5}$$

We discuss the details on the states $|EJTi\rangle$ in section 3.4, since matrix elements (2.5) will be the starting point of our investigations of three-particle interactions.

We obtain these matrix elements from Navrátil's MANYEFF code [13]. He uses the regulator function $F(q^2;\Lambda) = \exp\left(-\frac{q^4}{\Lambda^4}\right)$ depending on the momentum transfer $\vec{q}$ with $\Lambda = 500\,\text{MeV}$. Also for the N3LO two-body interaction a regulator depending on the momentum transfer is used. Additionally, the two LECs c_D and c_E have to be fixed. The standard three-nucleon observable used for constraining these parameters is the triton binding energy. As second constraint several choices have been studied in the literature, e.g. the nd scattering length [11], or the ^{4}He binding energy [5]. The most consistent way is to fix the parameters entirely in the three-body system, since then no additional many-body contributions can influence their values. As outlined in [14] and references therein, the parameter c_D also appears in the electroweak meson exchange current. Therefore, it is possible to determine its value from the triton β-decay halflife with help of fully converged ab initio calculations. Firstly, one computes trajectories in the c_D-c_E parameter space that reproduce the experimental ^{3}H binding energy and takes then only the region into account where the triton halflife is in agreement with experiment as well. The results are illustrated in fig. 3. The dotted lines yield the constraints

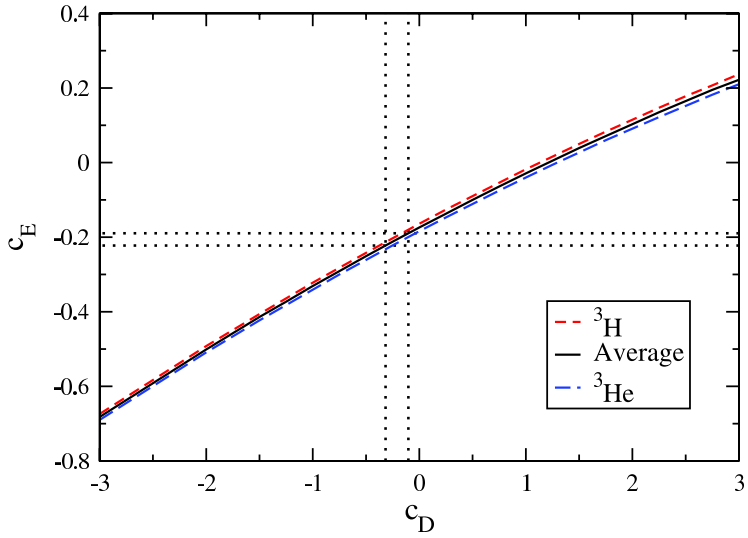

Figure 3 – *Trajectories in the c_D-c_E parameter space that reproduce ^{3}H and ^{3}He experimental binding energies. Additionally, the dotted lines show the region for which the experimental value of the Gamow-Teller matrix element, which is related to the triton β-decay halflife, is reproduced better than $\pm 0.54\%$ [14].*

$-0.3 \leq c_D \leq -0.1$ and $-0.220 \leq c_E \leq -0.189$. Therefore, the parameters we use are

$$c_D = -0.2 \tag{2.6}$$

$$c_E = -0.205\,. \tag{2.7}$$

There is still work left in order to include the three-body force in our IT-NCSM and Hartree-Fock codes, since we need matrix elements with respect to so-called three-body m-scheme harmonic oscillator states

$$|abc\rangle_a = |(n_a l_a, s_a) j_a m_a, (n_b l_b, s_b) j_b m_b, (n_c l_c, s_c) j_c m_c, t_a m_{t_a} t_b m_{t_b} t_c m_{t_c}\rangle_a\,. \tag{2.8}$$

Here, n_a, l_a are the single-particle harmonic oscillator radial and orbital angular momentum quantum numbers respectively. The parenthesis indicate the coupling of $\vec{l}_a$ with the spin $\vec{s}_a$ to total angular momentum $\vec{j}_a$, with corresponding projection quantum number m_a. Moreover, the isospin and its projection quantum number is denoted by t_a and m_{t_a}, respectively. The subscript $_a$ denotes that the states are antisymmetrized. In many-body calculations we use A-particle m-scheme states as basis of the A-particle Hilbert space. The advantages of this basis are the simple way of antisymmetrizing the states and that A-particle matrix elements can be reduced to three-particle m-scheme matrix elements using Slater rules [15]. Therefore, we have to transform the matrix elements (2.5) into the matrix elements with respect to states (2.8). As we need some basic mathematical

techniques to carry out this transformation, the next section will concentrate on all necessary points.

SECTION 3

Mathematical basics

In this section we discuss some mathematical basics that facilitate our investigations in the following sections and that are essential for a complete understanding of all details. Moreover, we introduce the notation used in the rest of this thesis. In the first subsection we focus on angular momentum coupling. Next, we introduce the so-called Jacobi coordinates in subsection 3.2 and study the harmonic oscillator brackets in 3.3. In subsection 3.4, we use all previously discussed elements to formulate a special method to construct an antisymmetrized basis of the three-particle Hilbert space.

3.1 Angular momentum coupling

As we will see in section 4, angular momentum (re-)coupling plays a crucial role in the transformation from the Jacobi-coordinate basis into the m-scheme basis. Therefore, we now briefly discuss different coupling scenarios and the corresponding transformation coefficients. Firstly, we deal with coupling of two angular momenta and the Clebsch-Gordan coefficients, next we investigate re-coupling including three angular momenta via so-called 6j-symbols. Then we discuss four momenta re-coupling with the corresponding 9j-symbols and finally we have a look at 3nj-symbols. For more details, e.g. regarding symmetry relations, see [16].

3.1.1 Clebsch-Gordan coefficients

Clebsch-Gordan coefficients occur if we couple two angular momenta $\vec{j}_1, \vec{j}_2$ to a total angular momentum $\vec{J}$. Assume we have the product state

$$|j_1 m_1, j_2 m_2\rangle \equiv |j_1 m_1\rangle \otimes |j_2 m_2\rangle \tag{3.1}$$

with arbitrary angular momenta quantum numbers j_1 and j_2 and corresponding magnetic quantum numbers m_1, m_2. We couple the two angular momenta by inserting an identity operator in the coupled basis representation

$$\mathbb{1} = \sum_{j_1,j_2,J,M} |(j_1,j_2)JM\rangle\langle(j_1,j_2)JM| \tag{3.2}$$

with J as the coupled momentum and M its corresponding magnetic quantum number. The parenthesis indicate that $\vec{\boldsymbol{j}}_1$ couples with $\vec{\boldsymbol{j}}_2$ to $\vec{\boldsymbol{J}}$. Using eq. (3.2) we can relate the uncoupled states to the coupled ones via

$$|j_1 m_1, j_2 m_2\rangle = \sum_{j_1',j_2',J,M} |(j_1',j_2')JM\rangle\langle(j_1',j_2')JM|j_1 m_1, j_2 m_2\rangle \tag{3.3}$$

$$= \sum_{J,M} |(j_1,j_2)JM\rangle\langle(j_1,j_2)JM|j_1 m_1, j_2 m_2\rangle\,. \tag{3.4}$$

The summations over j_1', j_2' vanish, as the state has to fulfill the eigenvalue equation of the squared angular momentum operators $\vec{\boldsymbol{j}}_1^2, \vec{\boldsymbol{j}}_2^2$ before and after insertion of the identity operator. The expansion coefficients on the right hand side of eq. (3.3) are called Clebsch-Gordan coefficients, which will be denoted in the following by

$$\left(\begin{array}{cc|c} j_1 & j_2 & J \\ m_1 & m_2 & M \end{array}\right) \equiv \langle(j_1,j_2)JM|j_1 m_1, j_2 m_2\rangle\,, \tag{3.5}$$

yielding

$$|j_1 m_1, j_2 m_2\rangle = \sum_{J,M} \left(\begin{array}{cc|c} j_1 & j_2 & J \\ m_1 & m_2 & M \end{array}\right) |(j_1,j_2)JM\rangle\,. \tag{3.6}$$

Likewise, we can expand the coupled states in the uncoupled basis

$$|(j_1,j_2)JM\rangle = \sum_{m_1,m_2} \left(\begin{array}{cc|c} j_1 & j_2 & J \\ m_1 & m_2 & M \end{array}\right) |j_1 m_1, j_2 m_2\rangle\,. \tag{3.7}$$

The Clebsch-Gordan coefficients can be chosen to be real numbers and they are nonzero only if the triangular condition

$$|j_1 - j_2| \leq J \leq j_1 + j_2 \tag{3.8}$$

as well as

$$m_1 + m_2 = M \tag{3.9}$$

are fulfilled. Additionally, the following two orthogonality relations hold true which will be useful later on:

$$\sum_{J,M} \left(\begin{matrix} j_1 & j_2 \\ m_1 & m_2 \end{matrix} \middle| \begin{matrix} J \\ M \end{matrix} \right) \left(\begin{matrix} j_1 & j_2 \\ m_1' & m_2' \end{matrix} \middle| \begin{matrix} J \\ M \end{matrix} \right) = \delta_{m_1,m_1'} \delta_{m_2,m_2'} \,, \tag{3.10}$$

$$\sum_{m_1,m_2} \left(\begin{matrix} j_1 & j_2 \\ m_1 & m_2 \end{matrix} \middle| \begin{matrix} J \\ M \end{matrix} \right) \left(\begin{matrix} j_1 & j_2 \\ m_1 & m_2 \end{matrix} \middle| \begin{matrix} J' \\ M' \end{matrix} \right) = \delta_{J,J'} \delta_{M,M'} \,. \tag{3.11}$$

There exist a number of symmetry relations for the Clebsch-Gordan coefficients, e.g. exchanging the first two columns yields

$$\left(\begin{matrix} j_1 & j_2 \\ m_1 & m_2 \end{matrix} \middle| \begin{matrix} J \\ M \end{matrix} \right) = (-1)^{J-j_1-j_2} \left(\begin{matrix} j_2 & j_1 \\ m_2 & m_1 \end{matrix} \middle| \begin{matrix} J \\ M \end{matrix} \right) \,. \tag{3.12}$$

At last, we note that the Clebsch-Gordan coefficients are proportional to Wigner's 3j-symbols

$$\left(\begin{matrix} j_1 & j_2 \\ m_1 & m_2 \end{matrix} \middle| \begin{matrix} J \\ M \end{matrix} \right) = (-1)^{j_1-j_2+M} \sqrt{2j_3+1} \begin{pmatrix} j_1 & j_2 & J \\ m_1 & m_2 & -M \end{pmatrix} \,, \tag{3.13}$$

with $\left(\begin{smallmatrix} j_1 & j_2 & J \\ m_1 & m_2 & -M \end{smallmatrix} \right)$ as Wigner's 3j-symbol. Though these 3j-symbols will not show up in any formula, they are used in our program when calculating Clebsch-Gordan coefficients.

3.1.2 6j-symbols

The 6j-symbols are the transformation coefficients for the conversion amongst different coupling schemes of three angular momenta. Three different possible coupling schemes exist:

1. $|[(j_1,j_2)J_{12},j_3]JM\rangle$
   $\vec{\boldsymbol{j}}_1$ couples with $\vec{\boldsymbol{j}}_2$ to $\vec{\boldsymbol{J}}_{12}$ and this "intermediate" angular momentum $\vec{\boldsymbol{J}}_{12}$ itself couples with $\vec{\boldsymbol{j}}_3$ to $\vec{\boldsymbol{J}}$.

2. $|[j_1,(j_2,j_3)J_{23}]JM\rangle$
   $\vec{\boldsymbol{j}}_2$ couples with $\vec{\boldsymbol{j}}_3$ to $\vec{\boldsymbol{J}}_{23}$, $\vec{\boldsymbol{j}}_1$ with $\vec{\boldsymbol{J}}_{23}$ to J.

3. $|[(j_1,j_3)J_{13},j_2]JM\rangle$
   $\vec{\boldsymbol{j}}_1$ couples with $\vec{\boldsymbol{j}}_3$ to $\vec{\boldsymbol{J}}_{13}$, $\vec{\boldsymbol{J}}_{13}$ with $\vec{\boldsymbol{j}}_2$ to $\vec{\boldsymbol{J}}$.

To express a state of the first coupling scheme in terms of states of the second one we again make use of an appropriate identity

$$|[(j_1,j_2)J_{12},j_3]JM\rangle = \sum_{J_{23},J',M'} |[j_1,(j_2,j_3)J_{23}]J'M'\rangle\langle[j_1,(j_2,j_3)J_{23}]J'M'|[(j_1,j_2)J_{12},j_3]JM\rangle. \tag{3.14}$$

The transformation coefficient is given by the relation

$$\begin{aligned}&\langle[j_1,(j_2,j_3)J_{23}]J'M'|[(j_1,j_2)J_{12},j_3]JM\rangle \\ &= \delta_{J,J'}\delta_{M,M'}(-1)^{j_1+j_2+j_3+J}\sqrt{(2J_{12}+1)(2J_{23}+1)}\begin{Bmatrix} j_1 & j_2 & J_{12} \\ j_3 & J & J_{23}\end{Bmatrix},\end{aligned} \tag{3.15}$$

which defines the Wigner 6j-symbol $\left\{ \begin{smallmatrix} j_1 & j_2 & J_{12} \\ j_3 & J & J_{23}\end{smallmatrix} \right\}$.
The 6j-symbol itself can be expressed with help of sums over three Clebsch-Gordan coefficients and thus are real numbers, too. They are nonzero only if the triangular conditions

$$\begin{aligned} &|j_1-j_2| \le J_{12} \le j_1+j_2, && |J_{12}-j_3| \le J \le J_{12}+j_3, \\ &|j_2-j_3| \le J_{23} \le j_3+j_3 \quad \text{and} && |J_{23}-j_1| \le J \le J_{23}+j_1 \end{aligned} \tag{3.16}$$

are fulfilled. Symmetry relations, orthogonality relations and formulas for the direct calculation of the 6j-symbols can be found in [16].

In general, there are three possible types of transformation coefficients depending on the states before and after the transformation. These three types are given by:

- $|[(j_1,j_2)J_{12},j_3]JM\rangle \longleftrightarrow |[j_1,(j_2,j_3)J_{23}]JM\rangle$
  The corresponding coefficient is given in eq. (3.15).

- $|[(j_1,j_2)J_{12},j_3]JM\rangle \longleftrightarrow |[(j_1,j_3)J_{13},j_2]JM\rangle$
  The coefficient is given by

$$\begin{aligned}&\langle[(j_1,j_2)J_{12},j_3]J'M'|[(j_1,j_3)J_{13},j_2]JM\rangle \\ &= \delta_{J,J'}\delta_{M,M'}(-1)^{j_2+j_3+J_{12}+J_{13}}\sqrt{(2J_{12}+1)(2J_{13}+1)}\begin{Bmatrix} j_2 & j_1 & J_{12} \\ j_3 & J & J_{13}\end{Bmatrix}.\end{aligned} \tag{3.17}$$

- $|[j_1,(j_2,j_3)J_{23}]J'M'\rangle \longleftrightarrow |[(j_1,j_3)J_{13},j_2]JM\rangle$
  The coefficient is given by

$$\begin{aligned}&\langle[j_1,(j_2,j_3)J_{23}]JM|[(j_1,j_3)J_{13},j_2]JM\rangle \\ &\quad = \quad \delta_{J,J'}\delta_{M,M'}(-1)^{j_1+J+J_{23}}\sqrt{(2J_{23}+1)(2J_{13}+1)}\begin{Bmatrix} j_1 & j_3 & J_{13} \\ j_2 & J & J_{23}\end{Bmatrix}. \end{aligned} \tag{3.18}$$

3.1.3 9j-symbols

The 9j-symbols are coefficients of unitary transformations between different coupling schemes of four angular momenta. They can be expressed as sums of products of three 6j-symbols or as sums of products of six Clebsch-Gordan coefficients, so they are also real numbers. Obviously there are many possibilities to couple four angular momenta, resulting in many different transformation coefficients. We will restrict ourselves to the cases that are relevant later on. The 9j-symbols will be denoted by

$$\begin{Bmatrix} a & b & c \\ d & e & f \\ g & h & j\end{Bmatrix}. \tag{3.19}$$

- $|[(j_1,j_2)J_{12},(j_3,j_4)J_{34}]JM\rangle \longleftrightarrow |[(j_1,j_3)J_{13},(j_2,j_4)J_{24}]JM\rangle$
  The notation $|[(j_1,j_2)J_{12},(j_3,j_4)J_{34}]JM\rangle$ again means that $\vec{\boldsymbol{j}}_1$ couples with $\vec{\boldsymbol{j}}_2$ to the intermediate $\vec{\boldsymbol{J}}_{12}$ and $\vec{\boldsymbol{j}}_3$ with $\vec{\boldsymbol{j}}_4$ to intermediate $\vec{\boldsymbol{J}}_{34}$. Then, the intermediates themselves couple to $\vec{\boldsymbol{J}}$. The transformation coefficient is given by

$$\begin{aligned}&\langle[(j_1,j_2)J_{12},(j_3,j_4)J_{34}]J'M'|[(j_1,j_3)J_{13},(j_2,j_4)J_{24}]JM\rangle \\ &\quad = \delta_{J,J'}\delta_{M,M'}\sqrt{(2J_{12}+1)(2J_{13}+1)(2J_{24}+1)(2J_{34}+1)}\begin{Bmatrix} j_1 & j_2 & J_{12} \\ j_3 & j_4 & J_{34} \\ J_{13} & J_{24} & J\end{Bmatrix}. \end{aligned} \tag{3.20}$$

- $|[(j_1,j_2)J_{12},(j_3,j_4)J_{34}]JM\rangle \longleftrightarrow |[(j_1,j_4)J_{14},(j_2,j_3)J_{23}]JM\rangle$
  The transformation coefficient is given by

$$\begin{aligned}&\langle[(j_1,j_2)J_{12},(j_3,j_4)J_{34}]J'M'|[(j_1,j_4)J_{14},(j_2,j_3)J_{23}]JM\rangle \\ &\quad = \delta_{J,J'}\delta_{M,M'}\sqrt{(2J_{12}+1)(2J_{14}+1)(2J_{23}+1)(2J_{34}+1)}(-1)^{j_3+j_4-J_{34}}\begin{Bmatrix} j_1 & j_2 & J_{12} \\ j_4 & j_3 & J_{34} \\ J_{14} & J_{23} & J\end{Bmatrix}. \end{aligned} \tag{3.21}$$

- $|[(j_1,j_3)J_{13},(j_2,j_4)J_{24}]JM\rangle \longleftrightarrow |[(j_1,j_4)J_{14},(j_2,j_3)J_{23}]JM\rangle$
  The transformation coefficient is given by

$$\begin{aligned}&\langle[(j_1,j_3)J_{13},(j_2,j_4)J_{24}]J'M'|[(j_1,j_4)J_{14},(j_2,j_3)J_{23}]JM\rangle \\ &= \delta_{J,J'}\delta_{M,M'}\sqrt{(2J_{13}+1)(2J_{14}+1)(2J_{24}+1)(2J_{23}+1)} \\ &\qquad\times(-1)^{j_3-j_4-J_{23}+J_{24}}\begin{Bmatrix} j_1 & j_3 & J_{13} \\ j_4 & j_2 & J_{24} \\ J_{14} & J_{23} & J \end{Bmatrix}.\end{aligned} \tag{3.22}$$

As usual many symmetry relations for the 9j-symbol exist, e.g. transposing all entries does not affect its value

$$\begin{Bmatrix} a & b & c \\ d & e & f \\ g & h & j \end{Bmatrix} = \begin{Bmatrix} a & d & g \\ b & e & h \\ c & f & j \end{Bmatrix}, \tag{3.23}$$

exchanging rows or columns produces phase factors. For details, see [16].
Finally, the following triangular conditions have to be fulfilled for a nonzero value of the 9j-symbols

$$\begin{aligned} &|a-b|\le c\le a+b\,, \qquad &&|d-e|\le f\le d+e\,, \qquad &&|g-h|\le j\le g+h\,, \\ &|a-d|\le g\le a+d\,, \qquad &&|b-e|\le h\le b+e\,, \qquad &&|c-f|\le j\le c+f\,. \end{aligned} \tag{3.24}$$

3.1.4 3nj-symbols

3nj-symbols are the generalization of 6j- and 9j-symbols, which are 3nj-symbols for $n=2$ and $n=3$, respectively. 3nj-symbols of higher orders are proportional to transformation coefficients needed for switching between different coupling schemes of five and more angular momenta. They can be written as sums of products of 6j-symbols and are real numbers, too. For our investigations on three-nucleon interactions we do not need 3nj-symbols for $n>3$, but if four-nucleon interactions would be considered someday they will come into play. For more details, see again [16].

3.2 Jacobi coordinates

In this section we give an introduction to Jacobi coordinates. We will use them quite frequently, so it is crucial to have a look at their definition. In principle, Jacobi coordinates are the generalization of the well-known two-body relative and center-of-mass coordinates. Given two particles with mass m_1 and m_2 and coordinates $\vec{r}_1$

and $\vec{r}_2$, respectively, these are defined as

$$\vec{R} = \frac{1}{m_1 + m_2}\left(m_1\vec{r}_1 + m_2\vec{r}_2\right) \qquad \text{(center-of-mass coordinate)}\,, \tag{3.25}$$

$$\vec{r} = \vec{r}_1 - \vec{r}_2 \qquad \text{(relative coordinate)}\,. \tag{3.26}$$

Jacobi coordinates are a generalization for more particles in the way that they are proportional to centers of mass of particle subclusters. Sometimes they are referred to as "relative coordinates for many-body systems". We denote Jacobi coordinates in this thesis with $\{\vec{\xi}_i\}$. One possible definition is given by

$$\vec{\xi}_0 = \sqrt{\frac{1}{A}}\left[\vec{r}_1 + \vec{r}_2 + \cdots + \vec{r}_A\right], \tag{3.27}$$

$$\vec{\xi}_1 = \sqrt{\frac{1}{2}}\left[\vec{r}_1 - \vec{r}_2\right], \tag{3.28}$$

$$\vdots$$

$$\vec{\xi}_{A-2} = \sqrt{\frac{A-2}{A-1}}\left[\frac{1}{A-2}(\vec{r}_1 + \vec{r}_2 + \cdots + \vec{r}_{A-2}) - \vec{r}_{A-1}\right], \tag{3.29}$$

$$\vec{\xi}_{A-1} = \sqrt{\frac{A-1}{A}}\left[\frac{1}{A-1}(\vec{r}_1 + \vec{r}_2 + \cdots + \vec{r}_{A-1}) - \vec{r}_A\right]. \tag{3.30}$$

Here we assumed A particles with same mass, as it will be the case in the atomic nucleus later on, since we will work in the isospin formalism. We see from eq. (3.27) that $\vec{\xi}_0$ is proportional to the center of mass of the A-particle system. The rest of the coordinates always depend linearly on centers of mass of nucleon subclusters: $\vec{\xi}_i$ is proportional to the relative vector between the center of mass of the first i particles and the position of the $(i+1)$*th* particle. The benefit of this coordinate system is that it allows to separate the center-of-mass motion of a system from the intrinsic motion. Since the motion of the center of mass is often irrelevant, this helps to simplify many problems. As the nuclear interaction does not effect the center of mass of the system, we will use later on harmonic oscillator states based on Jacobi coordinates. However, the set of Jacobi coordinates is not unique, but it is the most convenient for our purposes. For other sets and their applications in nuclear many-body calculations, see ref. [13]. For three-particle systems the equa-

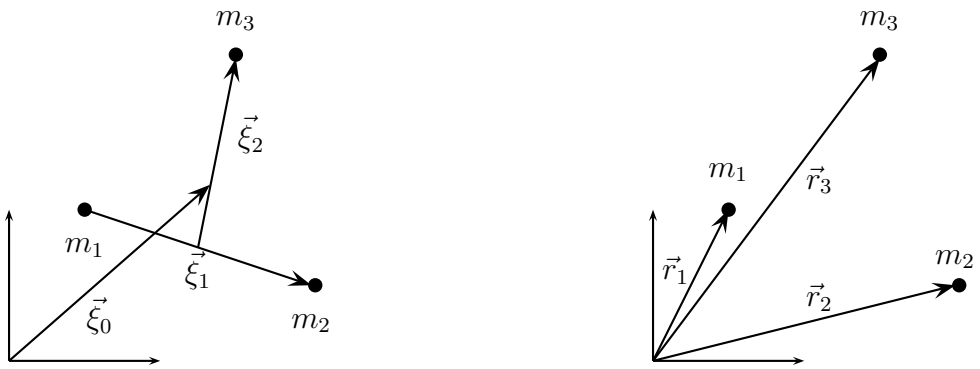

Figure 4 – *Three-particle system described in Jacobi coordinates (left) and in Cartesian coordinates (right).*

tions (3.27)-(3.30) become

$$\vec{\xi}_0 = \sqrt{\frac{1}{3}}\ [\vec{r}_1 + \vec{r}_2 + \vec{r}_3]\ , \tag{3.31}$$

$$\vec{\xi}_1 = \sqrt{\frac{1}{2}}\ [\vec{r}_1 - \vec{r}_2]\ , \tag{3.32}$$

$$\vec{\xi}_2 = \sqrt{\frac{2}{3}}\ \left[\frac{1}{2}(\vec{r}_1 + \vec{r}_2) - \vec{r}_3\right]\ . \tag{3.33}$$

Their geometric illustration is given in fig. 3.2: $\vec{\xi}_0$ points to the center of mass of the three-particle system, $\vec{\xi}_1$ is the relative vector between particles 1 and 2. Finally, coordinate $\vec{\xi}_2$ describes the coordinate of the third particle relative to the center of mass of particles 1 and 2. The same situation in Cartesian coordinates is shown on the right hand side. Here, each particle is described by its own position vector. The Jacobi momenta are defined analogously to the Jacobi coordinates. For a three-particle system they are given by

$$\vec{\pi}_0 = \sqrt{\frac{1}{3}}\ [\vec{p}_1 + \vec{p}_2 + \vec{p}_3]\ , \tag{3.34}$$

$$\vec{\pi}_1 = \sqrt{\frac{1}{2}}\ [\vec{p}_1 - \vec{p}_2]\ , \tag{3.35}$$

$$\vec{\pi}_2 = \sqrt{\frac{2}{3}}\ \left[\frac{1}{2}(\vec{p}_1 + \vec{p}_2) - \vec{p}_3\right]\ , \tag{3.36}$$

with $\vec{p}_i$ being the single-particle momentum.

3.3 Harmonic oscillator brackets (HOBs)

A typical problem known from nuclear structure calculations with two-body interactions is the transformation of harmonic oscillator matrix elements defined in relative coordinates into harmonic oscillator matrix elements based on single particle coordinates [17]. With states based on relative and center of mass coordinates we mean that the corresponding harmonic oscillator Hamilton operator is given by

$$\boldsymbol{H} = \frac{\vec{\boldsymbol{\pi}}_0^2}{2M} + \frac{1}{2}M\Omega^2\vec{\boldsymbol{\xi}}_0^2 + \frac{\vec{\boldsymbol{\pi}}_1^2}{2\mu} + \frac{1}{2}\mu\Omega^2\vec{\boldsymbol{\xi}}_1^2 \tag{3.37}$$

and also the orbital angular momentum operators are given by $\vec{\boldsymbol{L}}_{cm} = \vec{\boldsymbol{\xi}}_0 \times \vec{\boldsymbol{\pi}}_0$ and $\vec{\boldsymbol{L}}_{rel} = \vec{\boldsymbol{\xi}}_1 \times \vec{\boldsymbol{\pi}}_1$. Here, $\vec{\boldsymbol{\xi}}_{0,1}$ and $\vec{\boldsymbol{\pi}}_{0,1}$ are the position and momentum operators in Jacobi coordinates for the two-particle case respectively. In contrast, the Hamilton operator

$$\boldsymbol{H} = \frac{\vec{\boldsymbol{p}}_1^2}{2m_1} + \frac{1}{2}m_1\omega^2\vec{\boldsymbol{r}}_1^2 + \frac{\vec{\boldsymbol{p}}_2^2}{2m_2} + \frac{1}{2}m_2\omega^2\vec{\boldsymbol{r}}_2^2 \tag{3.38}$$

corresponds to the eigenstates based on single-particle coordinates. Here, the orbital angular momentum operators are given by $\vec{\boldsymbol{L}}_i = \vec{\boldsymbol{r}}_i \times \vec{\boldsymbol{p}}_i$. To distinguish these states we write the position, relevant for the orbital angular momentum quantum number, in parenthesis next to it:

$$|n_1 l_1(\vec{r}_1), n_2 l_2(\vec{r}_2)\rangle : \quad \text{state based on single-particle coordinates} \tag{3.39}$$

$$|NL(\vec{\xi}_0), nl(\vec{\xi}_1))\rangle : \quad \text{state based on cm. and rel. coordinates}\,. \tag{3.40}$$

States (3.40) are suitable to calculate interaction matrix elements of two-body interactions, since the center-of-mass part of the state is not affected by the interaction operator. The second advantage is that the operator of the relative orbital momentum is included in the operator structure of the interaction and, therefore, one can easily evaluate matrix elements using eigenstates of this operator. For many-body calculations in the no-core shell model (NCSM) framework matrix elements in states (3.39) are obligatory. So we need a technique to convert states (3.40) into states (3.39), the so called Talmi-Moshinsky transformation [18, 19]. We insert again the appropriate identity operator, while the resulting overlap is defined as the harmonic oscillator bracket (HOB). In general, HOBs cannot only be used to connect the well-known states given above, in fact they can connect states corresponding to any orthogonal coordinate transformation of the single-particle coordinates. We will use this property when we calculate matrix elements of the

antisymmetrizer in the next subsection and also later in the transformation presented in section 4. There are two different definitions of HOBs, distinguished by the order of the quantum numbers in the bra state. We first present the definition that we use in subsections 3.3.1 and 3.3.2. After that, we introduce the alternative definition in subsections 3.3.3 and 3.3.4. In subsection 3.3.5 we point out how to relate the two definitions to each other.

3.3.1 Definition of harmonic oscillator brackets – our version

The definition of the harmonic oscillator brackets that we use is given by

$$|[n_1 l_1, n_2 l_2]\Lambda\lambda\rangle = \sum_{NL,nl} \langle (NL, nl)\Lambda | (n_1 l_1, n_2 l_2)\Lambda\rangle_d \, |[NL, nl]\Lambda\lambda\rangle \,, \tag{3.41}$$

$$= \sum_{NL,nl} \langle\langle NL, nl; \Lambda | n_1 l_1, n_2 l_2\rangle\rangle_d \, |[NL, nl]\Lambda\lambda\rangle \,, \tag{3.42}$$

with $\langle\langle NL, nl; \Lambda | n_1 l_1, n_2 l_2\rangle\rangle_d$ as the HOB, where d is a non-negative real number [20]. The corresponding coordinate transformation matrix is given by the general form of an orthogonal transformation

$$\begin{pmatrix} \vec{R} \\ \vec{r} \end{pmatrix} = \begin{pmatrix} \sqrt{\frac{d}{1+d}} & \sqrt{\frac{1}{1+d}} \\ \sqrt{\frac{1}{1+d}} & -\sqrt{\frac{d}{1+d}} \end{pmatrix} \begin{pmatrix} \vec{r}_1 \\ \vec{r}_2 \end{pmatrix} \,. \tag{3.43}$$

For $d = 1$ this is a transformation from single-particle coordinates to relative and center-of-mass coordinates. For other values of d we describe a general orthogonal transformation. Although it might in general be a bit misleading, we refer to N and L as the quantum numbers of the "center-of-mass" of the two particles, and to n and l as the quantum numbers of their "relative" motion. Here N and n are the radial quantum numbers of the harmonic oscillator. With the notation introduced in section 3.2 we should write $L(\vec{R}), l(\vec{r})$ and accordingly $l_1(\vec{r}_1)$ and $l_2(\vec{r}_2)$ for the different angular momentum quantum numbers. For brevity we drop this notation for the rest of this subsection. The quantum number Λ is the coupled orbital angular momentum of the two particles and λ the corresponding projection quantum number. If we want to calculate the HOB explicitly, we insert an identity operator

in coordinate basis representation

$$\begin{aligned}
&\langle\langle NL, nl; \Lambda | n_1 l_1, n_2 l_2 \rangle\rangle_d \\
&\quad = \iint \mathrm{d}^3 r_1 \mathrm{d}^3 r_2 \langle (NL, nl)\Lambda\lambda | \vec{r}_1, \vec{r}_2 \rangle \langle \vec{r}_1, \vec{r}_2 | (n_1 l_1, n_2 l_2)\Lambda\lambda \rangle \\
&\quad = \iint \mathrm{d}^3 r_1 \mathrm{d}^3 r_2 \langle (NL, nl)\Lambda\lambda | \vec{R}, \vec{r} \rangle \langle \vec{r}_1, \vec{r}_2 | (n_1 l_1, n_2 l_2)\Lambda\lambda \rangle \\
&\quad = \iint \mathrm{d}^3 r_1 \mathrm{d}^3 r_2 \{\phi_{NL}(\vec{R})\phi_{nl}(\vec{r})\}^\dagger_{\Lambda\lambda} \{\phi_{n_1 l_1}(\vec{r}_1)\phi_{n_2 l_2}(\vec{r}_2)\}_{\Lambda\lambda} \\
&\quad = \frac{1}{2\Lambda+1} \sum_\lambda \iint \mathrm{d}^3 r_1 \mathrm{d}^3 r_2 \{\phi_{NL}(\vec{R})\phi_{nl}(\vec{r})\}^\dagger_{\Lambda\lambda} \{\phi_{n_1 l_1}(\vec{r}_1)\phi_{n_2 l_2}(\vec{r}_2)\}_{\Lambda\lambda} \,,
\end{aligned} \tag{3.44}$$

where we introduced the coordinate space harmonic oscillator wave functions ϕ. The curly brackets indicate the angular momentum coupling. The sum over λ in the last line follows from the fact that the HOBs are independent of the projection quantum number λ. Furthermore, HOBs are nonzero only if the energy of the harmonic oscillator states in the bra and ket is equal, i.e.

$$\langle\langle NL, nl; \Lambda | n_1 l_1, n_2 l_2 \rangle\rangle_d \equiv \delta_{2N+L+2n+l, 2n_1+l_1+2n_2+l_2} \langle\langle NL, nl; \Lambda | n_1 l_1, n_2 l_2 \rangle\rangle_d \,. \tag{3.45}$$

This is a very helpful relation, because it implies that the summations in eq. (3.41) are finite. This is a special property of harmonic oscillator eigenstates. It also implies the useful relation

$$(-1)^{l_1+l_2} = (-1)^{L+l} \,. \tag{3.46}$$

Moreover, HOBs are real numbers, i.e.

$$\langle\langle NL, nl; \Lambda | n_1 l_1, n_2 l_2 \rangle\rangle_d = \langle\langle n_1 l_1, n_2 l_2; \Lambda | NL, nl \rangle\rangle_d \tag{3.47}$$

holds.

3.3.2 Symmetry relations

Now we derive a number of useful symmetry relations of HOBs. Let us start with the definition of a HOB in coordinate representation

$$\begin{aligned}
&\langle\langle n_1 l_1, n_2 l_2; \Lambda | NL, nl \rangle\rangle_d \\
&\quad = \frac{1}{2\Lambda+1} \sum_\lambda \iint \mathrm{d}^3 r_1 \mathrm{d}^3 r_2 \langle (n_1 l_1, n_2 l_2)\Lambda\lambda | \vec{r}_1, \vec{r}_2 \rangle \langle \vec{R}, \vec{r} | (NL, nl)\Lambda\lambda \rangle \,.
\end{aligned} \tag{3.48}$$

Now we make use of the fact that the same transformation matrix combines the coordinates in the following way

$$\begin{pmatrix} -\vec{r} \\ \vec{R} \end{pmatrix} = \begin{pmatrix} \sqrt{\frac{d}{1+d}} & \sqrt{\frac{1}{1+d}} \\ \sqrt{\frac{1}{1+d}} & -\sqrt{\frac{d}{1+d}} \end{pmatrix} \begin{pmatrix} \vec{r}_2 \\ -\vec{r}_1 \end{pmatrix} . \tag{3.49}$$

Note that $\vec{R} = \sqrt{\frac{d}{1+d}}\vec{r}_1 + \sqrt{\frac{1}{1+d}}\vec{r}_2$ and $\vec{r} = \sqrt{\frac{1}{1+d}}\vec{r}_1 - \sqrt{\frac{d}{1+d}}\vec{r}_2$ still are given as in eq. (3.43). This must always be fulfilled for all symmetry relations we derive in the following. Furthermore, we know the following relations

$$\begin{aligned} \langle (n_1 l_1, n_2 l_2)\Lambda\lambda | \vec{r}_1, \vec{r}_2 \rangle &= (-1)^{l_1}(-1)^{l_1+l_2-\Lambda}\langle (n_2 l_2, n_1 l_1)\Lambda\lambda | \vec{r}_2, -\vec{r}_1 \rangle , & (3.50) \\ \langle (EL, el)\Lambda\lambda | \vec{R}, \vec{r} \rangle &= (-1)^{l}(-1)^{l+L-\Lambda}\langle (el, EL)\Lambda\lambda | -\vec{r}, \vec{R} \rangle . & (3.51) \end{aligned}$$

The first phase factor with one orbital angular momentum in the exponent corresponds to the behavior of the harmonic oscillator wave functions under parity transformation. The second one, with three orbital angular momenta in the exponent, is exactly the one we know from eq. (3.12) and shows up because we reversed the coupling order of the angular momenta. Using these relations we can rewrite eq. (3.48) as

$$\begin{aligned} &\langle\langle n_1 l_1, n_2 l_2; \Lambda | NL, nl \rangle\rangle_d \\ &\quad = \frac{1}{2\Lambda+1}\sum_\lambda \iint \mathrm{d}^3 r_1 \mathrm{d}^3 r_2 \langle (n_2 l_2, n_1 l_1)\Lambda\lambda | \vec{r}_2, -\vec{r}_1 \rangle \langle -\vec{r}, \vec{R} | (nl, NL)\Lambda\lambda \rangle (-1)^{l_2+L} \\ &\quad = \frac{1}{2\Lambda+1}\sum_\lambda \iint \mathrm{d}^3 r_1 \mathrm{d}^3 r_2 \langle (n_2 l_2, n_1 l_1)\Lambda\lambda | \vec{r}_2, -\vec{r}_1 \rangle \langle \vec{r}_2, -\vec{r}_1 | (nl, NL)\Lambda\lambda \rangle (-1)^{l_2+L} \\ &\quad = (-1)^{l_2+L}\langle\langle n_2 l_2, n_1 l_1; \Lambda | nl, NL \rangle\rangle_d , \end{aligned} \tag{3.52}$$

where we used the identity

$$\mathbb{1} = \iint \mathrm{d}^3 r_1 \mathrm{d}^3 r_2 | \vec{r}_2, -\vec{r}_1 \rangle \langle \vec{r}_2, -\vec{r}_1 | . \tag{3.53}$$

To simplify the phase factor we used the fact that orbital angular momenta are integer and so $(-1)^{2l} \equiv 1$.

For the next symmetry relation we use that the transformation

$$\begin{pmatrix} \vec{R} \\ -\vec{r} \end{pmatrix} = \begin{pmatrix} \sqrt{\frac{1}{1+d}} & \sqrt{\frac{d}{1+d}} \\ \sqrt{\frac{d}{1+d}} & -\sqrt{\frac{1}{1+d}} \end{pmatrix} \begin{pmatrix} \vec{r}_2 \\ \vec{r}_1 \end{pmatrix} \tag{3.54}$$

connects the coordinates in the correct way, where we also changed $d \to \frac{1}{d}$ in the

matrix. Moreover, we can use the relations

$$\langle nl|\vec{r}\rangle = (-1)^l\langle nl|-\vec{r}\rangle\,, \tag{3.55}$$

$$\langle(n_1l_1,n_2l_2)\Lambda\lambda|\vec{r}_1,\vec{r}_2\rangle = (-1)^{l_1+l_2-\Lambda}\langle(n_2l_2,n_1l_1)\Lambda\lambda|\vec{r}_2,\vec{r}_1\rangle\,, \tag{3.56}$$

and rewrite eq. (3.48) as

$$\begin{aligned}
&\langle\langle n_1l_1,n_2l_2;\Lambda|NL,nl\rangle\rangle_d \\
&= \frac{1}{2\Lambda+1}\sum_\lambda\iint \mathrm{d}^3r_1\mathrm{d}^3r_2\langle(n_2l_2,n_1l_1)\Lambda\lambda|\vec{r}_2,\vec{r}_1\rangle\langle\vec{R},-\vec{r}|(NL,nl)\Lambda\lambda\rangle(-1)^{l+l_1+l_2-\Lambda} \\
&= \frac{1}{2\Lambda+1}\sum_\lambda\iint \mathrm{d}^3r_1\mathrm{d}^3r_2\langle(n_2l_2,n_1l_1)\Lambda\lambda|\vec{r}_2,\vec{r}_1\rangle\langle\vec{r}_2,\vec{r}_1|(NL,nl)\Lambda\lambda\rangle(-1)^{l+l_1+l_2-\Lambda} \\
&= (-1)^{L-\Lambda}\langle\langle n_2l_2,n_1l_1;\Lambda|NL,nl\rangle\rangle_{\frac{1}{d}}\,.
\end{aligned} \tag{3.57}$$

Here we take advantage of eq. (3.46) to simplify the phase factor.

For the last symmetry relation we use the transformation matrix

$$\begin{pmatrix}\vec{r}\\ \vec{R}\end{pmatrix} = \begin{pmatrix}\sqrt{\frac{1}{1+d}} & \sqrt{\frac{d}{1+d}}\\ \sqrt{\frac{d}{1+d}} & -\sqrt{\frac{1}{1+d}}\end{pmatrix}\begin{pmatrix}\vec{r}_1\\ -\vec{r}_2\end{pmatrix}\,, \tag{3.58}$$

again with $d\to\frac{1}{d}$, and the relations

$$\langle n_2l_2|\vec{r}_2\rangle = (-1)^{l_2}\langle n_2l_2|-\vec{r}_2\rangle\,, \tag{3.59}$$

$$\langle(EL,el)\Lambda\lambda|\vec{R},\vec{r}\rangle = (-1)^{l+L-\Lambda}\langle(el,EL)\Lambda\lambda|\vec{r},\vec{R}\rangle\,. \tag{3.60}$$

So we can again rewrite eq. (3.48)

$$\begin{aligned}
&\langle\langle n_1l_1,n_2l_2;\Lambda|NL,nl\rangle\rangle_d \\
&= \frac{1}{2\Lambda+1}\sum_\lambda\iint \mathrm{d}^3r_1\mathrm{d}^3r_2\langle(n_1l_1,n_2l_2)\Lambda\lambda|\vec{r}_1,-\vec{r}_2\rangle\langle\vec{r},\vec{R}|(nl,NL)\Lambda\lambda\rangle(-1)^{l_2+l+L-\Lambda} \\
&= \frac{1}{2\Lambda+1}\sum_\lambda\iint \mathrm{d}^3r_1\mathrm{d}^3r_2\langle(n_1l_1,n_2l_2)\Lambda\lambda|\vec{r}_1,-\vec{r}_2\rangle\langle\vec{r}_1,-\vec{r}_2|(nl,NL)\Lambda\lambda\rangle(-1)^{l_2+l+L-\Lambda} \\
&= (-1)^{2l_2+l_1-\Lambda}\langle\langle n_1l_1,n_2l_2;\Lambda|nl,NL\rangle\rangle_{\frac{1}{d}} \\
&= (-1)^{l_1-\Lambda}\langle\langle n_1l_1,n_2l_2;\Lambda|nl,NL\rangle\rangle_{\frac{1}{d}}\,.
\end{aligned} \tag{3.61}$$

Altogether, we have three symmetry relations and the fact that the harmonic oscil-

lator brackets are real. This can be summarized to:

$$\begin{aligned}
&\langle\langle n_1 l_1, n_2 l_2; \Lambda | NL, nl \rangle\rangle_d \\
&\quad = \langle\langle NL, nl; \Lambda | n_1 l_1, n_2 l_2 \rangle\rangle_d \\
&\quad = (-1)^{l_2+L} \langle\langle n_2 l_2, n_1 l_1; \Lambda | nl, NL \rangle\rangle_d \\
&\quad = (-1)^{L-\Lambda} \langle\langle n_2 l_2, n_1 l_1; \Lambda | NL, nl \rangle\rangle_{\frac{1}{d}} \\
&\quad = (-1)^{l_1-\Lambda} \langle\langle n_1 l_1, n_2 l_2; \Lambda | nl, NL \rangle\rangle_{\frac{1}{d}} \,.
\end{aligned} \tag{3.62}$$

3.3.3 Definition of harmonic oscillator brackets – alternative version

An alternative definition of the HOBs is given by

$$|(n_1 l_1, n_2 l_2) \Lambda \lambda\rangle = \sum_{NL,nl} \langle\langle nl, NL; \Lambda | n_1 l_1, n_2 l_2 \rangle\rangle_d^{\text{alt}} \, |(nl, NL) \Lambda \lambda\rangle \tag{3.63}$$

with $\langle\langle nl, NL; \Lambda | n_1 l_1, n_2 l_2 \rangle\rangle_d^{\text{alt}}$ as HOB, the superscript $^{\text{alt}}$ denotes that it is the alternative definition [21, 22]. Note the reversed order of the relative and center-of-mass quantum numbers in the bra. Additionally, the corresponding transformation matrix is now given by

$$\begin{pmatrix} \vec{R} \\ \vec{r} \end{pmatrix} = \begin{pmatrix} \sqrt{\frac{1}{1+d}} & \sqrt{\frac{d}{1+d}} \\ \sqrt{\frac{d}{1+d}} & -\sqrt{\frac{1}{1+d}} \end{pmatrix} \begin{pmatrix} \vec{r}_1 \\ \vec{r}_2 \end{pmatrix} . \tag{3.64}$$

The calculation of this HOB is equivalent to the calculation above in eq. (3.44):

$$\begin{aligned}
&\langle\langle nl, NL; \Lambda | n_1 l_1, n_2 l_2 \rangle\rangle_d^{\text{alt}} \\
&\quad = \iint \mathrm{d}^3 r_1 \mathrm{d}^3 r_2 \langle (nl, NL) \Lambda \lambda | \vec{r}_1, \vec{r}_2 \rangle \langle \vec{r}_1, \vec{r}_2 | (n_1 l_1, n_2 l_2) \Lambda \lambda \rangle \\
&\quad = \iint \mathrm{d}^3 r_1 \mathrm{d}^3 r_2 \langle (nl, NL) \Lambda \lambda | \vec{r}, \vec{R} \rangle \langle \vec{r}_1, \vec{r}_2 | (n_1 l_1, n_2 l_2) \Lambda \lambda \rangle \\
&\quad = \iint \mathrm{d}^3 r_1 \mathrm{d}^3 r_2 \big\{ \phi_{nl}(\vec{r}) \phi_{NL}(\vec{R}) \big\}^\dagger_{\Lambda\lambda} \big\{ \phi_{n_1 l_1}(\vec{r}_1) \phi_{n_2 l_2}(\vec{r}_2) \big\}_{\Lambda\lambda} \\
&\quad = \frac{1}{2\Lambda+1} \sum_\lambda \iint \mathrm{d}^3 r_1 \mathrm{d}^3 r_2 \big\{ \phi_{nl}(\vec{r}) \phi_{NL}(\vec{R}) \big\}^\dagger_{\Lambda\lambda} \big\{ \phi_{n_1 l_1}(\vec{r}_1) \phi_{n_2 l_2}(\vec{r}_2) \big\}_{\Lambda\lambda} \,.
\end{aligned} \tag{3.65}$$

3.3.4 Symmetry relations of the alternative HOBs

In the following we derive the symmetry relations for the alternative definition of HOBs from eq. (3.63). The steps are very similar to those in section 3.3.2. First we

write down the definition

$$\begin{aligned}&\langle\langle n_1 l_1, n_2 l_2; \Lambda | nl, NL\rangle\rangle_d^{\text{alt}} \\ &\quad = \frac{1}{2\Lambda+1}\sum_\lambda \iint \mathrm{d}^3 r_1 \mathrm{d}^3 r_2 \langle (n_1 l_1, n_2 l_2)\Lambda\lambda | \vec{r}_1, \vec{r}_2\rangle\langle \vec{r}, \vec{R} | (nl, NL)\Lambda\lambda\rangle \,. \end{aligned} \tag{3.66}$$

Now we see that the following transformation with the same transformation matrix as in eq. (3.64) also connects the coordinates in the correct way

$$\begin{pmatrix} -\vec{r} \\ \vec{R} \end{pmatrix} = \begin{pmatrix} \sqrt{\frac{1}{1+d}} & \sqrt{\frac{d}{1+d}} \\ \sqrt{\frac{d}{1+d}} & -\sqrt{\frac{1}{1+d}} \end{pmatrix} \begin{pmatrix} \vec{r}_2 \\ -\vec{r}_1 \end{pmatrix} , \tag{3.67}$$

meaning that $\vec{r} = \sqrt{\frac{d}{1+d}}\vec{r}_1 - \sqrt{\frac{1}{1+d}}\vec{r}_2$ and $\vec{R} = \sqrt{\frac{1}{1+d}}\vec{r}_1 + \sqrt{\frac{d}{1+d}}\vec{r}_2$ hold true. Additionally, we use the relations

$$\langle (el, EL)\Lambda\lambda | \vec{r}, \vec{R}\rangle = (-1)^l (-1)^{L+l-\Lambda} \langle (EL, el)\Lambda\lambda | \vec{R}, -\vec{r}\rangle \,, \tag{3.68}$$

$$\langle (n_1 l_1, n_2 l_2)\Lambda\lambda | \vec{r}_1, \vec{r}_2\rangle = (-1)^{l_1} (-1)^{l_1+l_2-\Lambda} \langle (n_2 l_2, n_1 l_1)\Lambda\lambda | \vec{r}_2, -\vec{r}_1\rangle \,, \tag{3.69}$$

and rewrite eq. (3.66) as

$$\begin{aligned}&\langle\langle n_1 l_1, n_2 l_2; \Lambda | nl, NL\rangle\rangle_d^{\text{alt}} \\ &\quad = \frac{1}{2\Lambda+1}\sum_\lambda \iint \mathrm{d}^3 r_1 \mathrm{d}^3 r_2 \langle (n_2 l_2, n_1 l_1)\Lambda\lambda | \vec{r}_2, -\vec{r}_1\rangle\langle \vec{R}, -\vec{r} | (NL, nl)\Lambda\lambda\rangle (-1)^{l_1+l} \\ &\quad = \frac{1}{2\Lambda+1}\sum_\lambda \iint \mathrm{d}^3 r_1 \mathrm{d}^3 r_2 \langle (n_2 l_2, n_1 l_1)\Lambda\lambda | \vec{r}_2, -\vec{r}_1\rangle\langle \vec{r}_2, -\vec{r}_1 | (NL, nl)\Lambda\lambda\rangle (-1)^{l_1+l} \\ &\quad = (-1)^{l_1+l} \langle\langle n_2 l_2, n_1 l_1; \Lambda | NL, nl\rangle\rangle_d^{\text{alt}} \,. \end{aligned} \tag{3.70}$$

Here we used eq. (3.46) that is also valid for the alternative HOB definition. For the next symmetry relation we investigate the following transformation matrix with the substitution $d \to \frac{1}{d}$

$$\begin{pmatrix} \vec{R} \\ -\vec{r} \end{pmatrix} = \begin{pmatrix} \sqrt{\frac{d}{1+d}} & \sqrt{\frac{1}{1+d}} \\ \sqrt{\frac{1}{1+d}} & -\sqrt{\frac{d}{1+d}} \end{pmatrix} \begin{pmatrix} \vec{r}_2 \\ \vec{r}_1 \end{pmatrix} , \tag{3.71}$$

and we use the relations

$$\langle nl | \vec{r}\rangle = (-1)^l \langle nl | -\vec{r}\rangle \tag{3.72}$$

$$\langle (n_1 l_1, n_2 l_2)\Lambda\lambda | \vec{r}_1, \vec{r}_2\rangle = (-1)^{l_1+l_2-\Lambda} \langle (n_2 l_2, n_1 l_1)\Lambda\lambda | \vec{r}_2, \vec{r}_1\rangle \,. \tag{3.73}$$

We can then rewrite eq. (3.66) into

$$\begin{aligned}
&\langle\langle n_1 l_1, n_2 l_2; \Lambda | nl, NL\rangle\rangle_d^{\text{alt}} \\
&\quad = \frac{1}{2\Lambda+1}\sum_\lambda \iint \mathrm{d}^3 r_1 \mathrm{d}^3 r_2 \langle (n_2 l_2, n_1 l_1)\Lambda\lambda | \vec{r}_2, \vec{r}_1\rangle \langle -\vec{r}, \vec{R} | (nl, NL)\Lambda\lambda\rangle (-1)^{l_1+l_2-\Lambda}(-1)^l \\
&\quad = \frac{1}{2\Lambda+1}\sum_\lambda \iint \mathrm{d}^3 r_1 \mathrm{d}^3 r_2 \langle (n_2 l_2, n_1 l_1)\Lambda\lambda | \vec{r}_2, \vec{r}_1\rangle \langle \vec{r}_2, \vec{r}_1 | (nl, NL)\Lambda\lambda\rangle (-1)^{l_1+l_2-\Lambda}(-1)^l \\
&\quad = (-1)^{2l+L-\Lambda}\langle\langle n_2 l_2, n_1 l_1; \Lambda | nl, NL\rangle\rangle_{\frac{1}{d}}^{\text{alt}} \\
&\quad = (-1)^{L-\Lambda}\langle\langle n_2 l_2, n_1 l_1; \Lambda | nl, NL\rangle\rangle_{\frac{1}{d}}^{\text{alt}}
\end{aligned} \tag{3.74}$$

Finally, for the last symmetry relation we use the transformation matrix

$$\begin{pmatrix} \vec{r} \\ \vec{R} \end{pmatrix} = \begin{pmatrix} \sqrt{\frac{d}{1+d}} & \sqrt{\frac{1}{1+d}} \\ \sqrt{\frac{1}{1+d}} & -\sqrt{\frac{d}{1+d}} \end{pmatrix} \begin{pmatrix} \vec{r}_1 \\ -\vec{r}_2 \end{pmatrix}, \tag{3.75}$$

where also $d \to \frac{1}{d}$ has been used. The relations we need here are given by

$$\langle (nl, NL)\Lambda\lambda | \vec{r}, \vec{R}\rangle = (-1)^{L+l-\Lambda}\langle (NL, nl)\Lambda\lambda | \vec{R}, \vec{r}\rangle \tag{3.76}$$

$$\langle n_2 l_2 | \vec{r}_2\rangle = (-1)^{l_2}\langle n_2 l_2 | -\vec{r}_2\rangle\,, \tag{3.77}$$

and we rewrite eq. (3.66) as

$$\begin{aligned}
&\langle\langle n_1 l_1, e_2 l_2; \Lambda | nl, NL\rangle\rangle_d^{\text{alt}} \\
&\quad = \frac{1}{2\Lambda+1}\sum_\lambda \iint \mathrm{d}^3 r_1 \mathrm{d}^3 r_2 \langle (n_1 l_1, n_2 l_2)\Lambda\lambda | \vec{r}_1, -\vec{r}_2\rangle \langle \vec{R}, \vec{r} | (NL, nl)\Lambda\lambda\rangle (-1)^{L+l-\Lambda+l_2} \\
&\quad = (-1)^{2l_2+l_1-\Lambda}\langle\langle n_1 l_1, n_2 l_2; \Lambda | NL, nl\rangle\rangle_{\frac{1}{d}}^{\text{alt}} \\
&\quad = (-1)^{l_1-\Lambda}\langle\langle n_1 l_1, n_2 l_2; \Lambda | NL, nl\rangle\rangle_{\frac{1}{d}}^{\text{alt}}\,.
\end{aligned} \tag{3.78}$$

So we derived the analogous relations as in section 3.3.2. The alternative HOBs are real as well, so we have the following summarized relations

$$\boxed{\begin{aligned}
&\langle\langle n_1 l_1, n_2 l_2; \Lambda | nl, NL\rangle\rangle_d^{\text{alt}} \\
&\quad = \langle\langle nl, NL; \Lambda | n_1 l_1, n_2 l_2\rangle\rangle_d^{\text{alt}} \\
&\quad = (-1)^{l_1+l}\langle\langle n_2 l_2, n_1 l_1; \Lambda | NL, nl\rangle\rangle_d^{\text{alt}} \\
&\quad = (-1)^{L-\Lambda}\langle\langle n_2 l_2, n_1 l_1; \Lambda | nl, NL\rangle\rangle_{\frac{1}{d}}^{\text{alt}} \\
&\quad = (-1)^{l_1-\Lambda}\langle\langle n_1 l_1, n_2 l_2; \Lambda | NL, nl\rangle\rangle_{\frac{1}{d}}^{\text{alt}}\,.
\end{aligned}} \tag{3.79}$$

These and more symmetry relations can be found in [22].

3.3.5 Connection between our and the alternative definition of the HOB

After we derived the symmetry relations for the two conventions of the HOBs in section 3.3.2 and 3.3.4 respectively, we want to construct the connection between the two definitions. We remark two differences between the two definitions

- Coupling order: $(l\,L) \leftrightarrow (L\,l)$ which will lead to a phase factor.
- Transformation matrix: Replace $d \to \frac{1}{d}$ in matrix (3.64) compared to (3.43).

Because the left-hand sides of eqs. (3.42) and (3.63) are equal we can derive a relation between the two definitions. If we change the coupling order in the alternative definition we find

$$|(n_1l_1, n_2l_2)\Lambda\lambda\rangle \overset{(3.42)}{=} \sum_{NL,nl} \langle\langle NL, nl; \Lambda | n_1l_1, n_2l_2\rangle\rangle_{\frac{1}{d}} \, |(NL, nl)\Lambda\lambda\rangle \,, \tag{3.80}$$

$$\overset{(3.63)}{=} \sum_{NL,nl} \langle\langle nl, NL; \Lambda | n_1l_1, n_2l_2\rangle\rangle_{d}^{\text{alt}} \, |(nl, NL)\Lambda\lambda\rangle \tag{3.81}$$

$$= \sum_{NL,nl} \langle\langle nl, NL; \Lambda | n_1l_1, n_2l_2\rangle\rangle_{d}^{\text{alt}} \, (-1)^{l+L-\Lambda} |(NL, nl)\Lambda\lambda\rangle \,. \tag{3.82}$$

If we now match coefficients of (3.80) and (3.81) we find

$$\langle\langle NL, nl; \Lambda | n_1l_1, n_2l_2\rangle\rangle_{\frac{1}{d}} = (-1)^{l+L-\Lambda} \langle\langle nl, NL; \Lambda | n_1l_1, n_2l_2\rangle\rangle_{d}^{\text{alt}} \,. \tag{3.83}$$

Now we are able to switch between our definition and the alternative definition of the HOBs. This is useful when we compare our derived formulas against results published using the alternative definitions.

3.3.6 Explicit formula for calculation of the HOBs

Finally, we present the explicit formula for the harmonic oscillator brackets that conforms with our definition [20]

$$
\begin{aligned}
&\langle\langle NL, nl; \Lambda | n_1 l_1, n_2 l_2 \rangle\rangle_d \\
&\quad = i^{-(l_1+l_2+L+l)}\, 2^{-(l_1+l_2+L+l)/4} \\
&\quad \times \sqrt{n_1! n_2! N! n! [2(n_1+l_1)+1]!! [2(n_2+l_2)+1]!! [2(N+L)+1]!! [2(n+l)+1]!!} \\
&\quad \times \sum_{abcdl_a l_b l_c l_d} (-1)^{l_a+l_b+l_c} 2^{(l_a+l_b+l_c+l_d)/2} d^{(2a+l_a+2d+l_d)/2} (1+d)^{-(2a+l_a+2b+l_b+2c+l_c+2d+l_d)/2} \\
&\quad \times \frac{[(2l_a+1)(2l_b+1)(2l_c+1)(2l_d+1)]}{a! b! c! d! [2(a+l_a)+1]!! [2(b+l_b)+1]!! [2(c+l_c)+1]!! [2(d+l_d)+1]!!} \\
&\quad \times \begin{Bmatrix} l_a & l_b & l_1 \\ l_c & l_d & l_2 \\ L & l & \Lambda \end{Bmatrix} \left(\begin{matrix} l_a\, l_c \\ 0\ 0 \end{matrix} \middle| \begin{matrix} L \\ 0 \end{matrix} \right) \left(\begin{matrix} l_b\, l_d \\ 0\ 0 \end{matrix} \middle| \begin{matrix} l \\ 0 \end{matrix} \right) \left(\begin{matrix} l_a\, l_b \\ 0\ 0 \end{matrix} \middle| \begin{matrix} l_1 \\ 0 \end{matrix} \right) \left(\begin{matrix} l_c\, l_d \\ 0\ 0 \end{matrix} \middle| \begin{matrix} l_2 \\ 0 \end{matrix} \right) .
\end{aligned}
\tag{3.84}
$$

Because of its symmetric appearance we can rewrite it in the form

$$
\begin{aligned}
&\langle\langle NL, nl; \Lambda | n_1 l_1, n_2 l_2 \rangle\rangle_d \\
&\quad = d^{(e_1-e)/2} (1+d)^{-(e_1+e_2)/2} \sum_{e_a l_a e_b l_b e_c l_c e_d l_d} (-d)^{e_d} \begin{Bmatrix} l_a & l_b & l_1 \\ l_c & l_d & l_2 \\ L & l & \Lambda \end{Bmatrix} \\
&\quad \times G(e_1 l_1; e_a l_a, e_b l_b)\, G(e_2 l_2; e_c l_c, e_d l_d)\, G(EL; e_a l_a, e_c l_c)\, G(el; e_b l_b, e_d l_d) ,
\end{aligned}
\tag{3.85}
$$

which is more convenient for implementation. Here we used $E = 2N+L$, $e = 2n+l$, $e_1 = 2n_1 + l_1$ and $e_2 = 2n_2 + l_2$. Moreover, the G-coefficients are given by

$$
\begin{aligned}
G(e_1 l_1; e_a l_a, e_b l_b) = &\sqrt{(2l_a+1)(2l_b+1)} \left(\begin{matrix} l_a\, l_b \\ 0\ 0 \end{matrix} \middle| \begin{matrix} l_1 \\ 0 \end{matrix} \right) \\
&\times \left[\binom{e_1 - l_1}{e_a - l_a; e_b - l_b} \binom{e_1 + l_1 + 1}{e_a + l_a + 1; e_b + l_b + 1} \right]^{1/2} ,
\end{aligned}
\tag{3.86}
$$

with trinomial coefficients

$$
\binom{x}{y;\ z} \equiv \frac{(x)!!}{(y)!!\ (z)!!} .
\tag{3.87}
$$

3.4 Antisymmetrizer in basis representation

In this section we present a technique to derive a translationally invariant three-nucleon basis that is antisymmetrized with respect to particle exchange. Moreover, we derive an explicit form for the projector on the antisymmetric part of the Hilbert space. We will need this technique in section 4 to guarantee the antisymmetrization of the bra and ket states of the three-nucleon interaction matrix elements.

The typical approach when one is interested in antisymmetrizing a given state, is to project this state onto the antisymmetric subspace of the Hilbert space using the antisymmetrizer $\mathcal{A}$:

$$|abc\rangle \xrightarrow{\text{projection}} \sqrt{3!}\mathcal{A}|abc\rangle = |abc\rangle_a \,, \tag{3.88}$$

where $|abc\rangle$ denotes an arbitrary three-particle state and $\mathcal{A} = \frac{1}{A!}\sum_{\mathcal{P}} \text{sgn}(\mathcal{P})\mathcal{P}$ the antisymmetrizer, including the permutation operator $\mathcal{P}$. The subscript $_a$ on the right hand side of eq. (3.88) indicates that the state is antisymmetrized. Typically, the permutation is explicitly performed, ending up with

$$|abc\rangle_a = \frac{1}{\sqrt{3!}}(|abc\rangle + |cab\rangle + |bca\rangle - |bac\rangle - |cba\rangle - |acb\rangle) \,. \tag{3.89}$$

We will now discuss an alternative and in some sense more elegant way to access an antisymmetrized three-body basis. Therefore, we calculate the matrix elements of the antisymmetrizer in the basis

$$|\alpha\rangle = |[(n_{12}l_{12}(\vec{\xi}_1), s_{ab})j_{12}, (n_3 l_3(\vec{\xi}_2), s_c)j_3]JM_J, (t_{ab}t_c)TM_T\rangle \,. \tag{3.90}$$

The quantum numbers n_{12}, l_{12}, n_3 and l_3 denote harmonic oscillator quantum numbers with respect to Jacobi coordinates $\vec{\xi}_1$ and $\vec{\xi}_2$ as described in section 3.2. For brevity we omit the explicit reminder on Jacobi coordinates by showing the dependencies on $\vec{\xi}_1, \vec{\xi}_2$ in the following. If necessary we will come back to this notation. Moreover, j_{12}, s_{ab} and t_{ab} are angular momentum, spin and isospin quantum numbers corresponding to nucleons 1 and 2. Here, s_{ab} is the quantum number of the coupled spins of the first nucleon $\vec{s}_a$ and the second nucleon $\vec{s}_b$ and analogously for the isospin t_{ab} quantum number. The quantum number l_3 is the orbital angular momentum of the third nucleon with respect to the center of mass of nucleons 1 and 2. The spin, isospin and angular momentum of particle 3 is given by $\vec{s}_c, \vec{t}_c$ and $\vec{j}_3$ respectively. Finally, J and T are the total angular momentum and isospin quantum numbers of the states, respectively. We will refer to the states $|\alpha\rangle$ as Jacobi

states.

In addition, the states $|\alpha\rangle$ are antisymmetrized with respect to particle exchange $1 \leftrightarrow 2$ only. This is assured by taking only states that obey $(-1)^{l_{12}+s_{ab}+t_{ab}} = -1$. It is not antisymmetrized for particle exchange $1 \leftrightarrow 3$ or $2 \leftrightarrow 3$.

Once the matrix representation of $\mathcal{A}$ is known, we can solve its eigenvalue problem to get access to the fully antisymmetrized states $|EJTi\rangle$ which are eigenstates of the antisymmetrizer $\mathcal{A}$. Because $\mathcal{A}\mathcal{A} = \mathcal{A}$ holds true due to the projection property of $\mathcal{A}$, we will find two eigenspaces. One corresponding to eigenvalue 1, spanned by the fully antisymmetrized states, and one corresponding to eigenvalue 0, made up of spurious states that we are not interested in. At the end we have the antisymmetric three-particle eigenstates $|EJTi\rangle$ as expansion in the basis states $|\alpha\rangle$

$$|EJTi\rangle = \sum_{\alpha} \langle\alpha|EJTi\rangle|\alpha\rangle = \sum_{\alpha} c_{\alpha,i}|\alpha\rangle \,. \tag{3.91}$$

The expansion coefficients $c_{\alpha,i}$ are called coefficients of fractional parentage (CFPs). The quantum number

$$E = 2n_{12} + l_{12} + 2n_3 + l_3 \tag{3.92}$$

corresponds to the total harmonic oscillator energy of the three-nucleon state. The i is no physical quantum number, it just labels states with same E, J and T in an arbitrary ordering.

Having the fully antisymmetrized three-particle relative states $|EJTi\rangle$ we can explicitly construct a projector on the antisymmetric relative Hilbert space by using the dyadic product

$$\mathcal{A}_{rel} = \sum_{E,J,M_J} \sum_{T,M_T} \sum_{i} |EJM_JTM_Ti\rangle\langle EJM_JTM_Ti| \,. \tag{3.93}$$

We can extend this to an antisymmetrizer of the complete Hilbert space simply by multiplying with a dyadic product of center-of-mass states

$$\begin{aligned}\mathcal{A} &= \sum_{\substack{n_{cm},l_{cm}\\ m_{cm}}} |n_{cm}l_{cm}m_{cm}\rangle\langle n_{cm}l_{cm}m_{cm}| \otimes \sum_{E,J,M_J} \sum_{T,M_T} \sum_{i} |EJM_JTM_Ti\rangle\langle EJM_JTM_Ti| \\ &\equiv \sum_{\substack{n_{cm},l_{cm}\\ m_{cm}}} \sum_{E,J,M_J} \sum_{T,M_T} \sum_{i} |n_{cm}l_{cm}m_{cm}\rangle \otimes |EJM_JTM_Ti\rangle\langle n_{cm}l_{cm}m_{cm}| \otimes \langle EJM_JTM_Ti| \,,\end{aligned} \tag{3.94}$$

since the center-of-mass states are invariant with respect to particle permutations.

After explaining the basic idea of the antisymmetrization procedure, we now

derive the matrix representation of $\mathcal{A}$ in detail. We start with writing the antisymmetrizer for a three-particle system in terms of transposition operators simply by rewriting the permutation operators

$$\mathcal{A} = \frac{1}{6}\left(\mathcal{P}_{123} + \mathcal{P}_{312} + \mathcal{P}_{231} - \mathcal{P}_{321} - \mathcal{P}_{132} - \mathcal{P}_{213}\right) \tag{3.95}$$

$$= \frac{1}{6}\left(\mathbb{1} + \mathcal{T}_{23}\mathcal{T}_{12} + \mathcal{T}_{13}\mathcal{T}_{12} - \mathcal{T}_{13} - \mathcal{T}_{23} - \mathcal{T}_{12}\right) , \tag{3.96}$$

where we used $\mathcal{P}_{123} = \mathbb{1}$. Next we use $\mathcal{T}_{13} = \mathcal{T}_{12}\mathcal{T}_{23}\mathcal{T}_{12}$ as well as $\mathcal{T}_{12} = -1$, since we work with states (3.90) that are antisymmetric for particle exchange $1 \leftrightarrow 2$. This yields

$$\mathcal{A} = \frac{1}{6}\left(2 - 2\mathcal{T}_{23} - \mathcal{T}_{12}\mathcal{T}_{23}\mathcal{T}_{12} - \mathcal{T}_{12}\mathcal{T}_{23}\mathcal{T}_{12}\right) \tag{3.97}$$

$$= \frac{1}{6}\left(2 - 4\mathcal{T}_{23}\right) \tag{3.98}$$

$$= \frac{1}{3}\left(1 - 2\mathcal{T}_{23}\right) . \tag{3.99}$$

If we now calculate matrix elements of the antisymmetrizer in the states $|\alpha\rangle$ only the matrix elements of the transposition operator $\mathcal{T}_{23}$ need further attention.

For calculating matrix elements of $\mathcal{T}_{23}$, it is convenient to cast states (3.90) into the form

$$|(n_{12}l_{12}, n_3l_3)LM_L\rangle \otimes |(s_{ab}, s_c)SM_S\rangle \otimes |(t_{ab}, t_c)TM_T\rangle . \tag{3.100}$$

This has the advantage that we can investigate the action of the transposition operator on the spatial, spin and isospin part of the state separately. Furthermore, we will have to employ a HOB which means that the orbital angular momenta have to be coupled anyway. The transformation of states (3.90) into states (3.100) needs two subsequent steps: First we have a recoupling of four angular momenta

$$|[(n_{12}l_{12}, s_{ab})j_{12}, (n_3l_3, s_c)j_3]J\rangle \longrightarrow |[(n_{12}l_{12}, n_3l_3)L, (s_{ab}, s_c)S]J\rangle , \tag{3.101}$$

which will introduce a 9j-symbol according to eq. (3.20). Second we have to break

up the (LS)-coupling using a Clebsch-Gordan coefficient. We arrive at

$$
\begin{aligned}
&|[(n_{12}l_{12}, s_{ab})j_{12}, (n_3 l_3, s_c)j_3]JM_J, (t_{ab}t_c)TM_T\rangle \\
&= \sum_{L,M_L}\sum_{S,M_S} \hat{j}_{12}\hat{j}_3\hat{L}\hat{S} \begin{Bmatrix} l_{12} & s_{ab} & j_{12} \\ l_3 & s_c & j_3 \\ L & S & J \end{Bmatrix} \left(\begin{array}{cc|c} L & S & J \\ M_L & M_S & M_J \end{array}\right) \\
&\qquad \times |(n_{12}l_{12}, n_3 l_3)LM_L, (s_{ab}, s_c)SM_S, (t_{ab}t_c)TM_T\rangle \,.
\end{aligned} \tag{3.102}
$$

The matrix element of $\mathcal{T}_{23}$ then reads

$$
\begin{aligned}
&\langle[(n'_{12}l'_{12}, s'_{ab})j'_{12}, (n'_3 l'_3, s_c)j'_3]J'M'_J, (t'_{ab}t_c)T'M'_T| \\
&\qquad\qquad \times \mathcal{T}_{23}|[(n_{12}l_{12}, s_{ab})j_{12}, (n_3 l_3, s_c)j_3]JM_J, (t_{ab}t_c)TM_T\rangle \\
&= \sum_{L',S'}\sum_{M'_L,M'_S}\sum_{L,S}\sum_{M_L,M_S} \hat{j}'_{12}\hat{j}'_3\hat{L}'\hat{S}'\hat{j}_{12}\hat{j}_3\hat{L}\hat{S} \\
&\quad \times \begin{Bmatrix} l_{12} & s_{ab} & j_{12} \\ l_3 & s_c & j_3 \\ L & S & J \end{Bmatrix} \begin{Bmatrix} l'_{12} & s'_{ab} & j'_{12} \\ l'_3 & s_c & j'_3 \\ L' & S' & J' \end{Bmatrix} \left(\begin{array}{cc|c} L & S & J \\ M_L & M_S & M_J \end{array}\right) \left(\begin{array}{cc|c} L' & S' & J' \\ M'_L & M'_S & M'_J \end{array}\right) \\
&\quad \times \langle(n'_{12}l'_{12}, n'_3 l'_3)L'M'_L|\mathcal{T}_{23}|(n_{12}l_{12}, n_3 l_3)LM_L\rangle \\
&\quad \times \langle(s'_{ab}, s_c)S'M'_S|\mathcal{T}_{23}|(s_{ab}, s_c)SM_S\rangle \,\langle(t'_{ab}, t_c)T'M'_T|\mathcal{T}_{23}|(t_{ab}, t_c)TM_T\rangle \,.
\end{aligned} \tag{3.103}
$$

We note that the structure of the spin and isospin matrix element is identical, so it is sufficient to work out one of them. We investigate the isospin matrix element

$$
\langle(t'_{ab}, t_c)T'M'_T|\mathcal{T}_{23}|(t_{ab}, t_c)TM_T\rangle \,, \tag{3.104}
$$

by considering the action of the transposition operator on the ket

$$
\begin{aligned}
&\mathcal{T}_{23}|(t_{ab}, t_c)TM_T\rangle \\
&\quad = \sum_{m_{t_a}m_{t_b}m_{t_c}} \left(\begin{array}{cc|c} t_a & t_b & t_{ab} \\ m_{t_a} & m_{t_b} & m_{t_{ab}} \end{array}\right) \left(\begin{array}{cc|c} t_{ab} & t_c & T \\ m_{t_{ab}} & m_{t_c} & M_T \end{array}\right) \mathcal{T}_{23}|t_a m_{t_a}, t_b m_{t_b}, t_c m_{t_c}\rangle \qquad (3.105) \\
&\quad = \sum_{m_{t_a}m_{t_b}m_{t_c}} \left(\begin{array}{cc|c} t_a & t_b & t_{ab} \\ m_{t_a} & m_{t_b} & m_{t_{ab}} \end{array}\right) \left(\begin{array}{cc|c} t_{ab} & t_c & T \\ m_{t_{ab}} & m_{t_c} & M_T \end{array}\right) |t_a m_{t_a}, t_c m_{t_c}, t_b m_{t_b}\rangle \,. \qquad (3.106)
\end{aligned}
$$

Now particle 3 is in the state $|t_b m_{t_b}\rangle$ and couples its isospin with particle 1 to the same quantum number t_{ab} as before. This is the same situation as if we rewrite the formula with exchanged quantum numbers $t_b \leftrightarrow t_c$

$$
\mathcal{T}_{23}|[(t_a, t_b)t_{ab}, t_c]TM_T\rangle = |[(t_a, t_c)t_{ab}, t_b]TM_T\rangle \,. \tag{3.107}
$$

Thus the isospin matrix element is given by

$$\langle[(t_a,t_b)t_{ab},t_c]TM_T|[(t_a,t_c)t'_{ab},t_c]T'M'_T\rangle = \delta_{T,T'}\,\delta_{M_T,M'_T}\,\hat{t}'_{ab}\hat{t}_{ab}(-1)^{1+t'_{ab}+t_{ab}}\begin{Bmatrix} t_a & t_b & t'_{ab} \\ t_c & T & t_{ab}\end{Bmatrix}, \tag{3.108}$$

where we introduced a 6j-symbol, since we have a recoupling of three isospins as in (3.17).

Analogously, we can construct the spin matrix element

$$\langle(s'_{ab},s'_c)S'M'_S|\mathcal{T}_{23}|(s_{ab},s_c)SM_S\rangle = \delta_{S,S'}\,\delta_{M_S,M'_S}\,\hat{s}'_{ab}\hat{s}_{ab}(-1)^{1+s'_{ab}+s_{ab}}\begin{Bmatrix} s_a & s_b & s'_{ab} \\ s_c & T & s_{ab}\end{Bmatrix}. \tag{3.109}$$

Finally, we have to calculate the spatial matrix element

$$\langle(n'_{12}l'_{12},n'_3l'_3)L'M'_L|\mathcal{T}_{23}|(n_{12}l_{12},n_3l_3)LM_L\rangle\,. \tag{3.110}$$

Again we investigate the action of $\mathcal{T}_{23}$ on the ket

$$\mathcal{T}_{23}|(n_{12}l_{12},n_3l_3)LM_L\rangle\,. \tag{3.111}$$

If particles 2 and 3 are exchanged, the operator definitions that correspond to the quantum numbers $l_{12}(\vec{\xi}_1)$ and $l_3(\vec{\xi}_2)$ change. In other words, the Jacobi coordinate definitions are different because the single-particle coordinates 2 and 3 are exchanged. The new coordinates read

$$\vec{\xi}'_1 = \sqrt{\frac{1}{2}}\,[\vec{r}_a - \vec{r}_c]\,, \tag{3.112}$$

$$\vec{\xi}'_2 = \sqrt{\frac{2}{3}}\left[\frac{1}{2}(\vec{r}_a+\vec{r}_c) - \vec{r}_b\right]. \tag{3.113}$$

We connect the primed coordinates with the original ones by an orthogonal transformation with parameter $d=\frac{1}{3}$. Using eq. (3.43) we have

$$\begin{pmatrix}\vec{\xi}'_1\\ \vec{\xi}'_2\end{pmatrix} = \begin{pmatrix}\sqrt{\frac{1}{4}} & \sqrt{\frac{3}{4}}\\ \sqrt{\frac{3}{4}} & -\sqrt{\frac{1}{4}}\end{pmatrix}\begin{pmatrix}\vec{\xi}_1\\ \vec{\xi}_2\end{pmatrix}. \tag{3.114}$$

with the unprimed coordinates defined in eq. (3.31). Therefore, we can expand the states depending on the primed coordinates $\{\vec{\xi}'_1,\vec{\xi}'_2\}$ in states depending on

the original Jacobi coordinates by using a HOB

$$
\begin{aligned}
&|(n_{12}l_{12}(\vec{\xi}_1'), n_3l_3(\vec{\xi}_2'))LM_L\rangle \\
&\quad = \sum_{\tilde{n}_{12}\tilde{l}_{12}} \sum_{\tilde{n}_3\tilde{l}_3} \langle\langle \tilde{n}_{12}\tilde{l}_{12}, \tilde{n}_3\tilde{l}_3; L|n_{12}l_{12}, n_3l_3\rangle\rangle_{\frac{1}{3}} \qquad (3.115)\\
&\qquad\qquad \times\delta_{2\tilde{n}_{12}+\tilde{l}_{12}+2\tilde{n}_3+\tilde{l}_3,2n_{12}+l_{12}+2n_3+l_3}\, |(\tilde{n}_{12}\tilde{l}_{12}(\vec{\xi}_1), \tilde{n}_3\tilde{l}_3(\vec{\xi}_2))LM_L\rangle\,.
\end{aligned}
$$

The spatial matrix element of the transposition operator follows as

$$
\begin{aligned}
&\langle (n_{12}'l_{12}', n_3'l_3')L'M_L'|\mathcal{T}_{23}|(n_{12}l_{12}, n_3l_3)LM_L\rangle \\
&\quad = \delta_{L',L}\,\delta_{M_L',M_L}\,\delta_{2n_{12}'+l_{12}'+2n_3'+l_3',2n_{12}+l_{12}+2n_3+l_3}\,\langle\langle n_{12}'l_{12}', n_3'l_3'; L|n_{12}l_{12}, n_3l_3\rangle\rangle_{\frac{1}{3}} \qquad (3.116)
\end{aligned}
$$

Combining the results in eq. (3.108), (3.109) and (3.116) leads to the total matrix element of the transposition operator

$$
\begin{aligned}
&\langle [(n_{12}'l_{12}', s_{ab}')j_{12}', (n_3'l_3', s_c)j_3']J'M_J', (t_{ab}'t_c)T'M_T'| \\
&\qquad\qquad \times \mathcal{T}_{23}|[(n_{12}l_{12}, s_{ab})j_{12}, (n_3l_3, s_c)j_3]JM_J, (t_{ab}t_c)TM_T\rangle \\
&= \sum_{L',S'} \sum_{M_L',M_S'} \sum_{L,S} \sum_{M_L,M_S} \hat{j}_{12}'\hat{j}_3'\hat{L}'\hat{S}'\hat{j}_{12}\hat{j}_3\hat{L}\hat{S}\hat{s}_{ab}'\hat{s}_{ab}\hat{t}'_{ab}\hat{t}_{ab} \\
&\quad \times \begin{Bmatrix} l_{12} & s_{ab} & j_{12} \\ l_3 & s_c & j_3 \\ L & S & J \end{Bmatrix} \begin{Bmatrix} l_{12}' & s_{ab}' & j_{12}' \\ l_3' & s_c & j_3' \\ L' & S' & J' \end{Bmatrix} \left(\begin{array}{cc|c} L & S & J \\ M_L & M_S & M_J \end{array}\right) \left(\begin{array}{cc|c} L' & S' & J' \\ M_L' & M_S' & M_J' \end{array}\right) \\
&\quad \times (-1)^{1+t_{ab}'+t_{ab}}(-1)^{1+s_{ab}'+s_{ab}} \begin{Bmatrix} t_a & t_b & t_{ab}' \\ t_c & T & t_{ab} \end{Bmatrix} \begin{Bmatrix} s_a & s_b & s_{ab}' \\ s_c & S & s_{ab} \end{Bmatrix} \\
&\quad \times \delta_{T,T'}\,\delta_{M_T,M_T'}\,\delta_{S,S'}\,\delta_{M_S,M_S'}\,\delta_{L',L}\,\delta_{M_L',M_L} \\
&\quad \times \delta_{2n_{12}+'l_{12}'+2n_3'+l_3',2n_{12}+l_{12}+2n_3+l_3}\,\langle\langle n_{12}'l_{12}', n_3'l_3'; L|n_{12}l_{12}, n_3l_3\rangle\rangle_{\frac{1}{3}}\,. \qquad (3.117)
\end{aligned}
$$

Now we can eliminate the summations over L', M_L', S', M_S' using the Kronecker deltas and the orthogonality relation

$$
\sum_{M_L,M_S} \left(\begin{array}{cc|c} L & S & J' \\ M_L & M_S & M_J' \end{array}\right) \left(\begin{array}{cc|c} L & S & J \\ M_L & M_S & M_J \end{array}\right) = \delta_{J',J}\,\delta_{M_J',M_J} \qquad (3.118)
$$

to arrive at the final result

$$\begin{aligned}
&\langle[(n'_{12}l'_{12}, s'_{ab})j'_{12}, (n'_3 l'_3, s_c)j'_3]J'M'_J, (t'_{ab}t_c)T'M'_T| \\
&\qquad\qquad \times \mathcal{T}_{23}|[(n_{12}l_{12}, s_{ab})j_{12}, (n_3 l_3, s_c)j_3]JM_J, (t_{ab}t_c)TM_T\rangle \\
&= \delta_{T,T'}\,\delta_{M_T,M'_T}\,\delta_{J',J}\,\delta_{M'_J,M_J}\,\delta_{2n_{12}+'l'_{12}+2n'_3+l'_3,2n_{12}+l_{12}+2n_3+l_3} \\
&\quad \times \sum_{L,S} \hat{L}^2\,\hat{S}^2\,\hat{j}'_{12}\,\hat{j}'_3\,\hat{j}_{12}\,\hat{j}_3\hat{s}'_{ab}\,\hat{s}_{ab}\,\hat{t}'_{ab}\,\hat{t}_{ab} \\
&\quad \times \begin{Bmatrix} l_{12} & s_{ab} & j_{12} \\ l_3 & s_c & j_3 \\ L & S & J \end{Bmatrix} \begin{Bmatrix} l'_{12} & s'_{ab} & j'_{12} \\ l'_3 & s_c & j'_3 \\ L' & S' & J' \end{Bmatrix} (-1)^{1+t'_{ab}+t_{ab}} (-1)^{1+s'_{ab}+s_{ab}} \begin{Bmatrix} t_a & t_b & t'_{ab} \\ t_c & T & t_{ab} \end{Bmatrix} \begin{Bmatrix} s_a & s_b & s'_{ab} \\ s_c & S & s_{ab} \end{Bmatrix} \\
&\quad \times \langle\langle n'_{12}l'_{12}, n'_3 l'_3; L|n_{12}l_{12}, n_3 l_3\rangle\rangle_{\frac{1}{3}}\,.
\end{aligned} \tag{3.119}$$

As we can see, the matrix elements of $\mathcal{T}_{23}$ are diagonal in the projection quantum numbers M_J, M_T and furthermore do not depend on them at all. Therefore, it is sufficient to use the states $|[(n_{12}l_{12}, s_{ab})j_{12}, (n_3 l_3, s_c)j_3]J, (t_{ab}t_c)T\rangle$ without projection quantum numbers M_J, M_T for the basis representation. This reduces the number of matrix elements significantly. Furthermore, it helps in practical computations, especially when the interaction matrix elements do not depend on the projection quantum numbers either, as it will be the case for the transformation in section 4.

In addition, we recognize that the antisymmetrizer is diagonal in the quantum numbers T, J and $E = 2n_{12} + l_{12} + 2n_3 + l_3$

$$\langle\alpha'|\mathcal{A}|\alpha\rangle = \begin{pmatrix} \boxed{TJE} & & & \\ & \boxed{TJE'} & & \\ & & \ddots & \\ & & & \boxed{} \end{pmatrix}. \tag{3.120}$$

This allows to solve the eigenvalue problem as well as the calculation of the trace for each block separately, which reduces the computational effort. As mentioned above, the physical states must have eigenvalue 1. Since there will be many physical states even in one TJE-block, the eigenspace is degenerate. Therefore, we introduce an additional "quantum number" i that labels the different degenerate states that correspond to a given TJE-block. The value of i is then determined by the eigenvalue solver we use. One crucial detail is that the ordering of the eigenstates as well as the eigenstates $|EJTi\rangle$ themselves are not unique since any or-

thogonal transformation of the degenerate eigenstates will build an eigenbasis, too. Only the total number of eigenstates $|EJTi\rangle$ which is given by the trace of the antisymmetrizer stays the same. Consequently, different numerical eigenvalue-problem solvers will produce different orderings and different eigenstates of the totally antisymmetrized basis states. Once we fixed these eigenstates and their ordering in our calculations, we have to stick to it for the rest of the calculation.

SECTION 4

Three-body Jacobi matrix element transformation into the m-scheme

As already mentioned at the end of section 2, the starting point of our investigation of the N2LO three-nucleon interaction are matrix elements with respect to antisymmetrized three-particle Jacobi states $|EJM_JTM_Ti\rangle$. Since m-scheme matrix elements are needed in our many-body calculations, we have to transform the given matrix elements into the m-scheme .

To investigate the transformation, we assume a charge invariant and rotational invariant interaction, meaning that the interaction does not depend on the M_T or M_J quantum numbers. Moreover, the interaction does not change the total relative angular momentum $\vec{\boldsymbol{J}}$ and the total isospin $\vec{\boldsymbol{T}}$ of the three nucleons. This summarizes to

$$\begin{aligned}&\langle EJM_JTM_Ti|\mathbf{V}^{NNN}|E'J'M'_JT'M'_Ti'\rangle \\ &\quad = \langle EJTi|\mathbf{V}^{NNN}|E'JTi'\rangle\ \delta_{J,J'}\,\delta_{M_J,M'_J}\,\delta_{T,T'}\,\delta_{M_T,M'_T}\ . \end{aligned} \tag{4.1}$$

Furthermore, we denote the interaction operator throughout this section as $\mathbf{V}^{NNN}$, indicating a three-nucleon interaction. Nevertheless, all formulas are valid also for two-plus-three-body interactions as long as their matrix elements are given in the basis $|EJTi\rangle$.

In subsection 4.1 we deal with the transformation into m-scheme matrix elements. During this transformation we encounter a complicated overlap that is calculated separately in subsection 4.2. In subsection 4.3 we discuss a serious limitation with the direct transformation into m-scheme matrix elements, since storing them as well as the overlap calculated in subsection 4.2 is very memory demand-

ing. Finally, in subsection 4.4, we present the solution of this problem by slightly changing our strategy into the calculation of matrix elements that maintain a total coupled angular momentum and isospin.

4.1 Matrix elements of the three-nucleon interaction at N2LO in the m-scheme

In the following, we derive the formula for the transformation of three-particle interaction matrix elements from the antisymmetrized Jacobi states $|EJTi\rangle$ into the antisymmetrized m-scheme basis

$$\langle EJTi|\mathbf{V}^{NNN}|E'JTi'\rangle \;\longrightarrow\; {}_a\langle abc|\mathbf{V}^{NNN}|a'b'c'\rangle_a \,. \tag{4.2}$$

We start with a non-antisymmetrized product state of (ls)-coupled single-particle harmonic oscillator states

$$|abc\rangle = |(n_a l_a, s_a) j_a m_a, (n_b l_b, s_b) j_b m_b, (n_c l_c, s_c) j_c m_c, t_a m_{t_a} t_b m_{t_b} t_c m_{t_c}\rangle \,. \tag{4.3}$$

In the first step, we couple the single-particle angular momenta $\vec{\boldsymbol{j}}_i$ to total angular momentum $\vec{\mathcal{J}}$ of the three nucleons

$$\begin{aligned} |abc\rangle = \sum_{J_{ab},\mathcal{J}} \left(\begin{array}{cc|c} j_a & j_b & J_{ab} \\ m_a & m_b & M_{ab} \end{array}\right) \left(\begin{array}{cc|c} J_{ab} & j_c & \mathcal{J} \\ M_{ab} & m_c & \mathcal{M} \end{array}\right) \\ \times |\{[(n_a l_a, s_a) j_a, (n_b l_b, s_b) j_b] J_{ab}, (n_c l_c, s_c) j_c\} \mathcal{J}\mathcal{M}, t_a m_{t_a} t_b m_{t_b} t_c m_{t_c}\rangle \,, \end{aligned} \tag{4.4}$$

with $M_{ab} = m_a + m_b$ and $\mathcal{M} = M_{ab} + m_c$. We used the Clebsch-Gordan coefficients defined in eq. (3.5) and eliminated the sums over projection quantum numbers using eq. (3.9).

In the next step we make use of the identity

$$\mathbb{1} = \sum_{n_{cm},l_{cm}} \sum_{\alpha} \sum_{\mathcal{J}',\mathcal{M}'} \{|n_{cm} l_{cm}\rangle \otimes |\alpha\rangle\}^{\mathcal{J}'\mathcal{M}'} \{\langle n_{cm} l_{cm}| \otimes \langle\alpha|\}^{\mathcal{J}'\mathcal{M}'} \,, \tag{4.5}$$

where n_{cm}, l_{cm} denote center-of-mass quantum numbers and

$$|\alpha\rangle = |[(n_{12} l_{12}, s_{ab}) j_{12}, (n_3 l_3, s_c) j_3] J M_J, (t_{ab} t_c) T M_T\rangle \tag{4.6}$$

again denotes the Jacobi state as already introduced in section 3.4. Here, one has to be careful, since $|\alpha\rangle$ does not contain the M_J quantum number if its total angular momentum is coupled, as in eq. (4.5). There, the curly brackets indicate the coupling of the center-of-mass orbital angular momentum with the total angular

momentum of the Jacobi state $|\alpha\rangle$. Moreover we introduced

$$\sum_{\alpha} \equiv \sum_{n_{12},l_{12}} \sum_{n_3,l_3} \sum_{s_{ab}} \sum_{j_{12},j_3} \sum_{J} \sum_{t_{ab}} \sum_{T,M_T} . \tag{4.7}$$

Inserting eq. (4.5) into eq. (4.4) yields

$$\begin{aligned} |abc\rangle = &\sum_{J_{ab},\mathcal{J}} \sum_{n_{cm},l_{cm}} \sum_{\alpha} \left(\begin{array}{cc|c} j_a & j_b & J_{ab} \\ m_a & m_b & M_{ab} \end{array}\right) \left(\begin{array}{cc|c} J_{ab} & j_c & \mathcal{J} \\ M_{ab} & m_c & \mathcal{M} \end{array}\right) \\ &\times T \begin{pmatrix} a & b & c & J_{ab} & J & \mathcal{J} \\ n_{cm} & l_{cm} & n_{12} & l_{12} & n_3 & l_3 \\ s_{ab} & j_{12} & j_3 & t_{ab} & T & M_T \end{pmatrix} \\ &\times \{|n_{cm} l_{cm}\rangle \otimes |\alpha\rangle\}^{\mathcal{J}\mathcal{M}} , \end{aligned} \tag{4.8}$$

with the T-coefficient defined as the overlap

$$\begin{aligned} &T \begin{pmatrix} a & b & c & J_{ab} & J & \mathcal{J} \\ n_{cm} & l_{cm} & n_{12} & l_{12} & n_3 & l_3 \\ s_{ab} & j_{12} & j_3 & t_{ab} & T & M_T \end{pmatrix} \\ &= \{\langle n_{cm} l_{cm}| \otimes \langle \alpha|\}^{\mathcal{J}\mathcal{M}} |\{[(n_a l_a, s_a) j_a, (n_b l_b, s_b) j_b] J_{ab}, (n_c l_c, s_c) j_c\} \mathcal{J}\mathcal{M}, t_a m_{t_a} t_b m_{t_b} t_c m_{t_c}\rangle . \end{aligned} \tag{4.9}$$

The sums over primed quantum numbers vanish because of the orthogonality relations. For clarity we postpone working out the formula for the T-coefficient to the next subsection, but we stress that the arrangement of the quantum numbers in the symbol of the T-coefficient has no physical meaning.

Since the nuclear interaction will only affect the relative part of the state, it is useful to decouple the relative angular momentum from the center-of-mass orbital angular momentum. Doing so, we encounter one further Clebsch-Gordan coefficient

$$\begin{aligned} |abc\rangle = &\sum_{J_{ab},\mathcal{J}} \sum_{\alpha} \sum_{n_{cm},l_{cm}} \sum_{m_{cm},M_J} \left(\begin{array}{cc|c} j_a & j_b & J_{ab} \\ m_a & m_b & M_{ab} \end{array}\right) \left(\begin{array}{cc|c} J_{ab} & j_c & \mathcal{J} \\ M_{ab} & m_c & \mathcal{M} \end{array}\right) \\ &\times \left(\begin{array}{cc|c} l_{cm} & J & \mathcal{J} \\ m_{cm} & M_J & \mathcal{M} \end{array}\right) T \begin{pmatrix} a & b & c & J_{ab} & J & \mathcal{J} \\ n_{cm} & l_{cm} & n_{12} & l_{12} & n_3 & l_3 \\ s_{ab} & j_{12} & j_3 & t_{ab} & T & M_T \end{pmatrix} \\ &\times |n_{cm} l_{cm} m_{cm}\rangle \otimes |\alpha\rangle . \end{aligned} \tag{4.10}$$

Finally, only one piece is missing: The left-hand side is still a non-antisymmetrized product state. Thus, the final step is to project it onto the antisymmetric

part of the Hilbert space. Consequently, we now make use of the representation of the antisymmetrizer that we worked out in section 3.4 in eq. (3.94)

$$\mathcal{A} = \sum_{\substack{n_{cm},l_{cm}\\ m_{cm}}} \sum_{E,J,M_J} \sum_{T,M_T} \sum_{i} |n_{cm}l_{cm}m_{cm}\rangle \otimes |EJM_JTM_Ti\rangle\langle n_{cm}l_{cm}m_{cm}| \otimes \langle EJM_JTM_Ti| \,. \tag{4.11}$$

If we multiply eq. (4.10) with the antisymmetrizer from the left, we have to consider the overlap

$$\begin{aligned}&\langle n'_{cm}l'_{cm}m'_{cm}|n_{cm}l_{cm}m_{cm}\rangle\langle EJ'M'_JT'M'_JT'M'_Ti|\alpha\rangle \\ &\quad = c_{\alpha,i}\,\delta_{J',J}\,\delta_{M'_J,M_J}\,\delta_{T',T}\,\delta_{M'_T,M_T}\,\delta_{n'_{cm},n_{cm}}\,\delta_{l'_{cm},l_{cm}}\,\delta_{m'_{cm},m_{cm}}\,\delta_{E,2n_{12}+l_{12}+2n_3+l_3}\ ,\end{aligned} \tag{4.12}$$

with the coefficient of fractional parentage $c_{\alpha,i}$ as defined in eq. (3.91). Using the Kronecker deltas of eq. (4.12), we eliminate the corresponding summations and obtain for the antisymmetrized m-scheme state

$$\begin{aligned}|abc\rangle_a =& \sqrt{3!} \sum_{J_{ab},\mathcal{J}} \sum_{\alpha} \sum_{\substack{l_{cm},n_{cm},\\ m_{cm}}} \sum_{M_J} \sum_{i} \\ &\times \left(\begin{array}{cc|c} j_a & j_b & J_{ab} \\ m_a & m_b & M_{ab} \end{array}\right) \left(\begin{array}{cc|c} J_{ab} & j_c & \mathcal{J} \\ M_{ab} & m_c & \mathcal{M} \end{array}\right) \left(\begin{array}{cc|c} l_{cm} & J & \mathcal{J} \\ m_{cm} & M_J & \mathcal{M} \end{array}\right) \\ &\times T\begin{pmatrix} a & b & c & J_{ab} & J & \mathcal{J} \\ n_{cm} & l_{cm} & n_{12} & l_{12} & n_3 & l_3 \\ s_{ab} & j_{12} & j_3 & t_{ab} & T & M_T \end{pmatrix} \\ &\times c_{\alpha,i} \quad |n_{cm}l_{cm}m_{cm}\rangle \otimes |EJM_JTM_Ti\rangle \,.\end{aligned} \tag{4.13}$$

The only remaining sum of (4.11) is the one with respect to i. The quantum number E is now constrained by $E = 2n_{12} + l_{12} + 2n_3 + l_3$. The additional factor $\sqrt{3!}$ shows up because of

$$|abc\rangle_a = \sqrt{3!}\,\mathcal{A}\,|abc\rangle \,, \tag{4.14}$$

and is needed to have a normalized state after the projection.

Now we are in the position to write down the interaction matrix element. We use the hermitian adjoint of $|abc\rangle_a$, as given in eq. (4.13), to sandwich the interac-

tion operator. This yields

$$
\begin{aligned}
&{}_a\langle abc|\mathbf{V}^{NNN}|a'b'c'\rangle_a \\
&= 3! \sum_{J_{ab},\mathcal{J}} \sum_{\alpha} \sum_{\substack{n_{cm},l_{cm} \\ m_{cm}}} \sum_{M_J} \sum_{i} \sum_{J'_{ab},\mathcal{J}'} \sum_{\alpha'} \sum_{\substack{n'_{cm},l'_{cm} \\ m'_{cm}}} \sum_{M'_J} \sum_{i'} \\
&\quad \times \left(\begin{array}{cc|c} j'_a & j'_b & J'_{ab} \\ m'_a & m'_b & M'_{ab} \end{array}\right) \left(\begin{array}{cc|c} J'_{ab} & j'_c & \mathcal{J}' \\ M'_{ab} & m'_c & \mathcal{M}' \end{array}\right) \left(\begin{array}{cc|c} l'_{cm} & J' & \mathcal{J}' \\ m'_{cm} & M'_J & \mathcal{M}' \end{array}\right) \\
&\quad \times \left(\begin{array}{cc|c} j_a & j_b & J_{ab} \\ m_a & m_b & M_{ab} \end{array}\right) \left(\begin{array}{cc|c} J_{ab} & j_c & \mathcal{J} \\ M_{ab} & m_c & \mathcal{M} \end{array}\right) \left(\begin{array}{cc|c} l_{cm} & J & \mathcal{J} \\ m_{cm} & M_J & \mathcal{M} \end{array}\right) \\
&\quad \times T\begin{pmatrix} a & b & c & J_{ab} & J & \mathcal{J} \\ n_{cm} & l_{cm} & n_{12} & l_{12} & n_3 & l_3 \\ s_{ab} & j_{12} & j_3 & t_{ab} & T & M_T \end{pmatrix} T\begin{pmatrix} a' & b' & c' & J'_{ab} & J' & \mathcal{J}' \\ n'_{cm} & l'_{cm} & n'_{12} & l'_{12} & n'_3 & l'_3 \\ s'_{ab} & j'_{12} & j'_3 & t'_{ab} & T' & M'_T \end{pmatrix} \\
&\quad \times c_{\alpha,i}\, c_{\alpha',i'} \\
&\quad \times \langle n_{cm}l_{cm}m_{cm}|n'_{cm}l'_{cm}m'_{cm}\rangle\, \langle EJM_JTM_Ti|\mathbf{V}^{NNN}|E'J'M'_JT'M'_Ti'\rangle\,.
\end{aligned}
\tag{4.15}
$$

Here we have already used that the nuclear interaction operator $\mathbf{V}^{NNN}$ does not affect the center-of-mass part of the state.

For further simplification we make use of

$$
\langle n_{cm}l_{cm}m_{cm}|n'_{cm}l'_{cm}m'_{cm}\rangle = \delta_{n_{cm},n'_{cm}}\, \delta_{l_{cm},l'_{cm}}\, \delta_{m_{cm},m'_{cm}} \tag{4.16}
$$

and properties of the interaction, which imply

$$
\begin{aligned}
&\langle EJM_JTM_Ti|\mathbf{V}^{NNN}|E'J'M'_JT'M'_Ti'\rangle \\
&\quad = \delta_{J,J'}\, \delta_{M_J,M'_J}\, \delta_{T,T'}\, \delta_{M'_T,M_T}\, \langle EJTi|\mathbf{V}^{NNN}|E'JTi'\rangle\,.
\end{aligned}
\tag{4.17}
$$

Note that this holds true only for interactions that are independent of M_T, meaning charge invariant interactions. So we explicitly omit the fact that the nuclear interaction is not perfectly charge invariant at this point. Applying eqs. (4.16) and (4.17) on eq. (4.15) eliminates the summations over

$$
n'_{cm}, l'_{cm}, m'_{cm}, J', M'_J, T', M'_T \tag{4.18}
$$

leading to

$$
\begin{aligned}
&{}_a\langle abc|\mathbf{V}^{NNN}|a'b'c'\rangle_a \\
&= 3! \sum_{J_{ab},\mathcal{J}} \sum_{\alpha} \sum_{\substack{n_{cm},l_{cm} \\ m_{cm}}} \sum_{M_J} \sum_{i} \sum_{J'_{ab},\mathcal{J}'} \sum_{\tilde{\alpha}'} \sum_{i'} \\
&\quad \times \left(\begin{array}{cc|c} j'_a & j'_b & J'_{ab} \\ m'_a & m'_b & M'_{ab} \end{array}\right) \left(\begin{array}{cc|c} J'_{ab} & j'_c & \mathcal{J}' \\ M'_{ab} & m'_c & \mathcal{M}' \end{array}\right) \left(\begin{array}{cc|c} l_{cm} & J & \mathcal{J}' \\ m_{cm} & M_J & \mathcal{M}' \end{array}\right) \\
&\quad \times \left(\begin{array}{cc|c} j_a & j_b & J_{ab} \\ m_a & m_b & M_{ab} \end{array}\right) \left(\begin{array}{cc|c} J_{ab} & j_c & \mathcal{J} \\ M_{ab} & m_c & \mathcal{M} \end{array}\right) \left(\begin{array}{cc|c} l_{cm} & J & \mathcal{J} \\ m_{cm} & M_J & \mathcal{M} \end{array}\right) \\
&\quad \times T\begin{pmatrix} a & b & c & J_{ab} & J & \mathcal{J} \\ n_{cm} & l_{cm} & n_{12} & l_{12} & n_3 & l_3 \\ s_{ab} & j_{12} & j_3 & t_{ab} & T & M_T \end{pmatrix} T\begin{pmatrix} a' & b' & c' & J'_{ab} & J & \mathcal{J}' \\ n_{cm} & l_{cm} & n'_{12} & l'_{12} & n'_3 & l'_3 \\ s'_{ab} & j'_{12} & j'_3 & t'_{ab} & T & M_T \end{pmatrix} \\
&\quad \times c_{\alpha,i}\, c_{\tilde{\alpha}',i'} \\
&\quad \times \langle EJTi|\mathbf{V}^{NNN}|E'JTi'\rangle \,.
\end{aligned}
\tag{4.19}
$$

Here, $\sum_\alpha$ still means a sum over $\{n_{12}, l_{12}, s_{ab}, j_{12}, n_3, l_3, j_3, J, t_{ab}, T, M_T\}$, whereas $\sum_{\tilde{\alpha}'}$ means a sum over $\{n'_{12}, l'_{12}, s'_{ab}, j'_{12}, n'_3, l'_3, j_3', t'_{ab}\}$.

Next we use the orthogonality relation (3.11) of the Clebsch-Gordan coefficients

$$
\sum_{m_{cm},M_J} \left(\begin{array}{cc|c} l_{cm} & J & \mathcal{J} \\ m_{cm} & M_J & \mathcal{M} \end{array}\right) \left(\begin{array}{cc|c} l_{cm} & J & \mathcal{J}' \\ m_{cm} & M_J & \mathcal{M}' \end{array}\right) = \delta_{\mathcal{J},\mathcal{J}'}\, \delta_{\mathcal{M},\mathcal{M}'} \tag{4.20}
$$

and the three-body m-scheme interaction matrix element finally reads

$$
\begin{aligned}
&{}_a\langle abc|\mathbf{V}^{NNN}|a'b'c'\rangle_a \\
&= 3! \sum_{J_{ab},\mathcal{J}} \sum_{\alpha} \sum_{n_{cm},l_{cm}} \sum_{i} \sum_{J'_{ab}} \sum_{\tilde{\alpha}'} \sum_{i'} \\
&\quad \times \left(\begin{array}{cc|c} j'_a & j'_b & J'_{ab} \\ m'_a & m'_b & M'_{ab} \end{array}\right) \left(\begin{array}{cc|c} J'_{ab} & j'_c & \mathcal{J} \\ M'_{ab} & m'_c & \mathcal{M} \end{array}\right) \left(\begin{array}{cc|c} j_a & j_b & J_{ab} \\ m_a & m_b & M_{ab} \end{array}\right) \left(\begin{array}{cc|c} J_{ab} & j_c & \mathcal{J} \\ M_{ab} & m_c & \mathcal{M} \end{array}\right) \\
&\quad \times T\begin{pmatrix} a & b & c & J_{ab} & J & \mathcal{J} \\ n_{cm} & l_{cm} & n_{12} & l_{12} & n_3 & l_3 \\ s_{ab} & j_{12} & j_3 & t_{ab} & T & M_T \end{pmatrix} T\begin{pmatrix} a' & b' & c' & J'_{ab} & J & \mathcal{J} \\ n_{cm} & l_{cm} & n'_{12} & l'_{12} & n'_3 & l'_3 \\ s'_{ab} & j'_{12} & j'_3 & t'_{ab} & T & M_T \end{pmatrix} \\
&\quad \times c_{\alpha,i}\, c_{\tilde{\alpha}',i'} \\
&\quad \times \langle EJTi|\mathbf{V}^{NNN}|E'JTi'\rangle\, \delta_{\mathcal{M},\mathcal{M}'} \,.
\end{aligned}
\tag{4.21}
$$

Or with all quantum numbers shown explicitly

$$
\begin{aligned}
&{}_a\langle abc|\mathbf{V}^{NNN}|a'b'c'\rangle_a \\
&= 3! \sum_{J_{ab},J'_{ab}} \sum_{\mathcal{J}} \sum_{n_{cm},l_{cm}} \sum_{n_{12},n'_{12}} \sum_{l_{12},l'_{12}} \sum_{s_{ab},s'_{ab}} \sum_{j_{12},j'_{12}} \sum_{t_{ab},t'_{ab}} \sum_{n_3,n'_3} \sum_{l_3,l'_3} \sum_{j_3,j'_3} \sum_{J,T} \sum_{i,i'} \\
&\quad \times \left(\begin{array}{cc|c} j'_a & j'_b & J'_{ab} \\ m'_a & m'_b & M'_{ab} \end{array}\right) \left(\begin{array}{cc|c} J'_{ab} & j'_c & \mathcal{J} \\ M'_{ab} & m'_c & \mathcal{M} \end{array}\right) \left(\begin{array}{cc|c} j_a & j_b & J_{ab} \\ m_a & m_b & M_{ab} \end{array}\right) \left(\begin{array}{cc|c} J_{ab} & j_c & \mathcal{J} \\ M_{ab} & m_c & \mathcal{M} \end{array}\right) \\
&\quad \times T\begin{pmatrix} a & b & c & J_{ab} & J & \mathcal{J} \\ n_{cm} & l_{cm} & n_{12} & l_{12} & n_3 & l_3 \\ s_{ab} & j_{12} & j_3 & t_{ab} & T & M_T \end{pmatrix} T\begin{pmatrix} a' & b' & c' & J'_{ab} & J & \mathcal{J} \\ n_{cm} & l_{cm} & n'_{12} & l'_{12} & n'_3 & l'_3 \\ s'_{ab} & j'_{12} & j'_3 & t'_{ab} & T & M_T \end{pmatrix} \\
&\quad \times c_{\alpha,i}\begin{bmatrix} n_{12} & l_{12} & n_3 & l_3 \\ s_{ab} & j_{12} & j_3 & J \\ t_{ab} & T & M_T & i \end{bmatrix} c_{\tilde{\alpha}',i'}\begin{bmatrix} n'_{12} & l'_{12} & n'_3 & l'_3 \\ s'_{ab} & j'_{12} & j'_3 & J \\ t'_{ab} & T & M_T & i' \end{bmatrix} \\
&\quad \times \langle EJTi|\mathbf{V}^{NNN}|E'JTi'\rangle \,,
\end{aligned}
\tag{4.22}
$$

with

$$M_{ab} = m_a + m_b \,, \tag{4.23}$$

$$M'_{ab} = m'_a + m'_b \,, \tag{4.24}$$

$$\mathcal{M} = m_a + m_b + m_c = m'_a + m'_b + m'_c \,, \tag{4.25}$$

$$M_T = m_{t_a} + m_{t_b} + m_{t_c} = m'_{t_a} + m'_{t_b} + m'_{t_c} \,, \tag{4.26}$$

$$E = 2n_{12} + l_{12} + 2n_3 + l_3 \,. \tag{4.27}$$

The large number of summations and the fact that the T-coefficient depends on almost all of them leads to a complicated computational task. Obviously, the explicit execution of the summations would lead to inefficiently large run times. For details on our implementation we refer the interested reader to appendix A.

The remaining task is to calculate the T-coefficient defined in eq. (4.9), which will be done in the following subsection.

4.2 Calculation of the T-coefficient

In the last subsection we defined the T-coefficient as

$$T\begin{pmatrix} a & b & c & J_{ab} & J & \mathcal{J} \\ n_{cm} & l_{cm} & n_{12} & l_{12} & n_3 & l_3 \\ s_{ab} & j_{12} & j_3 & t_{ab} & T & M_T \end{pmatrix}$$

$$\begin{aligned} &= \left\{\langle n_{cm} l_{cm}| \otimes \langle\alpha|\right\}^{\mathcal{J}\mathcal{M}} |\{[(n_a l_a, s_a) j_a, (n_b l_b, s_b) j_b] J_{ab}, (n_c l_c, s_c) j_c\} \mathcal{J}\mathcal{M}, t_a m_{t_a} t_b m_{t_b} t_c m_{t_c}\rangle \\ &:= \left\{\langle n_{cm} l_{cm}| \otimes \langle\alpha|\right\}^{\mathcal{J}\mathcal{M}} \left\{\{|a\rangle \otimes |b\rangle\}^{J_{ab}} \otimes |c\rangle\right\}^{\mathcal{J}\mathcal{M}} . \end{aligned} \tag{4.28}$$

Now we will derive the explicit formula to compute it. Hence, we will start with the state $\left\{\{|a\rangle \otimes |b\rangle\}^{J_{ab}} \otimes |c\rangle\right\}^{\mathcal{J}\mathcal{M}}$ and express it stepwise by $\left\{|n_{cm} l_{cm}\rangle \otimes |\alpha\rangle\right\}^{\mathcal{J}\mathcal{M}}$. Obviously, we have to change the underlying coordinate system on our way through the transformation, since we must change quantum numbers of the relative and center-of-mass part of the three-nucleon system into single-particle quantum numbers. As outlined in section 3.3, we can achieve this with the help of HOBs. We will encounter two of them.

We start our transformations with coupling the isospin of $\left\{\{|a\rangle \otimes |b\rangle\}^{J_{ab}} \otimes |c\rangle\right\}^{\mathcal{J}\mathcal{M}}$ to total isospin quantum numbers T, M_T

$$\begin{aligned} &\left\{\{|a\rangle \otimes |b\rangle\}^{J_{ab}} \otimes |c\rangle\right\}^{\mathcal{J}\mathcal{M}} \\ &= \sum_{t_{ab}, T} \left(\begin{array}{cc|c} t_a & t_b & t_{ab} \\ m_{t_a} & m_{t_b} & m_{t_{ab}} \end{array}\right) \left(\begin{array}{cc|c} t_{ab} & t_c & T \\ m_{t_{ab}} & t_c & M_T \end{array}\right) \\ &\quad \times |\{[(n_a l_a, s_a) j_a, (n_b l_b, s_b) j_b] J_{ab}, (n_c l_c, s_c) j_c\} \mathcal{J}\mathcal{M}, [(t_a, t_b) t_{ab}, t_c] T M_T\rangle . \end{aligned} \tag{4.29}$$

As usual, we eliminated already the sums over the projection quantum numbers by $m_{t_{ab}} = m_{t_a} + m_{t_b}$ and $M_T = m_{t_{ab}} + m_{t_c}$. For the further steps the isospin part is dispensable, so we omit it for brevity.

In the following, we carry out a number of unitary transformations by inserting appropriate identity operators. How the parts of the state that are affected by the transformation change is always shown in the heading of each step. We encounter sums and transformation coefficients in every single step. We quote them only once in the step they are relevant for and highlight them with a box. At the end we will collect everything together and write down the complete formula. The same applies for the summation bounds: we specify them in each step and summarize them in a simplified form for a special ordering of the sums in appendix A.2.

Moreover, we will use the shorthand $\hat{x} = \sqrt{2x+1}$ and omit the projection quantum number $\mathcal{M}$ corresponding to $\mathcal{J}$ since it does not change during the transfor-

mations.

An overview with short description of the quantum numbers that we need during the various steps is given in table 1.

n_a, n_b, n_c	single-particle h.o. radial quantum numbers
l_a, l_b, l_c	single-particle h.o. orbital angular momentum quantum numbers
s_a, s_b, s_c	single-particle spin
j_a, j_b, j_c	(ls)-coupled single-particle angular momentum
t_a, t_b, t_c	single-particle isospin
s_{ab}	coupled spins (s_a, s_b)
t_{ab}	coupled isospins (t_a, t_b)
J_{ab}	coupled single-particle angular momenta $(j_a j_b)$
$\mathcal{J}$,$\mathcal{M}$	total angular momentum $(J_{ab} j_c)$ and projection quantum number
L_{ab}	coupled orbital angular momenta $(l_a l_b)$
$\mathcal{N}_{12}$	h.o. radial quantum number based on center of mass of particles 1 and 2
$\mathcal{L}_{12}$	orbital angular momentum based on center of mass of particles 1 and 2
n_{12}	h.o. radial quantum number of the first Jacobi coordinate $\vec{\xi}_1$
l_{12}	orbital angular momentum depending on the first Jacobi coordinate $\vec{\xi}_1$
$\mathcal{L}$	total orbital angular momentum $(L_{ab} l_c)$
S_3	total spin $(s_{ab} s_c)$
Λ	coupling of the orbital angular momenta $(\mathcal{L}_{12} l_c)$
n_3	h.o. radial quantum number depending on the Jacobi coordinate $\vec{\xi}_2$
l_3	orbital angular momentum depending on the Jacobi coordinate $\vec{\xi}_2$
L_3	total relative orbital angular momentum coupling $(l_{12} l_3)$
J	total angular momentum of the relative part of the state $(L_3 S_3)$
j_{12}	total angular momentum based on the first Jacobi coordinate (l_{12}, s_{ab})
j_3	total angular momentum based on the second Jacobi coordinate (l_3, s_c)

Table 1 – *Summary of all quantum numbers needed for the calculation of the T-coefficient. The shorthand h.o. means harmonic oscillator.*

► $[(n_a l_a, s_a) j_a, (n_b l_b, s_b) j_b] J_{ab} \;\rightarrow\; [(n_a l_a, n_b l_b) L_{ab}, (s_a, s_b) s_{ab}] J_{ab}$

Since we aim at the separation of the center-of-mass part of the state, it is clear that we have to deal with Talmi transformations. The first Talmi transformation will introduce the coordinate $c\vec{m}_{ab}$ of the center of mass of the first two particles and their corresponding relative coordinate $\vec{\xi}_1$. Before doing this, we have to change the (jj)-coupling of particles 1 and 2 into (LS)-coupling. We obtain this by inserting a suitable identity operator in eq. (4.29)

$$
\begin{aligned}
&|\{[(n_a l_a, s_a) j_a, (n_b l_b, s_b) j_b] J_{ab}, (n_c l_c, s_c) j_c\} \mathcal{J}\rangle \\
&= \sum_{L_{ab}, s_{ab}} |\{[(n_a l_a, n_b l_b) L_{ab}, (s_a, s_b) s_{ab}] J_{ab}, (n_c l_c, s_c) j_c\} \mathcal{J}\rangle \\
&\times \langle\{[(n_a l_a, n_b l_b) L_{ab}, (s_a, s_b) s_{ab}] J_{ab}, (n_c l_c, s_c) j_c\} \mathcal{J}| \\
&\qquad\qquad \times |\{[(n_a l_a, s_a) j_a, (n_b l_b, s_b) j_b] J_{ab}, (n_c l_c, s_c) j_c\} \mathcal{J}\rangle \,.
\end{aligned}
\tag{4.30}
$$

Since we have a recoupling of four angular momenta we can replace the overlap with a 9j-symbol by using eq. (3.20)

$$
\begin{aligned}
&\langle\{[(n_a l_a, n_b l_b) L_{ab}, (s_a, s_b) s_{ab}] J_{ab}, (n_c l_c, s_c) j_c\} \mathcal{J}| \\
&\qquad\qquad \times |\{[(n_a l_a, s_a) j_a, (n_b l_b, s_b) j_b] J_{ab}, (n_c l_c, s_c) j_c\} \mathcal{J}\rangle \\
&= \boxed{\hat{j}_a \hat{j}_b \hat{L}_{ab} \hat{s}_{ab} \begin{Bmatrix} l_a & l_b & L_{ab} \\ s_a & s_b & s_{ab} \\ j_a & j_b & J_{ab} \end{Bmatrix}} .
\end{aligned}
\tag{4.31}
$$

So the right-hand side of eq. (4.30) becomes

$$
\sum_{L_{ab}, s_{ab}} \hat{j}_a \hat{j}_b \hat{L}_{ab} \hat{s}_{ab} \begin{Bmatrix} l_a & l_b & L_{ab} \\ s_a & s_b & s_{ab} \\ j_a & j_b & J_{ab} \end{Bmatrix} |\{[(n_a l_a, n_b l_b) L_{ab}, (s_a, s_b) s_{ab}] J_{ab}, (n_c l_c, s_c) j_c\} \mathcal{J}\rangle \,. \tag{4.32}
$$

The summation bounds of the two sums are determined by the triangular conditions (3.24) that must be fulfilled for the 9j-symbol.

► $(n_a l_a, n_b l_b) L_{ab} \longrightarrow (\mathcal{N}_{12}\mathcal{L}_{12}(c\vec{m}_{ab}), n_{12} l_{12}(\vec{\xi}_1)) L_{ab}$

Now we carry out the first Talmi transformation. It changes the single-particle coordinates $\vec{r}_a$ and $\vec{r}_b$ into the coordinate of the center of mass $c\vec{m}_{ab}$ of the first two particles, and their relative Jacobi coordinate $\vec{\xi}_1$

$$c\vec{m}_{ab} = \sqrt{\frac{1}{2}}\,(\vec{r}_a + \vec{r}_b) \tag{4.33}$$

$$\vec{\xi}_1 = \sqrt{\frac{1}{2}}\,(\vec{r}_a - \vec{r}_b)\,. \tag{4.34}$$

For the corresponding transformation matrix (3.43) we have to choose the parameter $d = 1$, yielding

$$\begin{pmatrix} c\vec{m}_{ab} \\ \vec{\xi}_1 \end{pmatrix} = \begin{pmatrix} \sqrt{\frac{1}{2}} & \sqrt{\frac{1}{2}} \\ \sqrt{\frac{1}{2}} & -\sqrt{\frac{1}{2}} \end{pmatrix} \begin{pmatrix} \vec{r}_a \\ \vec{r}_b \end{pmatrix}\,. \tag{4.35}$$

As we have seen in section 3.3, the transformation coefficient is given by the HOB

$$\boxed{\langle\langle \mathcal{N}_{12}\mathcal{L}_{12}, n_{12} l_{12}; L_{ab} | n_a l_a, n_b l_b \rangle\rangle_1 \; \delta_{2\mathcal{N}_{12}+\mathcal{L}_{12}+2n_{12}+l_{12},2n_a+l_a+2n_b+l_b}}\,. \tag{4.36}$$

The new quantum numbers $\mathcal{N}_{12}, \mathcal{L}_{12}$ are the harmonic oscillator radial and orbital angular momentum quantum numbers that describe the center of mass of the first two particles, respectively. The harmonic oscillator depending on the first Jacobi coordinate $\vec{\xi}_1$ defines the quantum numbers n_{12} and l_{12}. Accordingly, the result of this transformation is given by

$$\begin{aligned} &|\{[(n_a l_a, n_b l_b) L_{ab}, (s_a, s_b) s_{ab}] J_{ab}, (n_c l_c, s_c) j_c\} \mathcal{J}\rangle \\ &= \sum_{\mathcal{N}_{12},\mathcal{L}_{12}} \sum_{n_{12},l_{12}} \langle\langle \mathcal{N}_{12}\mathcal{L}_{12}, n_{12} l_{12}; L_{ab} | n_a l_a, n_b l_b \rangle\rangle_1 \; \delta_{2\mathcal{N}_{12}+\mathcal{L}_{12}+2n_{12}+l_{12},2n_a+l_a+2n_b+l_b} \\ &\qquad \times |\{[(\mathcal{N}_{12}\mathcal{L}_{12}(c\vec{m}_{ab}), n_{12} l_{12}(\vec{\xi}_1)) L_{ab}, (s_a, s_b) s_{ab}] J_{ab}, (n_c l_c, s_c) j_c\} \mathcal{J}\rangle \end{aligned} \tag{4.37}$$

The summation bounds are constrained by the energy condition

$$2\mathcal{N}_{12} + \mathcal{L}_{12} + 2n_{12} + l_{12} = 2n_a + l_a + 2n_b + l_b\,. \tag{4.38}$$

► $[(L_{ab}, s_{ab})J_{ab}, (l_c, s_c)j_c]\mathcal{J} \longrightarrow [(L_{ab}, l_c)\mathcal{L}, (s_{ab}, s_c)S_3]\mathcal{J}$

For the second Talmi transformation that introduces the Jacobi coordinate $\vec{\xi}_2$, we need couplings of pure orbital angular momenta. Thus, we break up the $(L_{ab}s_{ab})$-coupling of the total orbital angular momentum of particles 1 and 2 with their coupled spin $\vec{s}_{ab}$ in this step. Instead, we couple $\vec{L}_{ab}$ with the orbital angular momentum of the third particle $\vec{l}_c$ to orbital angular momentum $\vec{\mathcal{L}}$. Inserting the appropriate identity operator leads to

$$
\begin{aligned}
&|(\mathcal{N}_{12}\mathcal{L}_{12}, n_{12}l_{12})L_{ab}, (s_a, s_b)s_{ab}]J_{ab}, (n_c l_c, s_c)j_c\}\mathcal{J}\rangle \\
&= \sum_{\mathcal{L},S_3} |\{[(\mathcal{N}_{12}\mathcal{L}_{12}, n_{12}l_{12})L_{ab}, n_c l_c]\mathcal{L}, [(s_a, s_b)s_{ab}, s_c]S_3\}\mathcal{J}\rangle \\
&\times \langle\{[(\mathcal{N}_{12}\mathcal{L}_{12}, n_{12}l_{12})L_{ab}, n_c l_c]\mathcal{L}, [(s_a, s_b)s_{ab}, s_c]S_3\}\mathcal{J}| \qquad (4.39) \\
&\qquad\qquad \times |\{[(\mathcal{N}_{12}\mathcal{L}_{12}, n_{12}l_{12})L_{ab}, (s_a, s_b)s_{ab}]J_{ab}, (n_c l_c, s_c)j_c\}\mathcal{J}\rangle
\end{aligned}
$$

Again, we have a recoupling of four angular momenta and we use eq. (3.20) to replace the overlap by a 9j-symbol

$$
\begin{aligned}
&\langle\{[(\mathcal{N}_{12}\mathcal{L}_{12}, n_{12}l_{12})L_{ab}, n_c l_c]\mathcal{L}, [(s_a s_b)s_{ab}, s_c]S_3\}\mathcal{J}| \\
&\qquad\qquad \times |\{[(\mathcal{N}_{12}\mathcal{L}_{12}, n_{12}l_{12})L_{ab}, (s_a, s_b)s_{ab}]J_{ab}, (n_c l_c, s_c)j_c\}\mathcal{J}\rangle \\
&= \boxed{\hat{\mathcal{L}}\hat{S}_3\hat{J}_{ab}\hat{j}_c \begin{Bmatrix} L_{ab} & l_c & \mathcal{L} \\ s_{ab} & s_c & S_3 \\ J_{ab} & j_c & \mathcal{J} \end{Bmatrix}}. \qquad (4.40)
\end{aligned}
$$

The right hand side of eq. (4.39) then reads

$$
\sum_{\mathcal{L},S_3} \hat{\mathcal{L}}\hat{S}_3\hat{J}_{ab}\hat{j}_c \begin{Bmatrix} L_{ab} & l_c & \mathcal{L} \\ s_{ab} & s_c & S_3 \\ J_{ab} & j_c & \mathcal{J} \end{Bmatrix} |\{[(\mathcal{N}_{12}\mathcal{L}_{12}, n_{12}l_{12})L_{ab}, n_c l_c]\mathcal{L}, [(s_a s_b)s_{ab}, s_c]S_3\}\mathcal{J}\rangle\,. \qquad (4.41)
$$

The summation bounds are again determined by the triangular conditions of the 9j-symbol, given in eq. (3.24).

► $[(\mathcal{N}_{12}\mathcal{L}_{12}, n_{12}l_{12})L_{ab}, n_c l_c]\mathcal{L} \longrightarrow [(\mathcal{N}_{12}\mathcal{L}_{12}, n_c l_c)\Lambda, n_{12}l_{12}]\mathcal{L}$

Before we carry out the second Talmi transformation that leads us to the complete set of Jacobi coordinates defined in eq. (3.31), we have to couple $\vec{\mathcal{L}}_{12}$ with $\vec{l}_c$. This is necessary because we can only transform the coordinates that correspond to these angular momenta using the transformation matrix (3.43) into the coordinates $\vec{\xi}_0$ and $\vec{\xi}_2$. Again we do the recoupling by inserting a representation for the identity operator and receive

$$\begin{aligned}
&|\{[(\mathcal{N}_{12}\mathcal{L}_{12}, n_{12}l_{12})L_{ab}, n_c l_c]\mathcal{L}, [(s_a, s_b)s_{ab}, s_c]S_3\}\mathcal{J}\rangle \\
&= \sum_{\Lambda} |\{[(\mathcal{N}_{12}\mathcal{L}_{12}, n_c l_c)\Lambda, n_{12}l_{12}]\mathcal{L}, [(s_a, s_b)s_{ab}, s_c]S_3\}\mathcal{J}\rangle \\
&\times \langle\{[(\mathcal{N}_{12}\mathcal{L}_{12}, n_c l_c)\Lambda, n_{12}l_{12}]\mathcal{L}, [(s_a, s_b)s_{ab}, s_c]S_3\}\mathcal{J}| \qquad (4.42)\\
&\qquad\qquad \times |\{[(\mathcal{N}_{12}\mathcal{L}_{12}, n_{12}l_{12})L_{ab}, n_c l_c]\mathcal{L}, [(s_a, s_b)s_{ab}, s_c]S_3\}\mathcal{J}\rangle
\end{aligned}$$

Now we have a recoupling of three angular momenta, so we replace the overlap by a 6j-symbol. The relation we use is given in eq. (3.17)

$$\begin{aligned}
&\langle\{[(\mathcal{N}_{12}\mathcal{L}_{12}, n_c l_c)\Lambda, n_{12}l_{12}]\mathcal{L}, [(s_a, s_b)s_{ab}, s_c]S_3\}\mathcal{J}| \\
&\qquad\qquad \times |\{[(\mathcal{N}_{12}\mathcal{L}_{12}, n_{12}l_{12})L_{ab}, n_c l_c]\mathcal{L}, [(s_a, s_b)s_{ab}, s_c]S_3\}\mathcal{J}\rangle \\
&= \boxed{(-1)^{l_c+l_{12}+\Lambda+L_{ab}}\hat{L}_{ab}\hat{\Lambda}\begin{Bmatrix} l_c & \mathcal{L}_{12} & \Lambda \\ l_{12} & \mathcal{L} & L_{ab}\end{Bmatrix}}. \qquad (4.43)
\end{aligned}$$

This yields for the right hand side of eq. (4.42)

$$\sum_{\Lambda}(-1)^{l_c+l_{12}+\Lambda+L_{ab}}\hat{L}_{ab}\hat{\Lambda}\begin{Bmatrix} l_c & \mathcal{L}_{12} & \Lambda \\ l_{12} & \mathcal{L} & L_{ab}\end{Bmatrix}|\{[(\mathcal{N}_{12}\mathcal{N}_{12}, n_c l_c)\Lambda, n_{12}l_{12}]\mathcal{L}, [(s_a, s_b)s_{ab}, s_c]S_3\}\mathcal{J}\rangle. \qquad (4.44)$$

Here, the summation bounds for Λ are given by the triangular conditions eq. (3.16) for the 6j-symbol.

► $(\mathcal{N}_{12}\mathcal{L}_{12}(c\vec{m}_{ab}), n_c l_c(\vec{r}_c))\Lambda \longrightarrow (n_{cm}l_{cm}(\vec{\xi}_0), n_3 l_3(\vec{\xi}_2))\Lambda$

Since the orbital angular momentum corresponding to $\vec{\xi}_1$ is now coupled with the orbital angular momentum with respect to the position of the third nucleon, we are able to perform the second Talmi transformation. This will introduce the center-of-mass coordinate of the three nucleons $\vec{\xi}_0$ and the Jacobi coordinate $\vec{\xi}_2$

$$\vec{\xi}_0 = \sqrt{\frac{1}{3}}\ [\vec{r}_a + \vec{r}_b + \vec{r}_c]\ , \tag{4.45}$$

$$\vec{\xi}_2 = \sqrt{\frac{2}{3}}\ \left[\frac{1}{2}(\vec{r}_a + \vec{r}_b) - \vec{r}_c\right]\ . \tag{4.46}$$

Comparison with the matrix (3.43) reveals that $d = 2$ is the correct parameter for the Talmi transformation. Therefore, the coordinate-transformation matrix reads

$$\begin{pmatrix} \vec{\xi}_0 \\ \vec{\xi}_2 \end{pmatrix} = \begin{pmatrix} \sqrt{\frac{2}{3}} & \sqrt{\frac{1}{3}} \\ \sqrt{\frac{1}{3}} & -\sqrt{\frac{2}{3}} \end{pmatrix} \begin{pmatrix} c\vec{m}_{ab} \\ \vec{r}_c \end{pmatrix}\ . \tag{4.47}$$

Thus, the transformation coefficient is given by the HOB

$$\boxed{\langle\langle n_{cm}l_{cm}, n_3 l_3; \Lambda | \mathcal{N}_{12}\mathcal{L}_{12}, n_c l_c\rangle\rangle_2\ \delta_{2n_{cm}+l_{cm}+2n_3+l_3, 2\mathcal{N}_{12}+\mathcal{L}_{12}+2n_c+l_c}}\ , \tag{4.48}$$

and the result of the Talmi transformation is

$$\begin{aligned} &|\{[(\mathcal{N}_{12}\mathcal{L}_{12}, n_c l_c)\Lambda, n_{12}l_{12}]\mathcal{L}, [(s_a, s_b)s_{ab}, s_c]S_3\}\mathcal{J}\rangle \\ &= \sum_{n_{cm}, l_{cm}} \sum_{n_3, l_3} \langle\langle n_{cm}l_{cm}, n_3 l_3; \Lambda | \mathcal{N}_{12}\mathcal{L}_{12}, n_c l_c\rangle\rangle_2\ \delta_{2n_{cm}+l_{cm}+2n_3+l_3, 2\mathcal{N}_{12}+\mathcal{L}_{12}+2n_c+l_c} \\ &\qquad \times |\{[(n_{cm}l_{cm}(\vec{\xi}_0), n_3 l_3(\vec{\xi}_2))\Lambda, n_{12}l_{12}]\mathcal{L}, [(s_a, s_b)s_{ab}, s_c]S_3\}\mathcal{J}\rangle \end{aligned} \tag{4.49}$$

Here the summations are restricted by the energy conserving condition of the HOBs, i.e.

$$2n_{cm} + l_{cm} + 2n_3 + l_3 = 2\mathcal{N}_{12} + \mathcal{L}_{12} + 2n_c + l_c\,. \tag{4.50}$$

► $[(n_{cm}l_{cm}, n_3l_3)\Lambda, n_{12}l_{12}]\mathcal{L} \longrightarrow [n_{cm}l_{cm}, (n_3l_3, n_{12}l_{12})L_3]\mathcal{L}$

In the final state, $\left\{|n_{cm}l_{cm}\rangle \otimes |\alpha\rangle\right\}^{\mathcal{JM}}$, the center-of-mass angular momentum is coupled with the total relative angular momentum including spin. So we have to break up the coupling of $\vec{l}_{cm}$ with other orbital angular momenta in two steps. In this first step we recouple $\vec{l}_{cm}$ with the total orbital angular momentum of the relative part of the state $\vec{L}_3$ by again inserting an appropriate identity operator

$$
\begin{aligned}
&|\{[(n_{cm}l_{cm}, n_3l_3)\Lambda, n_{12}l_{12}]\mathcal{L}, [(s_a, s_b)s_{ab}, s_c]S_3\}\mathcal{J}\rangle \\
&= \sum_{L_3} |\{[n_{cm}l_{cm}, (n_3l_3, n_{12}l_{12})L_3]\mathcal{L}, [(s_as_b)s_{ab}, s_c]S_3\}\mathcal{J}\rangle \\
&\times \langle\{[n_{cm}l_{cm}, (n_3l_3, n_{12}l_{12})L_3]\mathcal{L}, [(s_as_b)s_{ab}, s_c]S_3\}\mathcal{J}| \qquad (4.51) \\
&\qquad\qquad \times |\{[(n_{cm}l_{cm}, n_3l_3)\Lambda, n_{12}l_{12}]\mathcal{L}, [(s_a, s_b)s_{ab}, s_c]S_3\}\mathcal{J}\rangle
\end{aligned}
$$

Again, we replace the overlap by a 6j-symbol, this time with help of eq. (3.15)

$$
\begin{aligned}
&\langle\{[n_{cm}l_{cm}, (n_3l_3, n_{12}l_{12})L_3]\mathcal{L}, [(s_as_b)s_{ab}, s_c]S_3\}\mathcal{J}| \\
&\qquad\qquad \times |\{[(n_{cm}l_{cm}, n_3l_3)\Lambda, n_{12}l_{12}]\mathcal{L}, [(s_a, s_b)s_{ab}, s_c]S_3\}\mathcal{J}\rangle \\
&= \boxed{(-1)^{l_{cm}+l_3+l_{12}+\mathcal{L}}\hat{\Lambda}\hat{L}_3 \begin{Bmatrix} l_{cm} & l_3 & \Lambda \\ l_{12} & \mathcal{L} & L_3 \end{Bmatrix}}. \qquad (4.52)
\end{aligned}
$$

Hence, we obtain for the right-hand side of eq. (4.51)

$$
\sum_{L_3}(-1)^{l_{cm}+l_3+l_{12}+\mathcal{L}}\hat{\Lambda}\hat{L}_3 \begin{Bmatrix} l_{cm} & l_3 & \Lambda \\ l_{12} & \mathcal{L} & L_3 \end{Bmatrix} |\{[n_{cm}l_{cm}, (n_3l_3, n_{12}l_{12})L_3]\mathcal{L}, [(s_as_b)s_{ab}, s_c]S_3\}\mathcal{J}\rangle\,. \qquad (4.53)
$$

The summation bounds are given by the triangular conditions of the 6j-symbols defined in eq. (3.16).

► $[(n_{cm}l_{cm}, L_3)\mathcal{L}, S_3]\mathcal{J} \longrightarrow [n_{cm}l_{cm}, (L_3, S_3)J]\mathcal{J}$

With this step we arrive at the already mentioned situation that $\vec{l}_{cm}$ couples with the total angular momentum of the relative part of the state $\vec{J}$. Thus the center-of-mass part of the state has the desired form after this transformation step and will not be changed further. We employ the corresponding identity operator that conducts the transformation and gain

$$\begin{aligned}
&|\{[n_{cm}l_{cm}, (n_3l_3, n_{12}l_{12})L_3]\mathcal{L}, [(s_as_b)s_{ab}, s_c]S_3\}\mathcal{J}\rangle \\
&= \sum_J |\{n_{cm}l_{cm}, [(n_3l_3, n_{12}l_{12})L_3, [(s_a, s_b)s_{ab}, s_c]S_3]J\}\mathcal{J}\rangle \\
&\times \langle\{n_{cm}l_{cm}, [(n_3l_3, n_{12}l_{12})L_3, [(s_a, s_b)s_{ab}, s_c]S_3]J\}\mathcal{J}| \qquad (4.54)\\
&\qquad\qquad \times |\{[n_{cm}l_{cm}, (n_3l_3, n_{12}l_{12})L_3]\mathcal{L}, [(s_as_b)s_{ab}, s_c]S_3\}\mathcal{J}\rangle\,.
\end{aligned}$$

and the overlap can be replaced with help of eq. (3.15) again by a 6j-symbol

$$\begin{aligned}
&\langle\{n_{cm}l_{cm}, [(n_3l_3, n_{12}l_{12})L_3, [(s_a, s_b), s_{ab}, s_c]S_3]J\}\mathcal{J}| \\
&\qquad\qquad \times |\{[n_{cm}l_{cm}, (n_3l_3, n_{12}l_{12})L_3]\mathcal{L}, [(s_as_b)s_{ab}, s_c]S_3\}\mathcal{J}\rangle \\
&= \boxed{(-1)^{l_{cm}+L_3+S_3+\mathcal{J}}\hat{\mathcal{L}}\hat{J}\begin{Bmatrix} l_{cm} & L_3 & \mathcal{L} \\ S_3 & \mathcal{J} & J \end{Bmatrix}}. \qquad (4.55)
\end{aligned}$$

The right hand side results in

$$\sum_J (-1)^{l_{cm}+L_3+S_3+\mathcal{J}}\hat{\mathcal{L}}\hat{J}\begin{Bmatrix} l_{cm} & L_3 & \mathcal{L} \\ S_3 & \mathcal{J} & J \end{Bmatrix}|\{n_{cm}l_{cm}, [(n_3l_3, n_{12}l_{12})L_3, [(s_a, s_b), s_{ab}, s_c]S_3]J\}\mathcal{J}\rangle, \qquad (4.56)$$

and again the bounds of the sum over J are determined by the triangular conditions of the 6j-symbols, given in eq. (3.16).

► $[(n_3 l_3, n_{12} l_{12}) L_3, (s_{ab}, s_c) S_3] J \longrightarrow [(n_3 l_3, s_c) j_3, (n_{12} l_{12}, s_{ab}) j_{12}] J$

This final transformation leads to the coupling scheme of the state $|\alpha\rangle$. We have to change the internal coupling of angular momenta and spins into mixed coupling, meaning $\vec{l}_3$ couples with $\vec{s}_c$ and $\vec{l}_{12}$ with $\vec{s}_{ab}$. The new coupled quantum numbers are then denoted by j_3 and j_{12}, respectively. Again, we insert an appropriate identity operator

$$\begin{aligned}
&|\{n_{cm} l_{cm}, [(n_3 l_3, n_{12} l_{12}) L_3, [(s_a, s_b) s_{ab}, s_c] S_3] J\} \mathcal{J}\rangle \\
&= \sum_{j_{12}, j_3} |\{n_{cm} l_{cm}, [(n_3 l_3, s_c) j_3, (n_{12} l_{12}, s_{ab}) j_{12}] J\} \mathcal{J}\rangle \\
&\times \langle\{n_{cm} l_{cm}, [(n_3 l_3, s_c) j_3, (n_{12} l_{12}, s_{ab}) j_{12}] J\} \mathcal{J}| \qquad (4.57) \\
&\qquad\qquad \times |\{n_{cm} l_{cm}, [(n_3 l_3, n_{12} l_{12}) L_3, [(s_a, s_b) s_{ab}, s_c] S_3] J\} \mathcal{J}\rangle \, .
\end{aligned}$$

The overlap can be replaced with help of eq. (3.21) by

$$\begin{aligned}
&\langle\{n_{cm} l_{cm}, [(n_3 l_3, s_c) j_3, (n_{12} l_{12}, s_{ab}) j_{12}] J\} \mathcal{J}| \\
&\qquad\qquad \times |\{n_{cm} l_{cm}, [(n_3 l_3, n_{12} l_{12}) L_3, [(s_a, s_b) s_{ab}, s_c] S_3] J\} \mathcal{J}\rangle \\
&= (-1)^{s_{ab}+s_c-S_3} \hat{L}_3 \hat{j}_3 \hat{j}_{12} \hat{S}_3 \begin{Bmatrix} l_3 & l_{12} & L_3 \\ s_c & s_{ab} & S_3 \\ j_3 & j_{12} & J \end{Bmatrix} \qquad (4.58) \\
&= (-1)^{s_{ab}+s_c-S_3} \hat{L}_3 \hat{j}_3 \hat{j}_{12} \hat{S}_3 \begin{Bmatrix} l_{12} & l_3 & L_3 \\ s_{ab} & s_c & S_3 \\ j_{12} & j_3 & J \end{Bmatrix} (-1)^{l_{12}+l_3+L_3+s_{ab}+s_c+S_3+j_{12}+j_3+J} \, . \qquad (4.59)
\end{aligned}$$

In the last manipulation we used a symmetry relation of the 9j-symbols. We exchanged the first two columns and, therefore, have to pick up the phase factor with the sum over all appearing quantum numbers. At this point the right hand side of eq. (4.57) reads

$$\begin{aligned}
&\sum_{j_{12}, j_3} (-1)^{l_{12}+l_3+L_3+j_{12}+j_3+J+2s_c} \hat{L}_3 \hat{j}_3 \hat{j}_{12} \hat{S}_3 \begin{Bmatrix} l_{12} & l_3 & L_3 \\ s_{ab} & s_c & S_3 \\ j_{12} & j_3 & J \end{Bmatrix} \\
&\qquad\qquad \times |\{n_{cm} l_{cm}, [(n_3 l_3, s_c) j_3, (n_{12} l_{12}, s_{ab}) j_{12}] J\} \mathcal{J}\rangle \, , \qquad (4.60)
\end{aligned}$$

where we simplified the phase factor using the fact that s_{ab} is an integer. Additionally, we have to reverse the coupling order from $(j_3 j_{12})$ into $(j_{12} j_3)$ to have the same ordering as in $|\alpha\rangle$. Thereby we collect a phase $(-1)^{j_{12}+j_3-J}$ due to the symmetry

relation of the Clebsch-Gordan coefficients, given in eq. (3.12). Then we can further simplify the phase factor using that two times a half-integral number is always odd. This applies for $2j_3$ and implies that $2s_c + 2j_3$ is even. Furthermore, we know that j_{12} is an integer and so $(-1)^{2j_{12}} = 1$. Altogether the right hand side of eq. (4.57), including the simplified transformation coefficient for this step, reads

$$\sum_{j_{12},j_3} \boxed{(-1)^{l_3+l_{12}+L_3}\hat{L}_3\hat{j}_3\hat{j}_{12}\hat{S}_3 \begin{Bmatrix} l_{12} & l_3 & L_3 \\ s_{ab} & s_c & S_3 \\ j_{12} & j_3 & J \end{Bmatrix}} |\{n_{cm}l_{cm}, [(n_{12}l_{12}, s_{ab})j_{12}, (n_3l_3, s_c)j_3]J\}\mathcal{J}\rangle \,. \tag{4.61}$$

Now we have done all transformation steps. We obtain the complete result of

$$\left\{\{|a\rangle \otimes |b\rangle\}^{J_{ab}} \otimes |c\rangle\right\}^{\mathcal{J}\mathcal{M}} \;\rightarrow\; \left\{|n_{cm}l_{cm}\rangle \otimes |\alpha\rangle\right\}^{\mathcal{J}\mathcal{M}} \tag{4.62}$$

by collecting all transformation coefficients and the corresponding summations. In the following formula they are arranged in the order they appeared in the derivation

$$\begin{aligned}
&\left\{\{|a\rangle \otimes |b\rangle\}^{J_{ab}} \otimes |c\rangle\right\}^{\mathcal{J}\mathcal{M}} \\
&\quad= \sum_{t_{ab},m_{t_{ab}}} \sum_{T,M_T} \sum_{L_{ab},s_{ab}} \sum_{\mathcal{N}_{12},\mathcal{L}_{12}} \sum_{n_{12},l_{12}} \sum_{\mathcal{L},S_3} \sum_{\Lambda} \sum_{n_{cm},l_{cm}} \sum_{n_3,l_3} \sum_{L_3} \sum_{J} \sum_{j_{12},j_3} \\
&\quad\times \left(\begin{array}{cc|c} t_a & t_b & t_{ab} \\ m_{t_a} & m_{t_b} & m_{t_{ab}} \end{array}\right) \left(\begin{array}{cc|c} t_{ab} & t_c & T \\ m_{t_{ab}} & m_{t_c} & M_T \end{array}\right) \begin{Bmatrix} l_a & l_b & L_{ab} \\ s_a & s_b & s_{ab} \\ j_a & j_b & J_{ab} \end{Bmatrix} \hat{j}_a\hat{j}_b\hat{L}_{ab}\hat{s}_{ab} \\
&\quad\times \langle\langle \mathcal{N}_{12}\mathcal{L}_{12}, n_{12}l_{12}; L_{ab}|n_al_a, n_bl_b\rangle\rangle_1 \; \delta_{2\mathcal{N}_{12}+\mathcal{L}_{12}+2n_{12}+l_{12},2n_a+l_a+2n_b+l_b} \\
&\quad\times \hat{\mathcal{L}}\hat{S}_3\hat{J}_{ab}\hat{j}_c \begin{Bmatrix} L_{ab} & l_c & \mathcal{L} \\ s_{ab} & s_c & S_3 \\ J_{ab} & j_c & \mathcal{J} \end{Bmatrix} (-1)^{l_c+l_{12}+\Lambda+L_{ab}}\hat{L}_{ab}\hat{\Lambda} \begin{Bmatrix} l_c & \mathcal{L}_{12} & \Lambda \\ l_{12} & \mathcal{L} & L_{ab} \end{Bmatrix} \\
&\quad\times \langle\langle n_{cm}l_{cm}, n_3l_3; \Lambda|\mathcal{N}_{12}\mathcal{L}_{12}, n_cl_c\rangle\rangle_2 \; \delta_{2n_{cm}+l_{cm}+2n_3+l_3,2\mathcal{N}_{12}+\mathcal{L}_{12}+2n_c+l_c} \\
&\quad\times (-1)^{l_{cm}+l_3+l_{12}+\mathcal{L}}\hat{\Lambda}\hat{L}_3 \begin{Bmatrix} l_{cm} & l_3 & \Lambda \\ l_{12} & \mathcal{L} & L_3 \end{Bmatrix} (-1)^{l_{cm}+L_3+S_3+\mathcal{J}}\hat{\mathcal{L}}\hat{J} \begin{Bmatrix} l_{cm} & L_3 & \mathcal{L} \\ S_3 & \mathcal{J} & J \end{Bmatrix} \\
&\quad\times (-1)^{l_3+l_{12}+L_3}\hat{L}_3\hat{j}_3\hat{j}_{12}\hat{S}_3 \begin{Bmatrix} l_{12} & l_3 & L_3 \\ s_{ab} & s_c & S_3 \\ j_{12} & j_3 & J \end{Bmatrix} \left\{|n_{cm}l_{cm}\rangle \otimes |\alpha\rangle\right\}^{\mathcal{J}\mathcal{M}} .
\end{aligned} \tag{4.63}$$

In order to calculate the T-coefficient from that we multiply (4.63) from the left with $\left\{\langle n'_{cm} l'_{cm}| \otimes \langle \alpha'|\right\}^{\mathcal{JM}}$ and get Kronecker deltas

$$\delta_{n'_{cm},n_{cm}}\,\delta_{l'_{cm},l_{cm}}\,\delta_{n'_{12},n_{12}}\,\delta_{l'_{12},l_{12}}\,\delta_{s'_{ab},s_{ab}}\,\delta_{j'_{12},j_{12}}\,\delta_{n'_3,j_3}\,\delta_{l'_3,l_3}\,\delta_{j'_3,j_3}\,\delta_{J',J}\,\delta_{t'_{ab},t_{ab}}\,\delta_{m'_{t_{ab}},m_{t_{ab}}}\delta_{T',T}\,\delta_{M'_T,M_T}\,. \tag{4.64}$$

They eliminate the corresponding summations, leading to

$$\begin{aligned}
&\left\{\langle n_{cm} l_{cm}| \otimes \langle \alpha|\right\}^{\mathcal{JM}} \left\{\{|a\rangle \otimes |b\rangle\}^{J_{ab}} \otimes |c\rangle\right\}^{\mathcal{JM}} \\
&\quad = \sum_{L_{ab}} \sum_{\mathcal{N}_{12},\mathcal{L}_{12}} \sum_{\mathcal{L}} \sum_{S_3} \sum_{\Lambda} \sum_{L_3} \\
&\quad \times \delta_{2\mathcal{N}_{12}+\mathcal{L}_{12}+2n_{12}+l_{12},2n_a+l_a+2n_b+l_b}\,\delta_{2n_{cm}+l_{cm}+2n_3+l_3,2\mathcal{N}_{12}+\mathcal{L}_{12}+2n_c+l_c} \\
&\quad \times \left(\begin{array}{cc|c} t_a & t_b & t_{ab} \\ m_{t_a} & m_{t_b} & m_{t_{ab}} \end{array}\right) \left(\begin{array}{cc|c} t_{ab} & t_c & T \\ m_{t_{ab}} & m_{t_c} & M_T \end{array}\right) \\
&\quad \times \langle\langle \mathcal{N}_{12}\mathcal{L}_{12}, n_{12} l_{12}; L_{ab}|n_a l_a, n_b l_b\rangle\rangle_1\ \langle\langle n_{cm} l_{cm}, n_3 l_3; \Lambda|\mathcal{N}_{12}\mathcal{L}_{12}, n_c l_c\rangle\rangle_2 \\
&\quad \times \begin{Bmatrix} l_a & l_b & L_{ab} \\ s_a & s_b & s_{ab} \\ j_a & j_b & J_{ab} \end{Bmatrix} \hat{j}_a \hat{j}_b \hat{L}_{ab} \hat{s}_{ab} \begin{Bmatrix} L_{ab} & l_c & \mathcal{L} \\ s_{ab} & s_c & S_3 \\ J_{ab} & j_c & \mathcal{J} \end{Bmatrix} \hat{\mathcal{L}} \hat{S}_3 \hat{J}_{ab} \hat{j}_c \\
&\quad \times (-1)^{l_c+l_{12}+\Lambda+L_{ab}} \hat{L}_{ab} \hat{\Lambda} \begin{Bmatrix} l_c & \mathcal{L}_{12} & \Lambda \\ l_{12} & \mathcal{L} & L_{ab} \end{Bmatrix} (-1)^{l_{cm}+l_3+l_{12}+\mathcal{L}} \hat{\Lambda} \hat{L}_3 \begin{Bmatrix} l_{cm} & l_3 & \Lambda \\ l_{12} & \mathcal{L} & L_3 \end{Bmatrix} \\
&\quad \times (-1)^{l_{cm}+L_3+S_3+\mathcal{J}} \hat{\mathcal{L}} \hat{J} \begin{Bmatrix} l_{cm} & L_3 & \mathcal{L} \\ S_3 & \mathcal{J} & J \end{Bmatrix} (-1)^{l_3+l_{12}+L_3} \hat{L}_3 \hat{j}_3 \hat{j}_{12} \hat{S}_3 \begin{Bmatrix} l_{12} & l_3 & L_3 \\ s_{ab} & s_c & S_3 \\ j_{12} & j_3 & J \end{Bmatrix}\,.
\end{aligned} \tag{4.65}$$

Here we dropped the primes and rearranged the terms for convenience. Lastly, we can eliminate the sum over $\mathcal{N}_{12}$ with help of the first Kronecker delta. Then, the remaining Kronecker delta reads

$$\delta_{2n_a+l_a+2n_b+l_b+2n_c+l_c,2n_{cm}+l_{cm}+2n_3+l_3+2n_{12}+l_{12}} \tag{4.66}$$

and our final result for the T-coefficient is

$$
\begin{aligned}
&T\begin{pmatrix} a & b & c & J_{ab} & J & \mathcal{J} \\ n_{cm} & l_{cm} & n_{12} & l_{12} & n_3 & l_3 \\ s_{ab} & j_{12} & j_3 & t_{ab} & T & M_T \end{pmatrix} \\
&= \left\{ \langle n_{cm} l_{cm}| \otimes \langle \alpha| \right\}^{\mathcal{J}\mathcal{M}} \left\{ \{|a\rangle \otimes |b\rangle\}^{J_{ab}} \otimes |c\rangle \right\}^{\mathcal{J}\mathcal{M}} \\
&= \sum_{L_{ab}} \sum_{\mathcal{L}_{12}} \sum_{\mathcal{L}} \sum_{S_3} \sum_{\Lambda} \sum_{L_3} \\
&\quad \times \delta_{2n_a+l_a+2n_b+l_b+2n_c+l_c, 2n_{cm}+l_{cm}+2n_3+l_3+2n_{12}+l_{12}} \\
&\quad \times \left(\begin{array}{cc|c} t_a & t_b & t_{ab} \\ m_{t_a} & m_{t_b} & m_{t_{ab}} \end{array} \right) \left(\begin{array}{cc|c} t_{ab} & t_c & T \\ m_{t_{ab}} & m_{t_c} & M_T \end{array} \right) \\
&\quad \times \langle \langle \mathcal{N}_{12}\mathcal{L}_{12}, n_{12} l_{12}; L_{ab} | n_a l_a, n_b l_b \rangle \rangle_1 \langle \langle n_{cm} l_{cm}, n_3 l_3; \Lambda | \mathcal{N}_{12}\mathcal{L}_{12}, n_c l_c \rangle \rangle_2 \\
&\quad \times \begin{Bmatrix} l_a & l_b & L_{ab} \\ s_a & s_b & s_{ab} \\ j_a & j_b & J_{ab} \end{Bmatrix} \begin{Bmatrix} L_{ab} & l_c & \mathcal{L} \\ s_{ab} & s_c & S_3 \\ J_{ab} & j_c & \mathcal{J} \end{Bmatrix} \begin{Bmatrix} l_{12} & l_3 & L_3 \\ s_{ab} & s_c & S_3 \\ j_{12} & j_3 & J \end{Bmatrix} \\
&\quad \times \begin{Bmatrix} l_c & \mathcal{L}_{12} & \Lambda \\ l_{12} & \mathcal{L} & L_{ab} \end{Bmatrix} \begin{Bmatrix} l_{cm} & l_3 & \Lambda \\ l_{12} & \mathcal{L} & L_3 \end{Bmatrix} \begin{Bmatrix} l_{cm} & L_3 & \mathcal{L} \\ S_3 & \mathcal{J} & J \end{Bmatrix} \\
&\quad \times \hat{j}_a \hat{j}_b \hat{j}_c \hat{J}_{ab} \hat{j}_{12} \hat{j}_3 \hat{s}_{ab} \hat{J} \hat{S}_3^2 \hat{\mathcal{L}}^2 \hat{\Lambda}^2 \hat{L}_3^2 \hat{L}_{ab}^2 (-1)^{l_c+\Lambda+L_{ab}+\mathcal{L}+S_3+l_{12}+\mathcal{J}} \,,
\end{aligned}
\tag{4.67}
$$

where we also simplified the phase factor.

Now we have all pieces together to calculate the m-scheme matrix element (4.21). For implementation of the formula it is convenient to precompute the T-coefficients, since for all matrix elements with fixed $|abc\rangle_a$ we always need the same T-coefficients and their calculation is computationally demanding. So the strategy must be to precompute as many quantities as possible. When we look back at eq. (4.21) we recognize that we can include the two Clebsch-Gordan coefficients of the $\mathcal{J}$-coupling and the corresponding sum over J_{ab} into the T-coefficients. Then

we can precalculate a new object that we denote by $\tilde{T}$. It is given by

$$
\begin{aligned}
&\tilde{T}\begin{pmatrix} a & b & c & & J & \mathcal{J} \\ n_{cm} & l_{cm} & n_{12} & l_{12} & n_3 & l_3 \\ s_{ab} & j_{12} & j_3 & t_{ab} & T & M_T \end{pmatrix} \\
&= \sum_{J_{ab}} \sum_{L_{ab}} \sum_{\mathcal{L}_{12}} \sum_{\mathcal{L}} \sum_{S_3} \sum_{\Lambda} \sum_{L_3} \\
&\quad \times \delta_{2n_a+l_a+2n_b+l_b+2n_c+l_c,2n_{cm}+l_{cm}+2n_3+l_3+2n_{12}+l_{12}} \\
&\quad \times \left(\begin{array}{cc|c} j_a & j_b & J_{ab} \\ m_a & m_b & M_{ab} \end{array}\right) \left(\begin{array}{cc|c} J_{ab} & j_c & \mathcal{J} \\ M_{ab} & m_c & \mathcal{M} \end{array}\right) \\
&\quad \times \left(\begin{array}{cc|c} t_a & t_b & t_{ab} \\ m_{t_a} & m_{t_b} & m_{t_{ab}} \end{array}\right) \left(\begin{array}{cc|c} t_{ab} & t_c & T \\ m_{t_{ab}} & m_{t_c} & M_T \end{array}\right) \\
&\quad \times \langle\langle \mathcal{N}_{12}\mathcal{L}_{12}, n_{12}l_{12}; L_{ab} | n_a l_a, n_b l_b \rangle\rangle_1 \langle\langle n_{cm} l_{cm}, n_3 l_3; \Lambda | \mathcal{N}_{12}\mathcal{L}_{12}, n_c l_c \rangle\rangle_2 \\
&\quad \times \begin{Bmatrix} l_a & l_b & L_{ab} \\ s_a & s_b & s_{ab} \\ j_a & j_b & J_{ab} \end{Bmatrix} \begin{Bmatrix} L_{ab} & l_c & \mathcal{L} \\ s_{ab} & s_c & S_3 \\ J_{ab} & j_c & \mathcal{J} \end{Bmatrix} \begin{Bmatrix} l_{12} & l_3 & L_3 \\ s_{ab} & s_c & S_3 \\ j_{12} & j_3 & J \end{Bmatrix} \\
&\quad \times \begin{Bmatrix} l_c & \mathcal{L}_{12} & \Lambda \\ l_{12} & \mathcal{L} & L_{ab} \end{Bmatrix} \begin{Bmatrix} l_{cm} & l_3 & \Lambda \\ l_{12} & \mathcal{L} & L_3 \end{Bmatrix} \begin{Bmatrix} l_{cm} & L_3 & \mathcal{L} \\ S_3 & \mathcal{J} & J \end{Bmatrix} \\
&\quad \times \hat{j}_a \hat{j}_b \hat{j}_c \hat{J}_{ab} \hat{j}_{12} \hat{j}_3 \hat{s}_{ab} \hat{J} \hat{S}_3^2 \hat{\mathcal{L}}^2 \hat{\Lambda}^2 \hat{L}_3^2 \hat{L}_{ab}^2 (-1)^{l_c+\Lambda+L_{ab}+\mathcal{L}+S_3+l_{12}+\mathcal{J}} \,,
\end{aligned}
\tag{4.68}
$$

Because $\sum_{J_{ab}}$ is now included in the $\tilde{T}$-coefficient, it is independent of J_{ab} and we drop J_{ab} in the symbol.

With this simplification the m-scheme matrix element is given by

$$
\begin{aligned}
&{}_a\langle abc | V_{NNN} | a'b'c' \rangle_a \\
&\quad = 3! \sum_{\mathcal{J}} \sum_{n_{cm}, l_{cm}} \\
&\quad \times \sum_{\alpha} \tilde{T}\begin{pmatrix} a & b & c & & J & \mathcal{J} \\ n_{cm} & l_{cm} & n_{12} & l_{12} & n_3 & l_3 \\ s_{ab} & j_{12} & j_3 & t_{ab} & T & M_T \end{pmatrix} \sum_{\tilde{\alpha}'} \tilde{T}\begin{pmatrix} a' & b' & c' & & J & \mathcal{J} \\ n_{cm} & l_{cm} & n'_{12} & l'_{12} & n'_3 & l'_3 \\ s'_{ab} & j'_{12} & j'_3 & t'_{ab} & T & M_T \end{pmatrix} \\
&\quad \times \sum_i c_{\alpha,i} \sum_{i'} c_{\tilde{\alpha}',i'} \\
&\quad \times \langle EJTi | V_{NNN} | E'JTi' \rangle \,.
\end{aligned}
\tag{4.69}
$$

Here we arranged the summations in the way we ordered them in the implementation. For more details on our implementation of the matrix elements see appendix A. For the ordering of the summations for the computation of the $\tilde{T}$-coeffi-

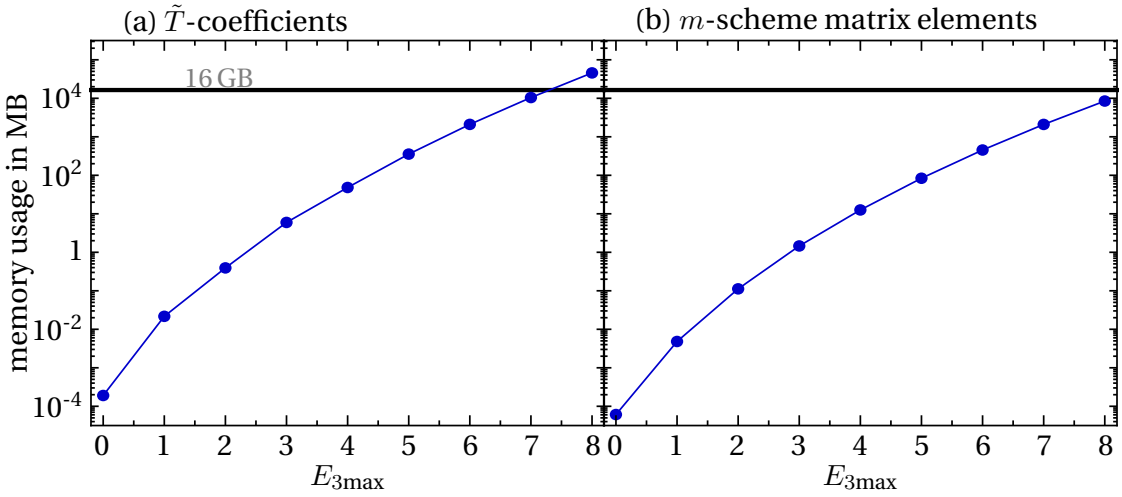

Figure 5 – *Memory usage for the $\tilde{T}$-coefficients (a) and for the m-scheme matrix elements (b) as a function of total three-nucleon energy E_{3max}. Also the maximum available memory on our computer cluster is shown at 16 GB. The single particle energies are truncated consistently, meaning $e_{max} = E_{3max}$.*

cient and the discussion of the corresponding summation bounds we also refer to appendix A.

4.3 Computational challenges

Using the result (4.69) for the m-scheme matrix elements we are in principle able to compute the matrix elements and then to perform first many-body calculations. But as already mentioned above, this is computationally demanding, especially regarding the memory requirements. Essentially two difficulties arise that we discuss in the following.

In figure 5(a) the memory needed for storing the precomputed nonzero $\tilde{T}$-coefficients is plotted against the total energy of the three nucleons $E_{3\max} = e_1 + e_2 + e_3$, with $e_i = 2n_i + l_i$. This used memory is composed of an array of structures in which besides the value of the $\tilde{T}$-coefficient also the corresponding quantum numbers $l_{cm}, \mathcal{J}$ and the number of the $|\alpha\rangle$ state is stored. The reasons for this storage scheme are discussed in appendix A.2. We recognize that the memory requirement increases dramatically if we increase the maximum three-nucleon energy. The maximal available memory on our cluster is 16 GB and we touch this limit already for $E_{3\max} = 8$. For the computation of the m-scheme matrix elements it is crucial to store all the relevant precomputed $\tilde{T}$-coefficients in the memory, because otherwise the runtime becomes inefficiently high. This means that already the computation of the m-scheme matrix elements for $E_{3\max} = 8$ is not possible with having all $\tilde{T}$-coefficients in memory, since we also have to store more than only the $\tilde{T}$. For $E_{3\max} = 10$ the situation becomes even worse, because 136 GB

memory are needed if we want to store all $\tilde{T}$-coefficients in memory. We tried to overcome this problem by reading the relevant $\tilde{T}$-coefficients from disk. Firstly, we read the $\tilde{T}$ for a given $|abc\rangle_a$. Having these in memory, we can calculate all matrix elements with this combination of single-particle quantum numbers. Therefore, we load the $\tilde{T}$ for each ${}_a\langle a'b'c'|$ in memory. This scheme allows to calculate matrix elements with higher three-particle energy $E_{3\text{max}} > 8$, but the calculation time increases significantly due to many disk accesses.

Additionally, there is a second problem concerning the m-scheme matrix elements themselves. In figure 5(b) we see the memory usage of the m-scheme matrix elements. This contains the value of the matrix element itself and two indices that specify the corresponding bra and ket states. Here, it is already taken into account that calculating a triangular matrix is sufficient and that the m-scheme states are antisymmetric and, therefore, only one permutation of single-particle quantum numbers needs to be included. Again, the critical 16 GB limit is reached for $E_{3\text{max}} = 8$. This is no problem while calculating them because we can write them into a file instead of storing in memory. But it is relevant for solving the many-body problem. There the m-scheme matrix elements must be available in memory if we stick to the strategy discussed so far. Otherwise the calculation becomes exceedingly slow, as every time one needs a m-scheme matrix element, it has to be read from hard disk. From experience with two-nucleon interactions one cannot expect converged many-body calculations using three-particle matrix elements only up to $E_{3\text{max}} = 8$. Converged refers here to the convergence with respect to model-space size.

The large numbers of $\tilde{T}$-coefficients and m-scheme matrix elements are caused by the many combinations of projection quantum numbers that must be included in the calculation. To get rid of these dependencies we change our strategy and work with states that provide a coupled total angular momentum $\mathcal{J}$ as well as total isospin T quantum number. We investigate the transformation of matrix elements with respect to the fully antisymmetrized states $|EJTi\rangle$ into the $\mathcal{J},T$-coupled scheme in the following subsection. The advantages of this scheme are discussed at the end of the next subsection.

4.4 $\mathcal{J},T$-coupling of the m-scheme matrix elements

As outlined in the last subsection, the handling of the m-scheme matrix elements is problematic because of the large number of $\tilde{T}$-coefficients and m-scheme matrix elements. To overcome these problems, we calculate $\mathcal{J},T$-coupled interaction

matrix elements

$$\langle[(j_a,j_b)J_{ab},j_c]\mathcal{J}\mathcal{M},[(t_a,t_b)t_{ab},t_c]TM_T|\mathbf{V}^{NNN}|[(j'_a,j'_b)J'_{ab},j'_c]\mathcal{J}\mathcal{M},[(t_a,t_b)t'_{ab},t_c]TM_T\rangle \tag{4.70}$$

instead of m-scheme matrix elements. Here, j_i are the single-particle angular momenta resulting from the (ls)-coupling of the single-particle states. We dropped the indication of these couplings for brevity. This will reduce the number of matrix elements significantly. We will discuss all advantages of this scheme after having derived the required formulas.

In the following we work out the formula for the transformation of the three-particle relative interaction matrix elements $|EJTi\rangle$ into the $\mathcal{J},T$-coupled states

$$\begin{aligned}&\langle EJTi|\mathbf{V}^{NNN}|E'JTi'\rangle\\ &\longrightarrow\\ &\langle[(j_a,j_b)J_{ab},j_c]\mathcal{J}\mathcal{M},[(t_a,t_b)t_{ab},t_c]TM_T|\mathbf{V}^{NNN}|[(j'_a,j'_b)J'_{ab},j'_c]\mathcal{J}\mathcal{M},[(t_a,t_b)t'_{ab},t_c]TM_T\rangle\,.\end{aligned} \tag{4.71}$$

We can use our result for the m-scheme matrix element derived in subsection 4.1.

We start with expanding the coupled states $|[(j_a,j_b)J_{ab},j_c]\mathcal{J}\mathcal{M},[(t_a,t_b)t_{ab},t_c]TM_T\rangle$ in terms of m-scheme states using Clebsch-Gordan coefficients

$$\begin{aligned}&|[(j_a,j_b)J_{ab},j_c]\mathcal{J}\mathcal{M},[(t_a,t_b)t_{ab},t_c]TM_T\rangle_a\\ &=\sum_{\substack{m_a,m_b\\M_{ab},m_c}}\sum_{\substack{m_{t_a},m_{t_b}\\m_{t_{ab}},m_{t_c}}}\left(\begin{array}{cc|c}j_a&j_b&J_{ab}\\m_a&m_b&M_{ab}\end{array}\right)\left(\begin{array}{cc|c}J_{ab}&j_c&\mathcal{J}\\M_{ab}&m_c&\mathcal{M}\end{array}\right)\left(\begin{array}{cc|c}t_a&t_a&t_{ab}\\m_{t_a}&m_{t_b}&m_{t_{ab}}\end{array}\right)\left(\begin{array}{cc|c}t_{ab}&t_c&T\\m_{t_{ab}}&m_{t_c}&M_T\end{array}\right)\\ &\qquad|(n_al_a,s_a)j_am_a,(n_bl_b,s_b)j_bm_b,(n_cl_c,s_c)j_cm_c,t_am_{t_a}t_bm_{t_b}t_cm_{t_c}\rangle_a\\ &=\sum_{\substack{m_a,m_b\\M_{ab},m_c}}\sum_{\substack{m_{t_a},m_{t_b}\\m_{t_{ab}},m_{t_c}}}\left(\begin{array}{cc|c}j_a&j_b&J_{ab}\\m_a&m_b&M_{ab}\end{array}\right)\left(\begin{array}{cc|c}J_{ab}&j_c&\mathcal{J}\\M_{ab}&m_c&\mathcal{M}\end{array}\right)\left(\begin{array}{cc|c}t_a&t_a&t_{ab}\\m_{t_a}&m_{t_b}&m_{t_{ab}}\end{array}\right)\left(\begin{array}{cc|c}t_{ab}&t_c&T\\m_{t_{ab}}&m_{t_c}&M_T\end{array}\right)\\ &\qquad|abc\rangle_a\,.\end{aligned} \tag{4.72}$$

With help of eq. (4.72) we can express matrix elements in the new coupled scheme with help of the previously derived m-scheme matrix elements of eq. (4.69). We

plug eq. (4.72) into eq. (4.70) and obtain

$$\begin{aligned}
&\langle[(j_a,j_b)J_{ab},j_c]\mathcal{J}\mathcal{M},[(t_a,t_b)t_{ab},t_c]TM_T|\mathbf{V}^{NNN}|[(j'_a,j'_b)J'_{ab},j'_c]\mathcal{J}\mathcal{M},[(t_a,t_b)t'_{ab},t_c]TM_T\rangle \\
&= \sum_{\substack{m_a,m_b\\M_{ab},m_c}}\sum_{\substack{m_{t_a},m_{t_b}\\m_{t_{ab}},m_{t_c}}}\sum_{\substack{m'_a,m'_b\\M'_{ab},m'_c}}\sum_{\substack{m'_{t_a},m'_{t_b}\\m'_{t_{ab}},m'_{t_c}}} \\
&\quad\times\left(\begin{array}{cc|c} j_a & j_b & J_{ab}\\ m_a & m_b & M_{ab}\end{array}\right)\left(\begin{array}{cc|c} J_{ab} & j_c & \mathcal{J}\\ M_{ab} & m_c & \mathcal{M}\end{array}\right)\left(\begin{array}{cc|c} t_a & t_a & t_{ab}\\ m_{t_a} & m_{t_b} & m_{t_{ab}}\end{array}\right)\left(\begin{array}{cc|c} t_{ab} & t_c & T\\ m_{t_{ab}} & m_{t_c} & M_T\end{array}\right) \\
&\quad\times\left(\begin{array}{cc|c} j'_a & j'_b & J'_{ab}\\ m'_a & m'_b & M'_{ab}\end{array}\right)\left(\begin{array}{cc|c} J'_{ab} & j'_c & \mathcal{J}\\ M'_{ab} & m'_c & \mathcal{M}\end{array}\right)\left(\begin{array}{cc|c} t_a & t_a & t'_{ab}\\ m'_{t_a} & m'_{t_b} & m'_{t_{ab}}\end{array}\right)\left(\begin{array}{cc|c} t'_{ab} & t_c & T\\ m'_{t_{ab}} & m'_{t_c} & M_T\end{array}\right) \\
&\quad\times {}_a\langle abc|V_{NNN}|a'b'c'\rangle_a\,. \qquad (4.73)
\end{aligned}$$

If we now look back at ${}_a\langle abc|V_{NNN}|a'b'c'\rangle_a$ in eq. (4.69), we recognize that further simplifications are possible. Therefore, we move the unprimed terms inclusive the corresponding sums of eq. (4.73) inside the unprimed $\tilde{T}$-coefficient of the m-scheme matrix element and the primed ones in the primed $\tilde{T}$-coefficient. We present the simplifications by showing only the relevant part of the m-scheme matrix element and $\tilde{T}$-coefficient, namely the sum over $J_{ab},\mathcal{J},t_{ab},T$ and the Clebsch-Gordan coefficients. Furthermore, we restrict ourselves to the simplification of the unprimed part from above, since the primed ones can be simplified by analogous steps.

The relevant part of the unprimed $\tilde{T}$ and the first four Clebsch-Gordans from eq. (4.73) with the corresponding sums read

$$\begin{aligned}
&\sum_{m_a,m_b}\sum_{M_{ab},m_c}\sum_{m_{t_a},m_{t_b}}\sum_{m_{t_{ab}},m_{t_c}} \\
&\times\left(\begin{array}{cc|c} j_a & j_b & J_{ab}\\ m_a & m_b & M_{ab}\end{array}\right)\left(\begin{array}{cc|c} J_{ab} & j_c & \mathcal{J}\\ M_{ab} & m_c & \mathcal{M}\end{array}\right)\left(\begin{array}{cc|c} t_a & t_a & t_{ab}\\ m_{t_a} & m_{t_b} & m_{t_{ab}}\end{array}\right)\left(\begin{array}{cc|c} t_{ab} & t_c & T\\ m_{t_{ab}} & m_{t_c} & M_T\end{array}\right) \\
&\times\sum_{\bar{\mathcal{J}}}\sum_{\bar{J}_{ab}}\sum_{\bar{t}_{ab}}\sum_{\bar{T}}\left(\begin{array}{cc|c} j_a & j_b & \bar{J}_{ab}\\ m_a & m_b & M_{ab}\end{array}\right)\left(\begin{array}{cc|c} J_{ab} & j_c & \bar{\mathcal{J}}\\ M_{ab} & m_c & \mathcal{M}\end{array}\right)\left(\begin{array}{cc|c} t_a & t_a & \bar{t}_{ab}\\ m_{t_a} & m_{t_b} & m_{t_{ab}}\end{array}\right)\left(\begin{array}{cc|c} t_{ab} & t_c & \bar{T}\\ m_{t_{ab}} & m_{t_c} & M_T\end{array}\right)\,. \qquad (4.74)
\end{aligned}$$

Here, $\sum_{\bar{\mathcal{J}}}$ is the sum over $\mathcal{J}$ from eq. (4.69) and $\sum_{\bar{t}_{ab}}$, $\sum_{\bar{T}}$ are also given in eq. (4.69), since they are implicit in $\sum_\alpha$. The summation $\sum_{\bar{J}_{ab}}$ is the one from inside the $\tilde{T}$-coefficient. Moreover, the projection quantum numbers do not require a tilde, since they are constrained to be the sum of the single-particle projection quantum

numbers. In the next step we only rearrange the terms, i.e.

$$\begin{aligned}
&\sum_{\bar{\mathcal{J}}}\sum_{\bar{J}_{ab}}\sum_{\bar{t}_{ab}}\sum_{\bar{T}} \\
&\times \sum_{M_{ab},m_c} \left(\begin{array}{cc|c} J_{ab} & j_c & \mathcal{J} \\ M_{ab} & m_c & \mathcal{M} \end{array}\right) \left(\begin{array}{cc|c} \bar{J}_{ab} & j_c & \bar{\mathcal{J}} \\ M_{ab} & m_c & \mathcal{M} \end{array}\right) \\
&\times \left[\sum_{m_a,m_b} \left(\begin{array}{cc|c} j_a & j_b & J_{ab} \\ m_a & m_b & M_{ab} \end{array}\right) \left(\begin{array}{cc|c} j_a & j_b & \bar{J}_{ab} \\ m_a & m_b & M_{ab} \end{array}\right)\right] \\
&\times \sum_{m_{t_{ab}},m_{t_c}} \left(\begin{array}{cc|c} t_{ab} & t_c & T \\ m_{t_{ab}} & m_{t_c} & M_T \end{array}\right) \left(\begin{array}{cc|c} \bar{t}_{ab} & t_c & \bar{T} \\ m_{t_{ab}} & m_{t_c} & M_T \end{array}\right) \\
&\times \left[\sum_{m_{t_a},m_{t_b}} \left(\begin{array}{cc|c} t_a & t_a & t_{ab} \\ m_{t_a} & m_{t_b} & m_{t_{ab}} \end{array}\right) \left(\begin{array}{cc|c} t_a & t_a & \bar{t}_{ab} \\ m_{t_a} & m_{t_b} & m_{t_{ab}} \end{array}\right)\right] .
\end{aligned} \tag{4.75}$$

Now, we can apply the orthogonality relation of the Clebsch-Gordan coefficients (3.11) to the terms inside the brackets, leading to Kronecker deltas that eliminate the corresponding sums over $\bar{J}_{ab}$ and $\bar{t}_{ab}$

$$\begin{aligned}
&\sum_{\bar{\mathcal{J}}}\sum_{\bar{J}_{ab}}\sum_{\bar{t}_{ab}}\sum_{\bar{T}} \\
&\times \sum_{M_{ab},m_c} \left(\begin{array}{cc|c} J_{ab} & j_c & \mathcal{J} \\ M_{ab} & m_c & \mathcal{M} \end{array}\right) \left(\begin{array}{cc|c} \bar{J}_{ab} & j_c & \bar{\mathcal{J}} \\ M_{ab} & m_c & \mathcal{M} \end{array}\right) \delta_{\bar{J}_{ab},J_{ab}}\,\delta_{M_{ab},M_{ab}} \\
&\times \sum_{m_{t_{ab}},m_{t_c}} \left(\begin{array}{cc|c} t_{ab} & t_c & T \\ m_{t_{ab}} & m_{t_c} & M_T \end{array}\right) \left(\begin{array}{cc|c} \bar{t}_{ab} & t_c & \bar{T} \\ m_{t_{ab}} & m_{t_c} & M_T \end{array}\right) \delta_{\bar{t}_{ab},t_{ab}}\,\delta_{m_{t_{ab}},m_{t_{ab}}}
\end{aligned} \tag{4.76}$$

$$\begin{aligned}
=&\sum_{\bar{\mathcal{J}}}\sum_{\bar{T}} \\
&\times \sum_{M_{ab},m_c} \left(\begin{array}{cc|c} J_{ab} & j_c & \mathcal{J} \\ M_{ab} & m_c & \mathcal{M} \end{array}\right) \left(\begin{array}{cc|c} J_{ab} & j_c & \bar{\mathcal{J}} \\ M_{ab} & m_c & \mathcal{M} \end{array}\right) \\
&\times \sum_{m_{t_{ab}},m_{t_c}} \left(\begin{array}{cc|c} t_{ab} & t_c & T \\ m_{t_{ab}} & m_{t_c} & M_T \end{array}\right) \left(\begin{array}{cc|c} t_{ab} & t_c & \bar{T} \\ m_{t_{ab}} & m_{t_c} & M_T \end{array}\right) .
\end{aligned} \tag{4.77}$$

We can again use the orthogonality relation (3.11), yielding

$$\sum_{\bar{\mathcal{J}}}\sum_{\bar{T}} \delta_{\bar{\mathcal{J}},\mathcal{J}}\,\delta_{\bar{T},T} . \tag{4.78}$$

We obtain the analogue result from simplification of the primed terms. Due to the Kronecker delta $\delta_{\bar{\mathcal{J}},\mathcal{J}}$, the sum over $\mathcal{J}$ in eq. (4.69) vanishes. Additionally, the sums over T and t_{ab} that are included in $\sum_\alpha$ in eq. (4.69) can be omitted.

The final expression for the $\mathcal{J}$-coupled matrix element (4.70) in terms of antisymmetric Jacobi matrix elements reads

$$
\begin{aligned}
&{}_a\langle[(j_a,j_b)J_{ab},j_c]\mathcal{J}\mathcal{M},[(t_a,t_b)t_{ab},t_c]TM_T|\mathbf{V}^{NNN}|[(j'_a,j'_b)J'_{ab},j'_c]\mathcal{J}\mathcal{M},[(t'_a,t'_b)t'_{ab},t_c]TM_T\rangle_a \\
&\quad = 3!\sum_{l_{cm}} \\
&\quad \times \sum_{\alpha} \tilde{T}_{\mathcal{J}}\begin{pmatrix} a & b & c & J_{ab} & J & \mathcal{J} \\ n_{cm} & l_{cm} & n_{12} & l_{12} & n_3 & l_3 \\ s_{ab} & j_{12} & j_3 & & & \end{pmatrix} \sum_{\alpha'} \tilde{T}_{\mathcal{J}}\begin{pmatrix} a' & b' & c' & J'_{ab} & J & \mathcal{J} \\ n_{cm} & l_{cm} & n'_{12} & l'_{12} & n'_3 & l'_3 \\ s'_{ab} & j'_{12} & j'_3 & & & \end{pmatrix} \\
&\quad \times \sum_i c_{\alpha,i} \sum_{i'} c_{\alpha',i'} \\
&\quad \times \langle EJTi|V_{NNN}|E'JTi'\rangle\,. \qquad (4.79)
\end{aligned}
$$

The $\tilde{T}_{\mathcal{J}}$-coefficients are now given by

$$
\begin{aligned}
&\tilde{T}_{\mathcal{J}}\begin{pmatrix} a & b & c & J_{ab} & J & \mathcal{J} \\ n_{cm} & l_{cm} & n_{12} & l_{12} & n_3 & l_3 \\ s_{ab} & j_{12} & j_3 & & & \end{pmatrix} \\
&= \sum_{L_{ab}}\sum_{\mathcal{L}_{12}}\sum_{\mathcal{L}}\sum_{S_3}\sum_{\Lambda}\sum_{L_3} \\
&\quad \times \delta_{2n_a+l_a+2n_b+l_b+2n_c+l_c,2n_{cm}+l_{cm}+2n_3+l_3+2n_{12}+l_{12}} \\
&\quad \times \langle\langle \mathcal{N}_{12}\mathcal{L}_{12},n_{12}l_{12};L_{ab}|n_al_a,n_bl_b\rangle\rangle_1\langle\langle n_{cm}l_{cm},n_3l_3;\Lambda|\mathcal{N}_{12}\mathcal{L}_{12},n_cl_c\rangle\rangle_2 \\
&\quad \times \begin{Bmatrix} l_a & l_b & L_{ab} \\ s_a & s_b & s_{ab} \\ j_a & j_b & J_{ab} \end{Bmatrix}\begin{Bmatrix} L_{ab} & l_c & \mathcal{L} \\ s_{ab} & s_c & S_3 \\ J_{ab} & j_c & \mathcal{J} \end{Bmatrix}\begin{Bmatrix} l_{12} & l_3 & L_3 \\ s_{ab} & s_c & S_3 \\ j_{12} & j_3 & J \end{Bmatrix} \\
&\quad \times \begin{Bmatrix} l_c & \mathcal{L}_{12} & \Lambda \\ l_{12} & \mathcal{L} & L_{ab} \end{Bmatrix}\begin{Bmatrix} l_{cm} & l_3 & \Lambda \\ l_{12} & \mathcal{L} & L_3 \end{Bmatrix}\begin{Bmatrix} l_{cm} & L_3 & \mathcal{L} \\ S_3 & \mathcal{J} & J \end{Bmatrix} \\
&\quad \times \hat{j}_a\hat{j}_b\hat{j}_c\hat{J}_{ab}\hat{j}_{12}\hat{j}_3\hat{s}_{ab}\hat{J}\hat{S}_3^2\hat{\mathcal{L}}^2\hat{\Lambda}^2\hat{L}_3^2\hat{L}_{ab}^2(-1)^{l_c+\Lambda+L_{ab}+\mathcal{L}+S_3+l_{12}+\mathcal{J}}\,, \qquad (4.80)
\end{aligned}
$$

In eq. (4.79), $\sum_\alpha$ denotes a sum over $\{n_{12},l_{12},s_{ab},j_{12},n_3,l_3,j_3,J\}$ and $\sum_{\alpha'}$ a sum over $\{n'_{12},l'_{12},s'_{ab},j'_{12},n'_3,l'_3,j'_3\}$. Moreover, the a,b,c in the symbol of the $\tilde{T}_{\mathcal{J}}$-coefficient indicate a dependence on n_a,l_a,j_a etc. but not a dependence on projection quantum numbers. Instead, they now depend on J_{ab}.

We can identify the advantages of this coupled scheme, from the last two equations. We have to calculate and store much fewer matrix elements, because single-particle projection quantum numbers are not resolved anymore. Furthermore, the matrix elements do not depend on the coupled $\mathcal{M}$ and M_T quantum num-

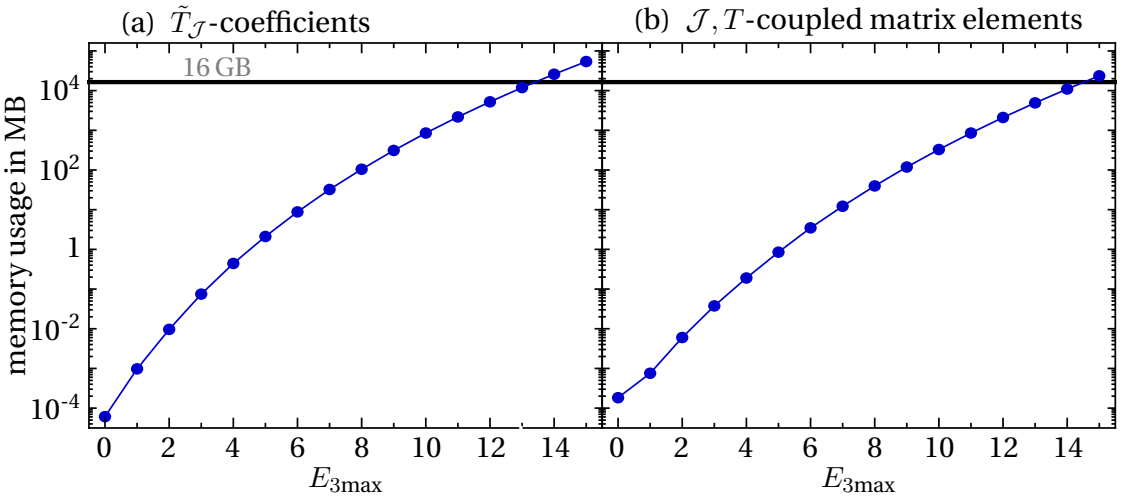

Figure 6 – *Memory usage of the $\tilde{T}_{\mathcal{J}}$-coefficients for the coupled scheme (a) and of the $\mathcal{J},T$-coupled matrix elements (b) as function of maximum total three-particle energy E_{3max}. The solid black line indicates the available memory of 16 GB in our cluster.*

bers. These properties are also translated into the new $\tilde{T}_{\mathcal{J}}$-coefficients, since all Clebsch-Gordan coefficients, which depend on projection quantum numbers, vanished. Instead the dependence on J_{ab} appears. But there are much less possible values for J_{ab} than for all projection quantum numbers.

We stress that in the many-body calculations m-scheme matrix elements are still needed. But, since the on-the-fly decoupling of the matrix elements (4.70), which can be stored in memory, is faster than retrieving the m-scheme matrix element from a file, the new coupled scheme is very helpful.

In fig. 6, we can see the improvement due to the $\mathcal{J}$-coupling. The memory usage of the precomputed $\tilde{T}_{\mathcal{J}}$-coefficients is shown in fig. 6(a) again as function of the maximum three-particle energy $E_{3\max}$. We still use the same storage scheme as for the $\tilde{T}$. However, we maintain a loop over the isospin T, despite the $\tilde{T}$-coefficients are independent of it, for convenience, because otherwise we would have to initialize a second $|\alpha\rangle$ basis. Now the $\tilde{T}$-memory usage reaches the 16 GB line relevant for our cluster for $E_{3\max} = 13$. Moreover, e.g. the $\tilde{T}_{\mathcal{J}}$-coefficients for $E_{3\max} = 10$ need now $\approx$ 850 MB memory which corresponds to by a factor 160 reduced memory demands compared with the $\tilde{T}$-coefficients we used before. This shows that the $\mathcal{J},T$-coupling of the states gives access to larger three-particle energies than the m-scheme states before. The same is true when we look at the memory usage of the $\mathcal{J},T$-coupled matrix elements, shown in figure 6(b). Here, calculations up to $E_{3\max} = 12$ are accessible, which was impossible with our old strategy using m-scheme matrix elements. The reduction of the memory usage for the matrix elements is not only due to the $\mathcal{J},T$-coupling, because we changed additionally the storage scheme. We now store only the bare double precision values of the matrix

elements in . The identification of the corresponding bra and ket states is done with help of the ordering of the matrix elements.

Obviously, the coupled scheme cannot completely remove the problems but it shifts the limits to higher three-particle energies and, therefore, enables much more reasonable calculations. At the moment our implementation can handle the calculation of coupled matrix elements up to $E_{3\text{max}} = 12$. Accordingly, we present results of NCSM calculations which use matrix elements up to this energy in section 6.

The next step will be to push the energy limit to $E_{3\text{max}} = 14$ and 16 by dividing the interaction matrix into appropriate parts so that its calculation can be spread over a number of nodes. Then, each node only needs a certain number of distinct $\tilde{T}_{\mathcal{J}}$-coefficients which will reduce the memory consumption per node. More details on our current implementation are given in appendix A.

SECTION 5

Similarity renormalization group transformation

The similarity renormalization group (SRG) transformation is a tool to soften an interaction, i.e. to pre-diagonalize its matrix representation. It was first formulated in light-front field theory [23] and in condensed matter physics [24, 25].

We apply the SRG transformation to the nuclear interaction to handle its short range correlations resulting from the strong repulsion at small inter-nucleon distances. The general concept of SRG is a unitary transformation of the considered Hamiltonian in the way that its matrix representation becomes band- or block-diagonal for a specific basis. As we will see in section 6, this leads to significantly improved convergence properties in many-body calculations with respect to model-space size.

In section 5.1 we present the general formalism of the SRG transformation, including the renormalization group flow equation. The solution of this flow equation is discussed in 5.2. For our applications in section 6 and the proper investigation of the impact of the three-nucleon force on our results, it is necessary to separate the three-nucleon force from the two-nucleon force. Since we get matrix elements of the combined interactions out of the SRG transformation, we investigate the decomposition into the three-nucleon and the two-nucleon contributions in section 5.3.

5.1 General formalism

The basic idea of a similarity renormalization group transformation is to carry out a unitary transformation of the Hamilton operator of a many-body system such

that its matrix representation becomes more diagonal with respect to a specific basis. Since the unitary transformation does not change the eigenvalues of the operator, we can use the transformed operator to solve the eigenvalue problem. This is advantageous, because due to the softer character of the transformed interaction we need smaller model spaces to obtain converged results in many-body calculations using the transformed Hamiltonian compared to calculations with the bare interaction.

For the transformation we employ a unitary operator $\boldsymbol{U}_\alpha$ depending continuously on a flow parameter α. Thus, the unitary transformation of the initial Hamiltonian $\boldsymbol{H}_0$ is given by

$$\boldsymbol{H}_\alpha = \boldsymbol{U}_\alpha^\dagger \boldsymbol{H}_0 \boldsymbol{U}_\alpha \,. \tag{5.1}$$

To derive the renormalization group flow equation we differentiate with respect to α, i.e.

$$\frac{\mathrm{d}}{\mathrm{d}\alpha}\boldsymbol{H}_\alpha = \big(\frac{\mathrm{d}}{\mathrm{d}\alpha}\boldsymbol{U}_\alpha^\dagger\big)\boldsymbol{H}_0\boldsymbol{U}_\alpha + \boldsymbol{U}_\alpha^\dagger\boldsymbol{H}_0\big(\frac{\mathrm{d}}{\mathrm{d}\alpha}\boldsymbol{U}_\alpha\big) \,. \tag{5.2}$$

For further simplification we can use $\boldsymbol{U}_\alpha\boldsymbol{U}_\alpha^\dagger = \mathbb{1}$, leading to

$$\frac{\mathrm{d}}{\mathrm{d}\alpha}\boldsymbol{U}_\alpha = -\boldsymbol{U}_\alpha\frac{\mathrm{d}\boldsymbol{U}_\alpha^\dagger}{\mathrm{d}\alpha}\boldsymbol{U}_\alpha \,. \tag{5.3}$$

Using this and eq. (5.1) we can simplify eq. (5.2), yielding

$$\begin{aligned}\frac{\mathrm{d}}{\mathrm{d}\alpha}\boldsymbol{H}_\alpha &= \frac{\mathrm{d}\boldsymbol{U}_\alpha^\dagger}{\mathrm{d}\alpha}\boldsymbol{U}_\alpha\boldsymbol{U}_\alpha^\dagger\boldsymbol{H}_0\boldsymbol{U}_\alpha + \boldsymbol{U}_\alpha^\dagger\boldsymbol{H}_0\boldsymbol{U}_\alpha\boldsymbol{U}_\alpha^\dagger\frac{\mathrm{d}\boldsymbol{U}_\alpha}{\mathrm{d}\alpha} \\ &= -\boldsymbol{U}_\alpha^\dagger\frac{\mathrm{d}\boldsymbol{U}_\alpha}{\mathrm{d}\alpha}\boldsymbol{H}_\alpha + \boldsymbol{H}_\alpha\boldsymbol{U}_\alpha^\dagger\frac{\mathrm{d}\boldsymbol{U}_\alpha}{\mathrm{d}\alpha} \\ &= \big[-\boldsymbol{U}_\alpha^\dagger\frac{\mathrm{d}\boldsymbol{U}_\alpha}{\mathrm{d}\alpha}, \boldsymbol{H}_\alpha\big] \,,\end{aligned} \tag{5.4}$$

where we introduced a commutator in the last line. Thus we have to solve an initial value problem with initial condition $\boldsymbol{H}_{\alpha=0} = \boldsymbol{H}_0$ to find the transformed Hamiltonian $\boldsymbol{H}_\alpha$. Moreover, we define

$$\boldsymbol{\eta}_\alpha = -\boldsymbol{U}_\alpha^\dagger\frac{\mathrm{d}\boldsymbol{U}_\alpha}{\mathrm{d}\alpha} \tag{5.5}$$

as the generator of the transformation. Finally, the flow equations for the Hamil-

tonian $\boldsymbol{H}_\alpha$ and analogously for any other observable $\boldsymbol{O}_\alpha$ are given by

$$\frac{\mathrm{d}\boldsymbol{H}_\alpha}{\mathrm{d}\alpha} = \left[\boldsymbol{\eta}_\alpha, \boldsymbol{H}_\alpha\right], \tag{5.6}$$

$$\frac{\mathrm{d}\boldsymbol{O}_\alpha}{\mathrm{d}\alpha} = \left[\boldsymbol{\eta}_\alpha, \boldsymbol{O}_\alpha\right]. \tag{5.7}$$

Obviously, the physics of the transformation is determined by the generator we use. Typically the generator contains the evolved Hamiltonian, so that the flow equation for observable $\boldsymbol{O}$ has to be solved simultaneously with the one for the Hamiltonian.

One important property of $\boldsymbol{\eta}_\alpha$ is its antihermitian character, since

$$\boldsymbol{\eta}_\alpha + \boldsymbol{\eta}_\alpha^\dagger = -\frac{\mathrm{d}}{\mathrm{d}\alpha}\left(\boldsymbol{U}_\alpha \boldsymbol{U}_\alpha^\dagger\right) = -\frac{\mathrm{d}}{\mathrm{d}\alpha}\mathbb{1} = 0 \;\Rightarrow\; \boldsymbol{\eta}_\alpha = -\boldsymbol{\eta}_\alpha^\dagger \tag{5.8}$$

holds. Thus, a typical choice for the generator is a commutator of a hermitian operator with the evolved Hamiltonian $\boldsymbol{H}_\alpha$, because this construct is always antihermitian.

In the literature, many possibilities of different generators are discussed. The first use of this approach by Wegner employed the generator

$$\boldsymbol{\eta}_\alpha = \left[\mathrm{diag}(\boldsymbol{H}_\alpha), \boldsymbol{H}_\alpha\right], \tag{5.9}$$

where $\mathrm{diag}(\boldsymbol{H}_\alpha)$ denotes the diagonal part of the Hamilton matrix in a certain basis [24]. Obviously, the generator does not affect the form of the matrix once it reached diagonal from during the flow, since the commutator vanishes in this case. Therefore, the basis used for representation of $\mathrm{diag}(\boldsymbol{H}_\alpha)$ defines the basis with respect to which the Hamiltonian is diagonalized. Furthermore, plugging this ansatz for the generator into the flow equation (5.6), one can show that the sum of the squares of the off-diagonal matrix elements decreases monotonically.

Throughout this thesis we employ the commutator of the intrinsic kinetic energy

$$\boldsymbol{T}_{int} = \boldsymbol{T} - \boldsymbol{T}_{cm} \tag{5.10}$$

with the evolved Hamiltonian as generator

$$\boldsymbol{\eta}_\alpha = (2\mu)^2 \left[\boldsymbol{T}_{int}, \boldsymbol{H}_\alpha\right]. \tag{5.11}$$

This form was proposed by Szpigel and Perry [26] and first used by Bogner et. al. [27]. The flow parameter α has dimension [length^4] due to the prefactor $(2\mu)^2$,

with $\mu = \frac{m_N}{2}$ as reduced nucleon mass. We omit the prefactor in the following for brevity. The square of the relative momentum operator, hidden in $\boldsymbol{T}_{int}$, can be rewritten as

$$\vec{\boldsymbol{q}}^2 = \vec{\boldsymbol{q}}_r^2 + \frac{\vec{\boldsymbol{L}}^2}{r^2}\,, \tag{5.12}$$

with $\vec{\boldsymbol{q}}_r$ as radial part of the momentum and $\vec{\boldsymbol{L}}$ as orbital angular momentum. Therefore, this generator leads to a band-diagonal matrix in momentum representation. This causes a decoupling of high- and low-momentum parts of the interaction with a conversion of the high momentum information of the interaction into the low-momentum regime. As a consequence, the short-range repulsion of the interaction is already taken into account in lower-momenta matrix elements of the transformed Hamiltonian. This causes a softer interaction and much better convergence properties in NCSM-type calculations, as we will see in section 6.

One crucial feature of the SRG transformation in an A-body system is the generation of irreducible many-body interactions up to the A-body level. This can be seen by explicitly working out the commutator relations on the right-hand side of eq. (5.6) with operators in second quantization. In general, a unitary transformation of a one-body operator is given by

$$\boldsymbol{U}^\dagger\, \boldsymbol{T}^{[1]}\, \boldsymbol{U} = \boldsymbol{T}^{[1]} + \tilde{\boldsymbol{T}}^{[2]} + \ldots + \tilde{\boldsymbol{T}}^{[A]}\,, \tag{5.13}$$

where the number in the brackets denotes the number of particles that are connected by the operator. The tilde indicates that short-range correlations are tamed in the operators in the sense that they are less repulsive at short distances. We see that the one-body component itself does not change via the unitary transformation. For all interactions of higher particle-order this is the case, e.g., a unitary transformation of a two-body operator yields

$$\boldsymbol{U}^\dagger\, \boldsymbol{V}_{NN}^{[2]}\, \boldsymbol{U} = \tilde{\boldsymbol{V}}_{NN}^{[2]} + \tilde{\boldsymbol{V}}_{NN}^{[3]} + \cdots + \tilde{\boldsymbol{V}}_{NN}^{[A]}\,, \tag{5.14}$$

with $\tilde{\boldsymbol{V}}_{NN}^{[2]}$ as the new two-body operator. Therefore, starting with a Hamiltonian including genuine three-body forces yields the following structure of the transformed Hamiltonian

$$\boldsymbol{U}^\dagger\, \boldsymbol{H}\, \boldsymbol{U} = \boldsymbol{T}^{[1]} + \left(\tilde{\boldsymbol{T}}^{[2]} + \tilde{\boldsymbol{V}}_{NN}^{[2]}\right) + \left(\tilde{\boldsymbol{T}}^{[3]} + \tilde{\boldsymbol{V}}_{NN}^{[3]} + \tilde{\boldsymbol{V}}_{NNN}^{[3]}\right) + \ldots\,. \tag{5.15}$$

For practical applications of the SRG transformation it is not possible to take all induced interactions into account. Therefore, we limit the evolution to two- or

three-body space. This implies that higher-order many-body interactions are discarded. Obviously, omitting of these higher-order many-body interactions destroys the unitarity of the transformation. We will find the signature of this truncation in our results in section 6. We refer to

$$\boldsymbol{V}_{ind}^{[3]} = \tilde{\boldsymbol{T}}^{[3]} + \tilde{\boldsymbol{V}}_{NN}^{[3]} \tag{5.16}$$

as induced three-particle interaction.

The next step is the solution of the flow equation (5.6) to obtain the transformed Hamiltonian $\boldsymbol{H}_\alpha$. Expansion of the commutators on the right-hand side leads to

$$\frac{\mathrm{d}\boldsymbol{H}_\alpha}{\mathrm{d}\alpha} = \boldsymbol{T}_{int}\boldsymbol{H}_\alpha\boldsymbol{H}_\alpha - 2\boldsymbol{H}_\alpha\boldsymbol{T}_{int}\boldsymbol{H}_\alpha + \boldsymbol{H}_\alpha\boldsymbol{H}_\alpha\boldsymbol{T}_{int}\,. \tag{5.17}$$

However, the solution of this operator equation is not trivial. Thus, we will switch to a matrix-element representation of eq. (5.17) for the practical implementation and solution, as described in the next subsection.

5.2 Solution of the flow equation

In this subsection we concentrate on the solution of the SRG flow equation for the Hamiltonian (5.17). Since we want to compare the impact of the induced three-body interaction that are lost during the SRG transformation in two-body space with the full inclusion of genuine three-nucleon forces later on, we have to solve the flow equations for three situations separately. Firstly, we investigate the evolution in three-body space including a genuine three-body force in subsection 5.2.1. In subsection 5.2.2 we discuss the flow in three-body space with an initial two-body force only. Finally, in subsection 5.2.3, we concentrate on the evolution in two-body space again with initial two-body force.

5.2.1 Evolution in three-body space including a genuine three-body force

We start with the evolution of the Hamiltonian including a two- plus three-nucleon force in the three-particle space. Thus, we use as initial Hamiltonian

$$\boldsymbol{H}_0 = \boldsymbol{T}_{int} + \boldsymbol{V}_{NN}^{N3LO} + \boldsymbol{V}_{NNN}^{N2LO}\,, \tag{5.18}$$

with the two-nucleon interaction at N3LO and the three-nucleon interaction at N2LO of χPT as introduced in section 2. For the solution of the flow equation (5.17), we use a matrix-element representation with respect to the fully antisymmetrized relative states $|EJTi\rangle$, defined in eq. (3.91). We sandwich eq. (5.17) with these

states and obtain

$$\begin{aligned}\frac{\mathrm{d}}{\mathrm{d}\alpha}\langle EJTi|\boldsymbol{H}_\alpha|E'J'T'i'\rangle = \quad & \langle EJTi|\boldsymbol{T}_{int}\boldsymbol{H}_\alpha\boldsymbol{H}_\alpha|E'J'T'i'\rangle \\ & -2\,\langle EJTi|\boldsymbol{H}_\alpha\boldsymbol{T}_{int}\boldsymbol{H}_\alpha|E'J'T'i'\rangle \\ & +\langle EJTi|\boldsymbol{H}_\alpha\boldsymbol{H}_\alpha\boldsymbol{T}_{int}|E'J'T'i'\rangle\,. \end{aligned} \tag{5.19}$$

We omitted the projection quantum numbers M_J and M_T for brevity. From the MANYEFF-code we obtain matrix elements of the intrinsic kinetic energy $\boldsymbol{T}_{int}$ and of the total Hamiltonian $\boldsymbol{H}_{\alpha=0}$, given in eq. (5.18). Therefore, we insert identity operators between all operators on the right-hand side of eq. (5.19), yielding

$$\begin{aligned}&\frac{\mathrm{d}}{\mathrm{d}\alpha}\langle EJTi|\boldsymbol{H}_\alpha|E'J'T'i'\rangle = \\ &\quad\sum_{E''J''T''i''}\sum_{E'''J'''T'''i'''} \\ &\quad\langle EJTi|\boldsymbol{T}_{int}|E''J''T''i''\rangle\langle E''J''T''i''|\boldsymbol{H}_\alpha|E'''J'''T'''i'''\rangle\langle E'''J'''T'''i'''|\boldsymbol{H}_\alpha|E'J'T'i'\rangle \\ &-2\,\langle EJTi|\boldsymbol{H}_\alpha|E''J''T''i''\rangle\langle E''J''T''i''|\boldsymbol{T}_{int}|E'''J'''T'''i'''\rangle\langle E'''J'''T'''i'''|\boldsymbol{H}_\alpha|E'J'T'i'\rangle \\ &\quad+\langle EJTi|\boldsymbol{H}_\alpha|E''J''T''i''\rangle\langle E''J''T''i''|\boldsymbol{H}_\alpha|E'''J'''T'''i'''\rangle\langle E'''J'''T'''i'''|\boldsymbol{T}_{int}|E'J'T'i'\rangle\,. \end{aligned} \tag{5.20}$$

Furthermore, we make use of the fact that the interaction does not change the J and T quantum numbers, i.e.,

$$\begin{aligned}&\frac{\mathrm{d}}{\mathrm{d}\alpha}\langle EJTi|\boldsymbol{H}_\alpha|E'JTi'\rangle = \\ &\sum_{E''i''}\sum_{E'''i'''} \quad \langle EJTi|\boldsymbol{T}_{int}|E''JTi''\rangle\langle E''JTi''|\boldsymbol{H}_\alpha|E'''JTi'''\rangle\langle E'''JTi'''|\boldsymbol{H}_\alpha|E'JTi'\rangle \\ &\quad -2\langle EJTi|\boldsymbol{H}_\alpha|E''JTi''\rangle\langle E''JTi''|\boldsymbol{T}_{int}|E'''JTi'''\rangle\langle E'''JTi'''|\boldsymbol{H}_\alpha|E'JTi'\rangle \\ &\quad +\langle EJTi|\boldsymbol{H}_\alpha|E''JTi''\rangle\langle E''JTi''|\boldsymbol{H}_\alpha|E'''JTi'''\rangle\langle E'''JTi'''|\boldsymbol{T}_{int}|E'JTi'\rangle\,. \end{aligned} \tag{5.21}$$

Moreover, we know that the interaction does not change the parity of the states. Therefore, the above coupled differential equations decouple for each T-J-parity block and they can be solved for each block separately.

For the solution of the system of ordinary differential equations, we use a Runge-Kutta algorithm with adaptive step size control. Adaptive step size control is indispensable, since the main effect of the flow occurs at the beginning for very low α parameters. Accordingly, these effects should be considered with very high precision, by using a very small step size. For larger α parameters the step size can be increased. Thus the adaptive step size enables reasonable run times of the algo-

rithm. For more technical details on the implementation we refer to app. A.

Special attention should be payed on the summation limits of the identity operators in eq. (5.21). In principle, they should run over an infinity number of states $|EJTi\rangle$. Since this is obviously impossible we truncate these summations by defining a maximum energy quantum number for these sums denoted by E_{3SRG}. We will study the convergence of the results of the SRG transformation with respect to this truncation in section 6 .

After the SRG transformation we subtract the initial intrinsic kinetic energy $\boldsymbol{T}_{int}$ to obtain the transformed interaction matrix element, i.e.,

$$\langle EJTi|\big(\boldsymbol{H}_\alpha - \boldsymbol{T}_{int}\big)|E'JTi'\rangle = \langle EJTi|\big(\tilde{\boldsymbol{T}}^{[2]}_{int} + \tilde{\boldsymbol{V}}^{[2]}_{NN} + \tilde{\boldsymbol{T}}^{[3]}_{int} + \tilde{\boldsymbol{V}}^{[3]}_{NN} + \tilde{\boldsymbol{V}}^{[3]}_{NNN}\big)|E'JTi'\rangle\,, \tag{5.22}$$

where $\tilde{\boldsymbol{T}}^{[3]}_{int} + \tilde{\boldsymbol{V}}^{[3]}_{NN}$ is the induced three-body force. Note that the SRG transformed contributions of the intrinsic kinetic energy is handled different from the interactions, because $\tilde{\boldsymbol{T}}^{[2]}_{int}$ is the *correction* to $\boldsymbol{T}_{int}$ on the two-body level.

In fig. 7(a) we see the absolute value of the intrinsic kinetic energy matrix elements in the $|EJTi\rangle$ basis up to $E = 28$ as it appears in the generator $\boldsymbol{\eta}_\alpha$ of the SRG flow equation. In figs. 7(b)-(f) and 8 we see the change of the absolute value of the interaction matrix elements (5.22) during the flow for various α parameters from $\alpha = 0.0\,\mathrm{fm}^4$ up to $\alpha = 5.52\,\mathrm{fm}^4$ for $J = \frac{1}{2}$, $T = \frac{1}{2}$ and positive parity. Zero values are indicated by black and larger values are indicated over yellow to white colors. The block structure that can be seen corresponds to the different blocks with E and E' quantum numbers.

We expect the interaction matrix to flow towards the matrix representation of the intrinsic kinetic energy, as this is a fix point of the flow equation. This behavior can be identified in the matrix plots. In fig. 7(b) we see the interaction matrix before the transformation which has all kinds of large matrix elements. During the flow the matrix elements in the upper right and lower left corner are suppressed. These are the matrix elements between high and low energy states. From $\alpha = 0.16\,\mathrm{fm}^4$ to $\alpha = 5.12\,\mathrm{fm}^4$ the changes of the far off-diagonal matrix elements is not that large, but in this range we recognize an enhancement of the matrix elements in the diagonal blocks which carry the same energy quantum number in bra and ket. Thus the matrix flows towards a band block-diagonal from that is similar to the matrix representation of the intrinsic kinetic energy.

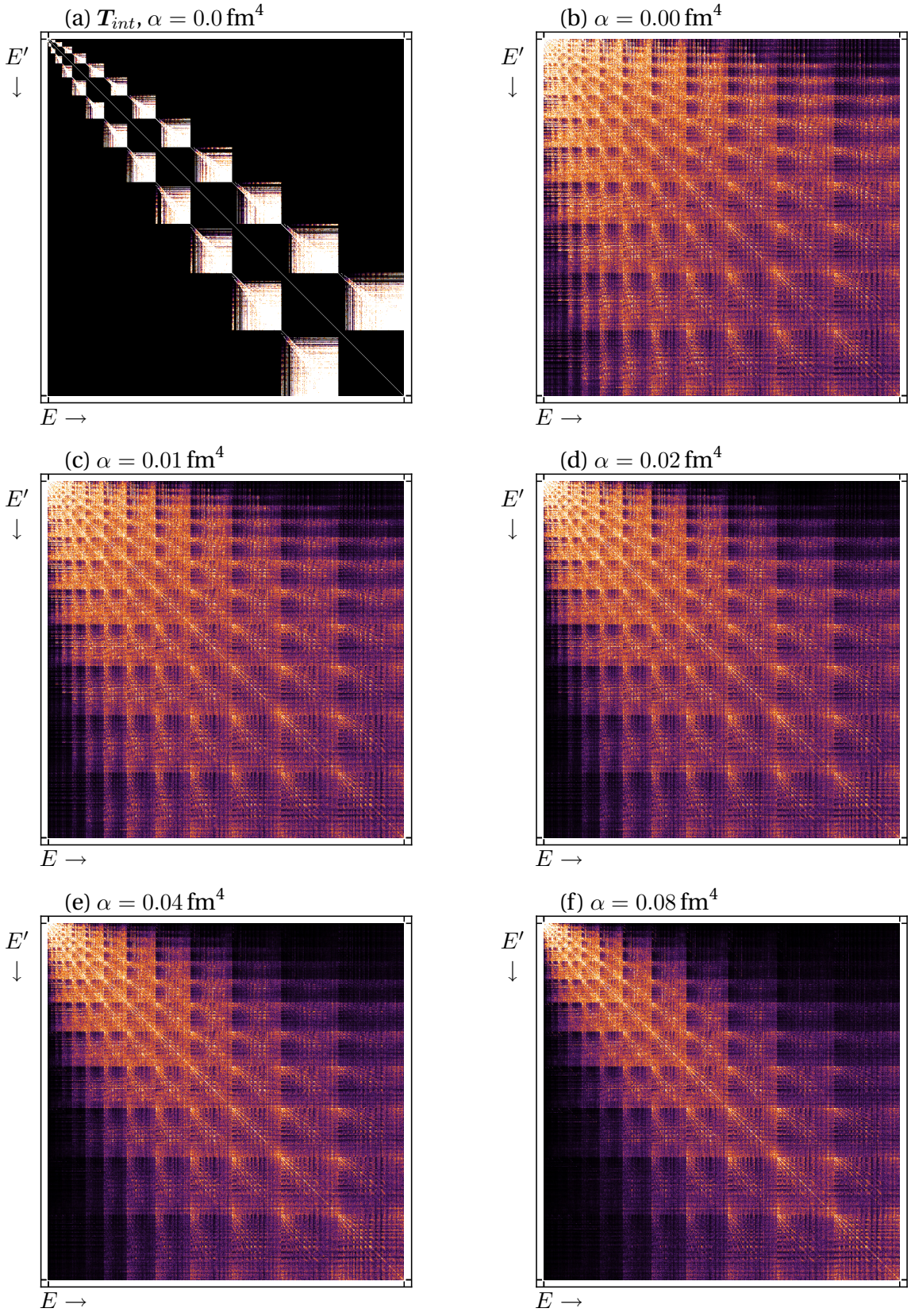

Figure 7 – *(a) Matrix elements of the intrinsic kinetic energy with respect to $|EJTi\rangle$ states as it appears in the generator η_α. (b)-(f) Interaction matrix elements with respect to $|EJTi\rangle$ states for $J = \frac{1}{2}$, $T = \frac{1}{2}$ and positive parity during the SRG flow up to $E = 28$.*

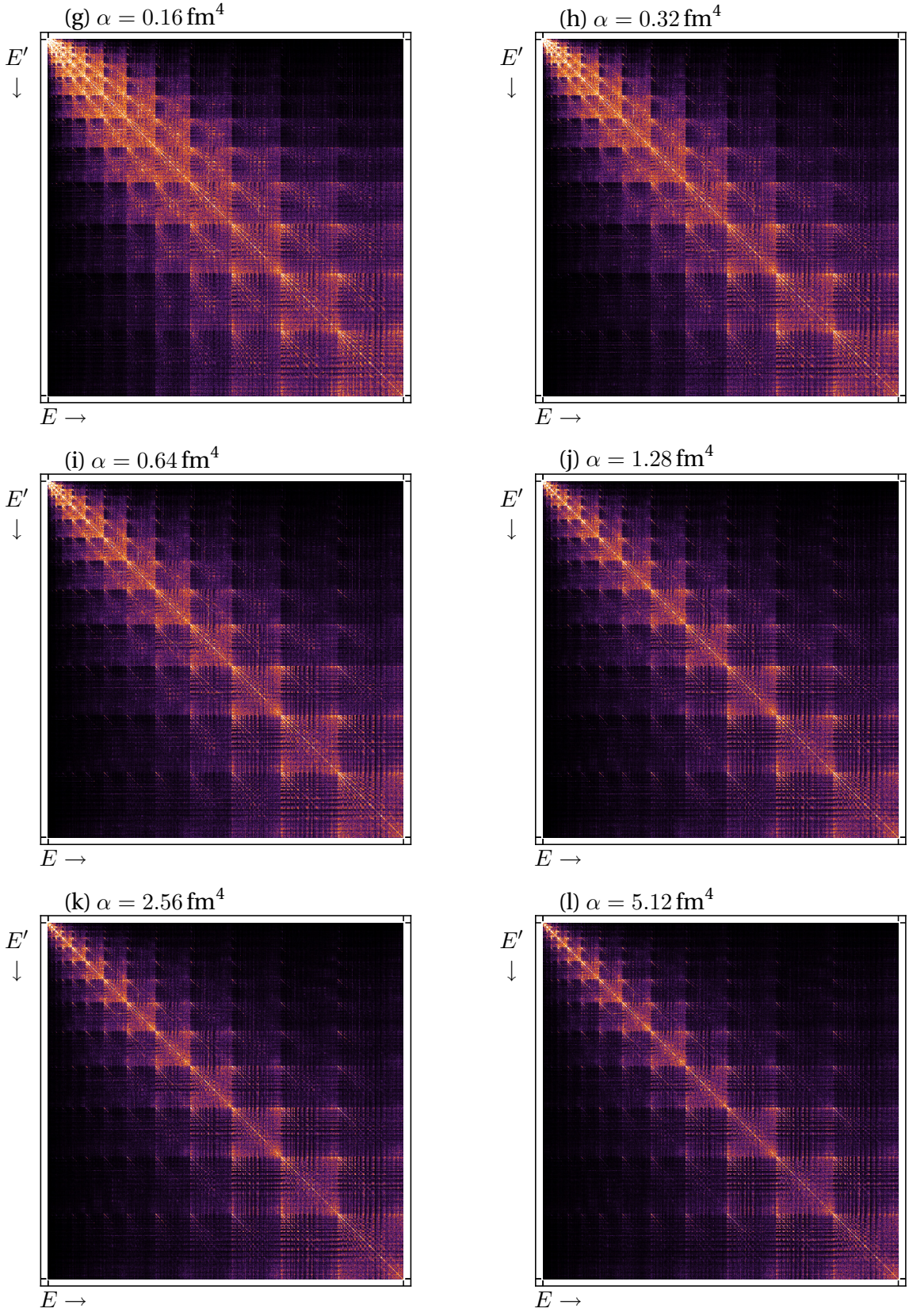

Figure 8 – *(g)-(l) Interaction matrix elements with respect to* $|EJTi\rangle$ *states for* $J = \frac{1}{2}$, $T = \frac{1}{2}$ *and positive parity during the SRG flow up to* $E = 28$.

5.2.2 Evolution in three-body space with initial two-nucleon interaction only

Now, we discuss the evolution of a Hamiltonian including only the N3LO two-body interaction in the three-body space. Even in the generator $\boldsymbol{\eta}_\alpha$ of the SRG transformation this Hamiltonian appears. Thus, the initial Hamiltonian and generator are given by

$$\boldsymbol{H}_0 = \boldsymbol{T}_{int} + \boldsymbol{V}_{NN}^{N3LO} \qquad \boldsymbol{\eta}_{\alpha=0} = \left[\boldsymbol{T}_{int}, \boldsymbol{H}_{\alpha=0}\right] . \tag{5.23}$$

Besides, there are no changes on the presented procedure of section 5.2.1. In particular, we use the same basis states $|EJTi\rangle$ for the matrix element representation and we again get the matrix elements from the MANYEFF-Code.

Since we work with three-nucleon states, the evolved matrix elements also include induced three-body forces, but no transformed parts of the genuine three-body interaction. Again, we subtract the intrinsic kinetic energy after the SRG transformation and obtain the SRG transformed interaction matrix elements as

$$\langle EJTi|\big(\boldsymbol{H}_\alpha - \boldsymbol{T}_{int}\big)|E'JTi'\rangle = \langle EJTi|\big(\tilde{\boldsymbol{T}}_{int}^{[2]} + \tilde{\boldsymbol{V}}_{NN}^{[2]} + \tilde{\boldsymbol{T}}_{int}^{[3]} + \tilde{\boldsymbol{V}}_{NN}^{[3]}\big)|E'JTi'\rangle\,, \tag{5.24}$$

where $\tilde{\boldsymbol{T}}_{int}^{[3]} + \tilde{\boldsymbol{V}}_{NN}^{[3]}$ is the induced three-body force.

We stress that the induced three-nucleon force here is different from the one we obtained in the last subsection. This is caused by the different generators. In the last subsection the generator contains initially the genuine three-body interaction, whereas it contains here initially only the two-body interaction. Later on we want to compare the influence of the genuine three-nucleon interactions on our results to the situation without initial genuine three-nucleon force. Therefore, we only investigate the induced three-body force from the evolution in three-body space without three-body interaction in the initial Hamiltonian separately, namely the one we identified in eq. (5.24).

5.2.3 Evolution in two-body space

Finally, we present the evolution in the two-body space of the Hamiltonian including a two-nucleon interaction. Therefore, the initial Hamilton operator reads again

$$\boldsymbol{H}_0 = \boldsymbol{T}_{int} + \boldsymbol{V}_{NN}^{N3LO}\,. \tag{5.25}$$

The difference to the evolution described in the last subsection is that we now work exclusively in the two-body space. The flow equation for the operator is the same

as in eq. (5.17), but now we use the J-coupled two-body relative states

$$|(nl,S)JM_J,TM_T\rangle\,. \tag{5.26}$$

for the transition into matrix-element representation. Here, n and l are two-body relative harmonic oscillator radial and orbital angular momentum quantum numbers. Moreover, $\vec{\boldsymbol{l}}$ couples with the coupled spin of the two particles $\vec{\boldsymbol{S}}$ to total angular momentum of the two nucleons denoted by the quantum number J and its projection quantum number M_J. Finally the isospins of both particles are coupled to total isospin $\vec{\boldsymbol{T}}$.

Since this is a two-body basis, no three- or higher-order many-body interactions remain during the SRG flow. Thus, the transformed interaction matrix elements are given by

$$\begin{aligned}&\langle(nl,S)JM_J,TM_T|\big(\boldsymbol{H}_\alpha-\boldsymbol{T}_{int}\big)|(n'l',S')JM_J,TM_T\rangle\\ &\quad=\ \langle(nl,S)JM_J,TM_T|\big(\tilde{\boldsymbol{T}}^{[2]}_{int}+\tilde{\boldsymbol{V}}^{[2]}_{NN}\big)|(n'l',S')JM_J,TM_T\rangle\end{aligned} \tag{5.27}$$

Finally, we stress that the operators $\tilde{\boldsymbol{T}}^{[2]}_{int}+\tilde{\boldsymbol{V}}^{[2]}_{NN}$ are the same as in eqs. (5.24) and (5.22), though different generators were used for the transformations. This results from the fact that two-particle interactions are not affected by the included three-particle interactions during the flow and can be verified by explicitly working out the commutators on the right-hand side of the flow equation.

To discuss the influence of the three-nucleon force, either induced or genuine, on the results of the many-body calculations we have to separate it from the two-nucleon force. This will be done in the following subsection.

5.3 Separation of the transformed three-nucleon interaction

In order to study the impact of the different interactions on the results of many-body calculations we have to subtract the two-body part of the interaction matrix elements in eqs. (5.24) and (5.22) yielding matrix elements of the induced three-body force and matrix elements of induced plus transformed genuine three-body forces, respectively.

To carry out calculations for a three-body system, e.g. the triton, we can use the matrix elements that result from the SRG transformation without any change. But in order to study A-particle systems we must subtract the two-body interaction contributions from the SRG transformed matrix elements, because otherwise the two-body interaction get the wrong weight during a direct calculation with the transformed matrix elements.

Now we investigate the separation of the three-nucleon force, therefore, we follow the strategy shown in the flow chart in fig. 9. In the following, we briefly discuss each step and give the formulas if necessary.

We see two main paths independent from each other until the matrix elements are subtracted. The left path describes how the matrix elements containing induced or induced-plus-genuine three-body forces have to be prepared for the subtraction. All necessary steps from this path were already discussed: first we solve the SRG flow equation in three-body space and obtain matrix elements including three-body forces. Then, these matrix elements are transformed into the $\mathcal{J},T$-coupled scheme as described in section 4.4. After that the matrix elements are ready for the subtraction of the two-nucleon part.

For a consistent subtraction we convert the matrix elements of the two-nucleon forces into three-particle matrix elements in the $\mathcal{J},T$-coupled scheme, too. The individual steps are shown in the right path of the flowchart in fig. 9. We start with matrix elements of $\boldsymbol{T}_{int} + \boldsymbol{V}_{NN}$ using the two-body Jacobi basis

$$|(nl,S)JM_J,TM_T\rangle\,, \tag{5.28}$$

as described in section 5.2.3, whereat we omitted the isospin in fig. 9 for brevity. The first step is to solve the SRG flow equation for these matrix elements, as described in section 5.2.3. The SRG transformed two-body relative interaction matrix elements

$$\langle(nl,S)JM_J,TM_T|\tilde{\boldsymbol{T}}^{[2]}_{int} + \tilde{\boldsymbol{V}}^{[2]}_{NN}|(n'l',S)JM_J,TM_T\rangle \tag{5.29}$$

are then converted into $\mathfrak{J}$-coupled two-body matrix elements including the center-of-mass degrees of freedom. This is the analogous transformation as in section 4, but on two-body level. Accordingly, this transformation is simpler and well-known from many applications, e.g. see [28]. The interested reader can find the transformation formulas in appendix B.

The $\mathfrak{J}$-coupled matrix elements read

$$\langle[(n_al_a,s_a)j_a,(n_bl_b,s_b)j_b]\mathfrak{J}\mathfrak{M}_\mathfrak{J},TM_T|\tilde{\boldsymbol{T}}^{[2]}_{int} + \tilde{\boldsymbol{V}}^{[2]}_{NN}|[(n'_al'_a,s_a)j'_a,(n'_bl'_b,s_b)j'_b]\mathfrak{J}\mathfrak{M}_\mathfrak{J},TM_T\rangle\,, \tag{5.30}$$

where the orbital angular momentum quantum numbers l_i are defined with respect to the single-particle coordinates.

Next, we break up the (jj)-coupling of the states, yielding two-body m-scheme matrix elements. Thereby, we encounter Clebsch-Gordan coefficients. The trans-

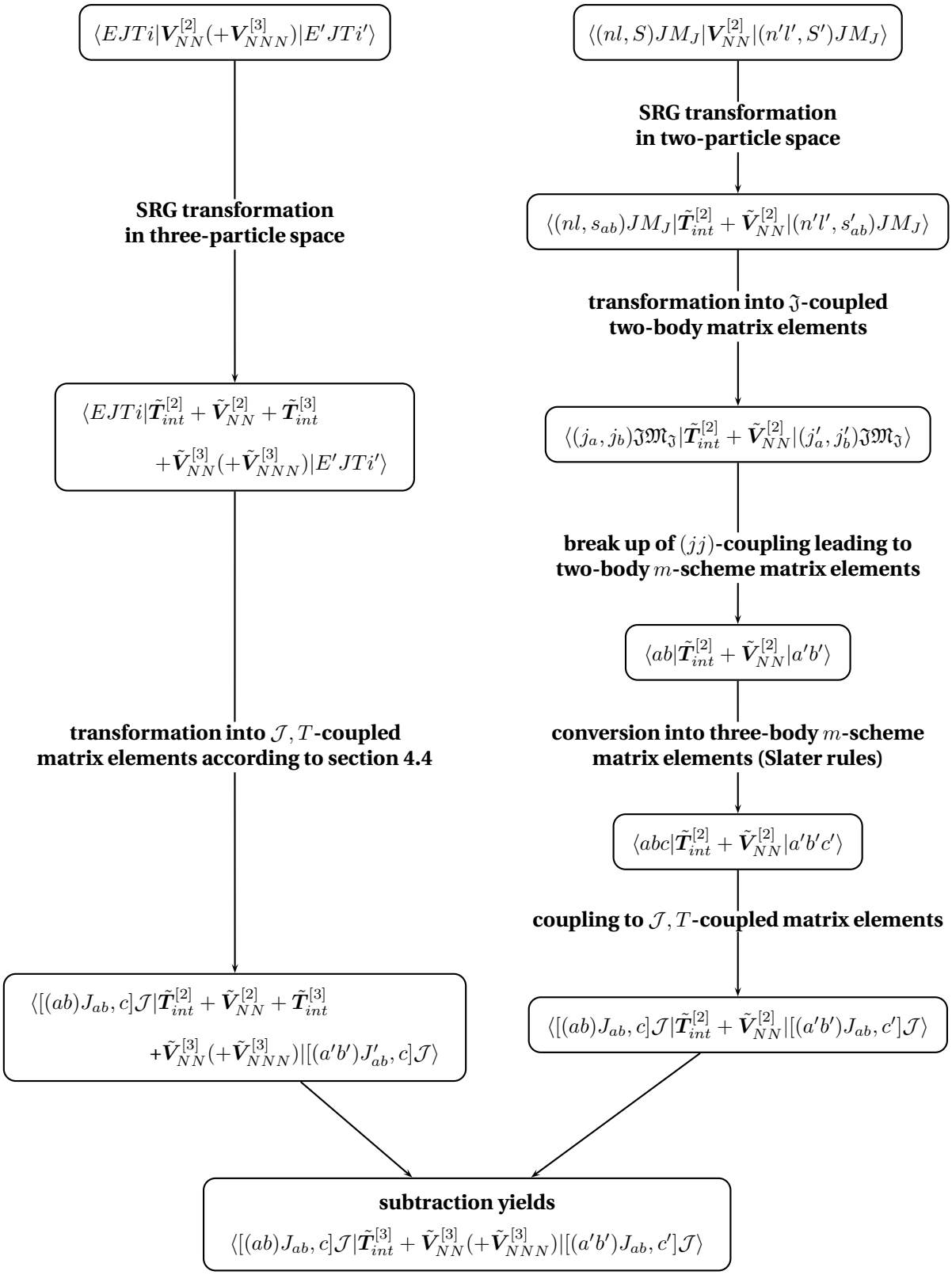

Figure 9 – *Steps towards the consistent separation of the three-nucleon force. The isospin is omitted for brevity.*

formation is given by

$$\langle (n_a l_a, s_a) j_a m_a, (n_b l_b, s_b) j_b m_b, t_a m_{t_a} t_b m_{t_b} | \tilde{\boldsymbol{T}}^{[2]}_{int} + \tilde{\boldsymbol{V}}^{[2]}_{NN} \times | (n'_a l'_a, s_a) j'_a m'_a, (n'_b l'_b, s_b) j'_b m'_b, t_a m'_{t_a} t_b m'_{t_b} \rangle$$

$$= \sum_{\mathfrak{J}\mathfrak{M}_\mathfrak{J}} \sum_{TM_T} \left(\begin{matrix} j_a & j_b \\ m_a & m_b \end{matrix} \middle| \begin{matrix} \mathfrak{J} \\ \mathfrak{M}_\mathfrak{J} \end{matrix} \right) \left(\begin{matrix} j'_a & j'_b \\ m'_a & m'_b \end{matrix} \middle| \begin{matrix} \mathfrak{J} \\ \mathfrak{M}_\mathfrak{J} \end{matrix} \right) \left(\begin{matrix} t_a & t_b \\ m_{t_a} & m_{t_b} \end{matrix} \middle| \begin{matrix} T \\ M_T \end{matrix} \right) \left(\begin{matrix} t_a & t_b \\ m'_{t_a} & m'_{t_b} \end{matrix} \middle| \begin{matrix} T \\ M_T \end{matrix} \right) \tag{5.31}$$

$$\times \langle [(n_a l_a, s_a) j_a, (n_b l_b, s_b) j_b] \mathfrak{J}\mathfrak{M}_\mathfrak{J}, TM_T | \tilde{\boldsymbol{T}}^{[2]}_{int} + \tilde{\boldsymbol{V}}^{[2]}_{NN} | [(n'_a l'_a, s_a) j'_a, (n'_b l'_b, s_b) j'_b] \mathfrak{J}\mathfrak{M}_\mathfrak{J}, TM_T \rangle$$

The matrix elements (5.31) are then converted into three-body matrix elements. We obtain them by evaluating matrix elements of the two-body interaction in the three-body m-scheme basis. Thereby we employ the so-called Slater rules, given here by

$$\begin{aligned}
{}_a\langle abc | \tilde{\boldsymbol{T}}^{[2]}_{int} + \tilde{\boldsymbol{V}}^{[2]}_{NN} | a'b'c' \rangle_a &= 0 && (5.32)\\
{}_a\langle abc | \tilde{\boldsymbol{T}}^{[2]}_{int} + \tilde{\boldsymbol{V}}^{[2]}_{NN} | a'b'c \rangle_a &= {}_a\langle ab | \tilde{\boldsymbol{T}}^{[2]}_{int} + \tilde{\boldsymbol{V}}^{[2]}_{NN} | a'b' \rangle_a && (5.33)\\
{}_a\langle abc | \tilde{\boldsymbol{T}}^{[2]}_{int} + \tilde{\boldsymbol{V}}^{[2]}_{NN} | a'bc \rangle_a &= {}_a\langle ab | \tilde{\boldsymbol{T}}^{[2]}_{int} + \tilde{\boldsymbol{V}}^{[2]}_{NN} | a'b \rangle_a + {}_a\langle ac | \tilde{\boldsymbol{T}}^{[2]}_{int} + \tilde{\boldsymbol{V}}^{[2]}_{NN} | a'c \rangle_a && (5.34)\\
{}_a\langle abc | \tilde{\boldsymbol{T}}^{[2]}_{int} + \tilde{\boldsymbol{V}}^{[2]}_{NN} | abc \rangle_a &= {}_a\langle ab | \tilde{\boldsymbol{T}}^{[2]}_{int} + \tilde{\boldsymbol{V}}^{[2]}_{NN} | ab \rangle_a + {}_a\langle ac | \tilde{\boldsymbol{T}}^{[2]}_{int} + \tilde{\boldsymbol{V}}^{[2]}_{NN} | ac \rangle_a \\
&\quad + {}_a\langle bc | \tilde{\boldsymbol{T}}^{[2]}_{int} + \tilde{\boldsymbol{V}}^{[2]}_{NN} | bc \rangle_a && (5.35)
\end{aligned}$$

where a, b and c summarize the quantum numbers for one particle, i.e.

$$|abc\rangle_a = |(n_a l_a, s_a) j_a m_a, (n_b l_b, s_b) j_b m_b, (n_c l_c, s_c) j_c m_c, t_a m_{t_a} t_b m_{t_b} t_c m_{t_c} \rangle_a \,. \tag{5.36}$$

Which one of the four rules above applies, depends on how many quantum numbers in the bra and ket are different. The primes in the ket indicate that the quantum numbers are different from all quantum numbers in the bra.

Thereafter, we have three-body m-scheme matrix elements of the SRG transformed Hamiltonian containing only two-body interactions

$$\langle abc | \tilde{\boldsymbol{T}}^{[2]}_{int} + \tilde{\boldsymbol{V}}^{[2]}_{NN} | a'b'c' \rangle \,. \tag{5.37}$$

Finally, we have to transform these states into the $\mathcal{J}, T$-coupled scheme, as we did for the three-body m-scheme matrix elements in section 4.4. We achieve this in the same way as in eq. (4.73).

At the end we have matrix elements

$$\langle [(j_a, j_b) J_{ab}, j_c] \mathcal{J}\mathcal{M}, (t_{ab}, t_c) TM_T | \tilde{\boldsymbol{T}}^{[2]}_{int} + \tilde{\boldsymbol{V}}^{[2]}_{NN} | [(j'_a, j'_b) J'_{ab}, j'_c] \mathcal{J}\mathcal{M}, (t'_{ab}, t_c) TM_T \rangle \tag{5.38}$$

in the $\mathcal{J}, T$-coupled scheme, that now can be used for consistent subtraction.

After the subtraction we end up with the matrix elements

$$\langle[(j_a, j_b)J_{ab}, j_c]\mathcal{J}\mathcal{M}, (t_{ab}, t_c)TM_T|\tilde{\boldsymbol{T}}^{[3]}_{int} + \tilde{\boldsymbol{V}}^{[3]}_{NN} + \tilde{\boldsymbol{V}}^{[3]}_{NNN}|[(j'_a, j'_b)J'_{ab}, j'_c]\mathcal{J}\mathcal{M}, (t'_{ab}, t_c)TM_T\rangle \tag{5.39}$$

including the three-body forces only. These can now be used for many-body calculations for any nuclei.

It is important to use the same truncation of the summations on the right-hand side of for the flow equations for the evolution with two- plus three-body interactions and with two-body interactions only. Therefore, we employ the same maximum three-particle energy E_{3SRG} in both cases.

We stress that all interactions used for the SRG transformation and the subtraction process are charge invariant, meaning the interaction matrix elements do not depend on the M_T quantum number. This translates in particular into the matrix elements (5.39). In the next section we present our results for NCSM and Hartree-Fock calculations including these matrix elements.

SECTION 6

Chiral three-body force in many-body calculations

In this section we present calculations with various combinations of the interactions we derived in the previous subsection. All calculations are in principle based on the same Hamiltonian, given by

$$\boldsymbol{H} = (\boldsymbol{T} - \boldsymbol{T}_{cm}) + \boldsymbol{V}_{NN} + \boldsymbol{V}_{NNN} \,. \tag{6.1}$$

The kinetic energy part is represented by $\boldsymbol{T} - \boldsymbol{T}_{cm}$, which is the intrinsic kinetic energy

$$\boldsymbol{T}_{int} = \frac{2}{A}\frac{1}{2\mu}\sum_{i<j}^{A} \vec{\boldsymbol{q}}_{ij}^{\,2} \,, \tag{6.2}$$

since properties of the investigated nuclei must not depend on its center-of-mass motion.

As two-body interaction we basically use the N3LO two-body interaction from χEFT by Entem and Machleidt [10]. Whenever we discuss SRG transformed interactions the complete Hamiltonian (6.1) is transformed consistently. For the many-body calculations we take the charge dependence of the two-body interaction into account. Consequently, interaction matrix elements of the two-body interaction depend on the projection quantum number of the total isospin M_T.

There exist at least two different choices for the three-body interaction. We use the abbreviations shown in table 2 to specify the used interaction. The term 'NN-only' refers to a calculation with the above mentioned N3LO two-body interaction only. A calculation with N3LO two-body interaction plus the corresponding in-

abbreviation	interaction type
NN-only	no three-body interaction, as in section 5.2.3 but with M_T dependence
NN+NNN-induced	NN + induced three-body interaction from SRG evolution in three-body space with initial two-body interaction
NN+NNN	NN + genuine N2LO three-body interaction + induced three-body force due to SRG in three-particle space

Table 2 – *Abbreviations for the different calculation types.*

duced three-body interaction is referred to as 'NN+NNN-induced'. This implies that there are no effects of genuine three-body forces included in these types of calculations. Finally, 'NN+NNN type' calculations include the genuine three-body forces as well as the induced three-body forces. Therefore, we can study the impact of the genuine N2LO three-body force by comparing the results of NN+NNN-induced calculations to those of NN+NNN calculations.

In the following, we present two kinds of calculations. Firstly, in section 6.1.1, we investigate the behavior of the three interaction types in the ab initio no-core shell model (NCSM) and the importance-truncated no-core shell model (IT-NCSM). Converged results with these methods are restricted to light nuclei, because heavier nuclei need to be considered in large, untractable model spaces to account for the complex properties of the nuclear interaction. Nevertheless, the advantage is that one can assess the quality of the nuclear interaction by comparing the converged results with experiments, since they are exact.

In contrast, the Hartree-Fock method provides only approximative calculations which are in return applicable to the whole nuclear chart and, therefore, are predestinated for first studies of the influence of three-body forces on the binding energy and charge radii systematics. This is discussed in section 6.2.

6.1 Studies of the N2LO three-body interactions in the (IT-)NCSM

6.1.1 (Importance-truncated) no-core shell model

In this section we briefly discuss the no-core shell model (NCSM) as one possibility to exactly solve the eigenvalue problem of the Hamilton operator. Afterwards, we investigate the importance-truncated no-core shell model (IT-NCSM) that enables calculations for heavier nuclei and larger model spaces than the NCSM.

The general idea of the NCSM is to translate the Hamilton operator of the nuclear many-body system into matrix representation and to solve the eigenvalue

problem of this matrix numerically. This matrix eigenvalue problem is given by

$$\begin{pmatrix} H_{11} & H_{12} & \cdots \\ H_{21} & H_{22} & \cdots \\ \vdots & \vdots & \ddots \end{pmatrix} \begin{pmatrix} C_1^\nu \\ C_2^\nu \\ \vdots \end{pmatrix} = E_\nu \begin{pmatrix} C_1^\nu \\ C_2^\nu \\ \vdots \end{pmatrix} , \tag{6.3}$$

where the matrix elements are $H_{ij} = \langle \phi_i | \boldsymbol{H} | \phi_j \rangle$. Moreover, the coefficients

$$C_i^\nu = \langle \phi_i | E_\nu \rangle \tag{6.4}$$

are the expansion coefficients of the eigenstate $|E_\nu\rangle$ in the chosen basis $\{|\phi_i\rangle\}$. In the NCSM these basis states $|\phi_i\rangle$ are Slater determinants of harmonic-oscillator single-particle states, equivalent to A-particle m-scheme states. Obviously, this Slater determinant basis consists of an infinite number of states and has to be truncated to make the model space finite and the eigenvalue problem tractable. This truncation is in the NCSM defined by a restriction on the maximum number of harmonic-oscillator excitation quanta $N_{\max}$. This means that all Slater determinants within the NCSM model space have unperturbed excitation energies up to $N_{\max}\hbar\Omega$, as illustrated in fig. 10. The use of harmonic oscillator states as basis combined with this truncation scheme has the advantage that one can guarantee the proper separation of the center-of-mass part of the state from its relative part. Therefore, spurious center-of-mass contaminations of the eigenstates are absent.

For the solution of the matrix eigenvalue problem one applies a Lanczos-type algorithm [29, 30]. This is a very efficient tool if only few eigenstates of the matrix have to be determined. This is the case for the nuclear Hamiltonian, since often only the energetically lowest eigenstates or eigenstates with certain quantum numbers are of interest. The only limitation of this approach is the model-space size that directly determines the dimension of the matrix. It grows factorially with $N_{\max}$ and particle number A. Currently, dimensions of 10^{10} are the upper limit of tractable matrices during the computations. Unfortunately, the model spaces often need to be that large (and larger) to account for all correlations of the nuclear system and to obtain converged results.

This is exactly where IT-NCSM comes into play. It is a tool to reduce the model space to tractable size without loss of accuracy of the eigenenergies compared to NCSM calculations (see [6] for a thorough discussion). The idea is to exploit that we are usually only interested in a few low-lying eigenstates of the Hamiltonian. This information is explicitly taken into account during the construction of the model space for the matrix representation. Therefore, the main ingredient is an a priori importance measure for the individual basis states $|\phi_i\rangle$.

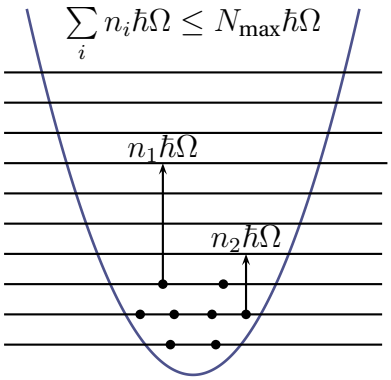

Figure 10 – *Illustration of the truncation scheme in the NCSM for 8 particles. We see the harmonic oscillator potential and its energy shells (horizontal lines). The dots indicate single-particle states that altogether build the unperturbed many-body ground state. In the NCSM model space all Slater determinants with excitation energy up to $N_{max}\hbar\Omega$ on top of this ground state are considered.*

The typical modus operandi for the model-space construction is outlined in the following: One starts with a given model space $\mathcal{M}$ spanned by Slater determinants $|\phi_i\rangle$ and a reference state $|\Psi_{\text{ref}}\rangle \in \mathcal{M}_{\text{ref}} \subset \mathcal{M}$ as approximation for the target state that we want to determine later by the diagonalization. This reference state already carries the correct quantum numbers of the target state, and it might result, e.g., from a NCSM-type diagonalization in $\mathcal{M}_{\text{ref}}$. The next step is to quantify the importance of the basis states of the model space $\mathcal{M}$ that are not included in $\mathcal{M}_{\text{ref}}$. For this we make use of multi-configuration many-body perturbation theory [31, 32] and consider the first perturbative correction for the reference state $|\Psi_{\text{ref}}\rangle$, given by

$$|\Psi^{(1)}\rangle = -\sum_{\phi_i \notin \mathcal{M}_{\text{ref}}} \frac{\langle\phi_i|\boldsymbol{H}|\Psi_{\text{ref}}\rangle}{\epsilon_i - \epsilon_{\text{ref}}}|\phi_i\rangle\,, \tag{6.5}$$

where ϵ_i are the unperturbed energies of the basis states from outside the reference space and $\epsilon_{\text{ref}} = \langle\Psi_{\text{ref}}|\boldsymbol{H}|\Psi_{\text{ref}}\rangle$ [6]. To evaluate the right-hand side we can insert $|\Psi_{\text{ref}}\rangle$ as expansion in terms of the basis states $|\phi_i\rangle$. In the special case that the reference state is given by a single Slater determinant, everything reduces to ordinary many-body perturbation theory. Now we can use the coefficient

$$\kappa_i = \frac{\langle\phi_i|\boldsymbol{H}|\Psi_{\text{ref}}\rangle}{\epsilon_i - \epsilon_{\text{ref}}} \tag{6.6}$$

as a priori importance measure for the basis state $|\phi_i\rangle$, since it indicates a large influence on the correction to the reference state if its absolute value is large. Therefore, all basis states with $|\kappa_i| \leq \kappa_{\min}$ are omitted, yielding the importance truncated

model space. The diagonalization of the matrix is then performed in this smaller space. Executing this procedure for different values of $\kappa_{\min}$ allows the extrapolation of the results for $\kappa_{\min} \to 0$. It turns out that these extrapolated results offer both, a reduction of the model space and results for eigenenergies and angular momentum quantum numbers that are in very good agreement with full NCSM calculations [6, 33].

From eq. (6.6) we can identify two reasons that imply a small importance measure: Firstly, the energy denominator can become large for energetically high basis states in the model space. Thus, the exclusion of these states corresponds in principle to the truncation in standard NCSM-type calculations, where states with high energies are also excluded by the $N_{\max}$ truncation. Secondly, the numerator in eq. (6.6) can be small due to specific properties of the Hamiltonian and the considered reference state. This type of truncation cannot be identified in the NCSM truncation and is the main advantage of IT-NCSM.

The outlined procedure for the importance truncation of the model space can be cast into a sequential scheme: One starts with a certain model space and reference state and reduces the model space with help of the importance measure (6.6). Then one diagonalizes the Hamiltonian in the importance truncated model space, yielding an eigenstate that can now be used as reference state for the next larger model space. Then the procedure starts again and one can progress to successively larger model spaces.

Altogether, the reduction of the model space is very powerful, since it facilitates calculations in regions that are not tractable with the standard NCSM. For example ^{16}O calculations for $N_{\max} = 10$, which are untractable in the NCSM framework, are possible within the IT-NCSM, since the model space dimension reduces from 10^{10} by several order of magnitude basis states. One can even go beyond $N_{\max} = 10$ up to $N_{\max} = 22$ importance truncated spaces with IT-NCSM.

In the following, we show results for ^{4}He and ^{6}Li in model spaces that are tractable also by the standard NCSM. Therefore, we employed IT-NCSM only for convenience, since the results are the same as the NCSM results but the computation is less demanding. The appearing error bars in the plots of the IT-NCSM data result from the extrapolation. The smallest $\kappa_{\min}$ we use is 10^{-5}.

6.1.2 Ground-state energy for ^{4}He including the bare N2LO three-body force

We start our investigations with the calculation of the ^{4}He ground-state energy via the NCSM with the bare, meaning not SRG transformed, N3LO two-body plus N2LO three-body force. The results for ground-state energies in different model spaces are shown in fig. 11 as function of the harmonic-oscillator frequency. Firstly,

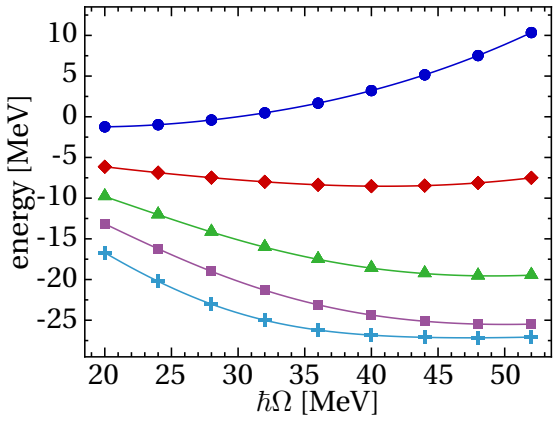

Figure 11 – *Ground-state energy of ^{4}He as function of the harmonic oscillator frequency for calculations in different model spaces: $N_{max} = 2$ (●), $N_{max} = 4$ (◆), $N_{max} = 6$ (▲), $N_{max} = 8$ (■), $N_{max} = 10$ (✚). Lines to guide the eye.*

the results are not converged with respect to model-space size, since every time we increase $N_{\max}$ the energy changes. Moreover, we recognize a strong dependence of the results for a certain model-space size on the harmonic-oscillator frequency. There seems to be a correlation between the rate of convergence and the frequency $\hbar\Omega$, since the results for frequencies above $\hbar\Omega = 30$ MeV reach the reasonable energy regime around -28 MeV much faster than e.g. computations with $\hbar\Omega = 20$ MeV. This behavior is already known from calculations including two-body interactions only.

We conclude that it is not trivial to obtain reasonable, converged results using the bare N2LO three-body interaction, even for ^{4}He. To overcome this obstacle we use the SRG transformed interactions as discussed in the next subsection.

Nevertheless, we stress that we carried out the first ^{4}He calculation within a $N_{\max} = 10$ model space build of m-scheme states. This is a result of our strategy to transform the antisymmetrized Jacobi matrix elements into $\mathcal{J}, T$-coupled matrix elements that are decoupled in the many-body calculation.

6.1.3 ^{4}He ground state energy with SRG transformed N2LO three-body interaction

In this section, we investigate results for the ^{4}He ground-state energy for different SRG flow parameters in NN+NNN IT-NCSM calculations with a harmonic oscillator frequency $\hbar\Omega = 28$ MeV. In fig. 12 we plot the ground-state energy against $N_{\max}$. The blue circles are the results with the bare interaction that we have seen already in the previous subsection.

As expected the SRG transformation drastically improves the convergence properties of the ground-state energy with respect to model-space size. The conver-

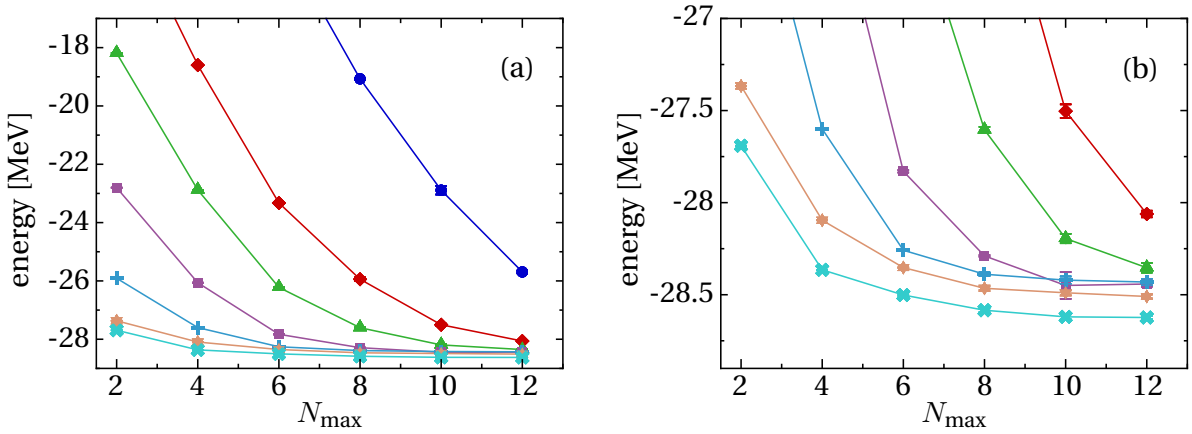

Figure 12 – *Ground-state energy of ^{4}He for different SRG parameters α in NN+NNN IT-NCSM calculations as function of N_{max}. The SRG parameters are $\alpha = 0.0$ fm^4 (●), 0.01 fm^4 (◆), 0.02 fm^4 (▲), 0.04 fm^4 (■), 0.08 fm^4 (✚), 0.16 fm^4 (★), 0.32 fm^4 (✖). Note the different energy ranges in plots (a) and (b). Lines to guide the eye.*

gence is accelerated when we increase the flow parameter α, which indicates a softer character of the interaction. Moreover, the energy is already converged for $N_{\text{max}} = 6$ using $\alpha = 0.08\,\text{fm}^4$. Furthermore, using $\alpha = 0.32\,\text{fm}^4$ yields converged results in the $N_{\text{max}} = 4$ model space.

Additionally, all calculations seem to converge to the same energy around -28.5 MeV which is the the ground-state energy that results from NCSM calculations with the bare interaction, too [34]. This would imply α-independence and mirror the unitarity of the SRG. However, if we zoom in, as shown in fig. 12(b), we recognize that only the results for $\alpha \leq 0.08\,\text{fm}^4$ approach the same energy. Increasing α to $0.16\,\text{fm}^4$ leads to ≈ 80 keV deviations although the results for $\alpha = 0.08\,\text{fm}^4$ are already converged at $N_{\text{max}} = 6$. The deviations increase to ≈ 190 keV when we use $\alpha = 0.32\,\text{fm}^4$ for the interaction. These deviations must be the signature of the lost induced four-body forces during the SRG transformation, as also found in [34]. Because we omitted these the transformation is only approximately unitary and, therefore, the eigenvalues of the Hamiltonian can change. Thus, we stay in the α-range up to $\alpha = 0.08\,\text{fm}^4$ for all further investigations.

We stress that this behavior is significantly improved compared to calculations with SRG transformed two-body interactions only. There results for interactions with different SRG parameters converge to completely different energies as we will see in subsection 6.1.5.

Before we investigate the contributions of the different parts of the three-body interaction to the results in fig. 12 in section 6.1.5, we study the influence of the truncated summations during the SRG transformation on our results.

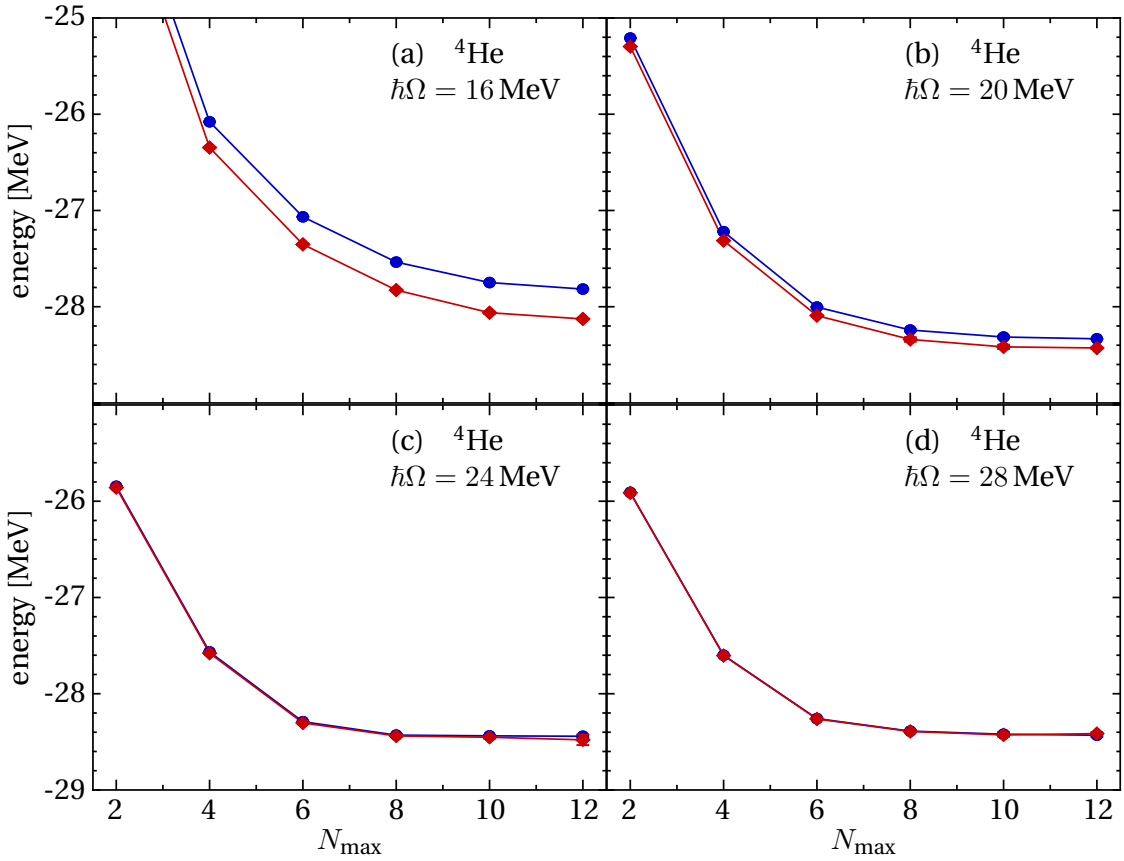

Figure 13 – *Comparison of NN+NNN IT-NCSM ^{4}He-ground-state energy calculations for different truncations of the summation bounds during the SRG transformation: $E_{3SRG} = 28$ (●), $E_{3SRG} = 32$ (◆). The SRG parameter is $\alpha = 0.08$ fm^4.*

6.1.4 Dependence on the energy cutoff $E_{3\mathrm{SRG}}$

In section 5.2.1 we mentioned the truncation of the summations on the right-hand side of the SRG flow equation (5.21) by defining a maximum harmonic oscillator quantum number $E_{3\mathrm{SRG}}$. It is important that our results are independent of this truncation. In the following we investigate whether this criterion is fulfilled. Therefore, we compare ^{4}He calculations with $E_{3\mathrm{SRG}} = 28$ to those with $E_{3\mathrm{SRG}} = 32$. The SRG parameter is $\alpha = 0.08\,\mathrm{fm}^4$ and the harmonic-oscillator frequency varies from 16 MeV to 28 MeV. The results for ^{4}He in fig. 13 and for ^{6}Li in fig. 14 show the importance of this study. For harmonic-oscillator frequency 28 MeV and also for 24 MeV the truncation is no problem, as the results of both truncations lie on top of each other for both nuclei. But the situation changes for lower frequencies: For ^{4}He and $\hbar\Omega = 20$ MeV we recognize a deviation of the results depending on $E_{3\mathrm{SRG}}$ of about 100 keV. These deviations increase to 300 keV for $\hbar\Omega = 16$ MeV, where, additionally, the results are not converged with respect to model space size. In case of ^{6}Li the deviations for $\hbar\Omega = 20$ MeV are about 0.2 MeV and for $\hbar\Omega = 16$ MeV

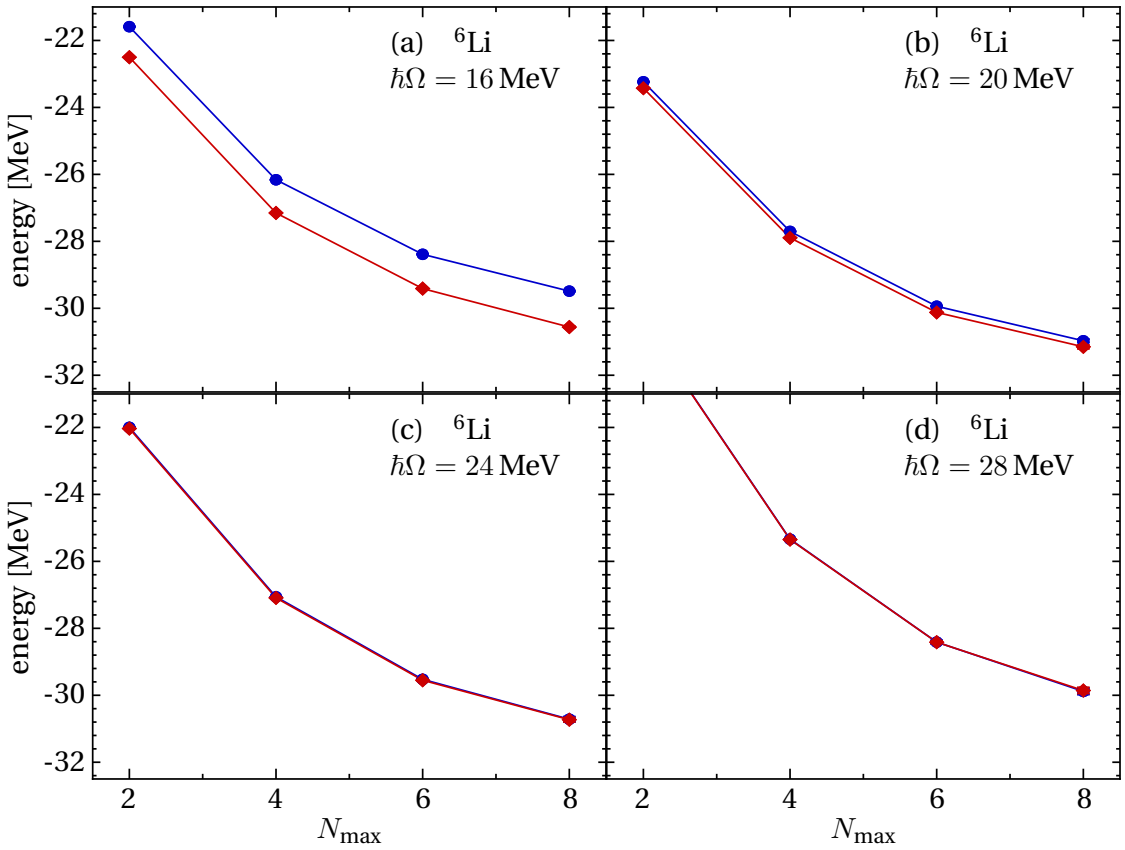

Figure 14 – *Comparison of NN+NNN IT-NCSM ^{6}Li-ground-state energy calculations for different truncations of the summation bounds during the SRG transformation: $E_{3SRG} = 28$ (●), $E_{3SRG} = 32$ (◆). The SRG parameter is $\alpha = 0.08$ fm^4.*

they increase to ≈ 1.1 MeV. Additionally, the results are not converged with respect to model space size. It is likely that for the low frequencies even the $E_{3\mathrm{SRG}} = 32$ truncation is not sufficient and one has to push $E_{3\mathrm{SRG}}$ to 36 or 40.

Whether the dependence on $E_{3\mathrm{SRG}}$ returns for higher harmonic-oscillator frequencies has to be investigated further. Moreover, it is interesting to study if it is sufficient to use a truncation scheme that depends on the total relative angular momentum quantum number of the matrix elements under consideration. For example, one could think of a high $E_{3\mathrm{SRG}}$ for the transformation of matrix elements with small total angular momentum quantum numbers J and to decrease it for matrix elements with larger J instead of using the same truncation for all matrix elements. This changed truncation might have no effects on the results, because one expects matrix elements including states with high J to be less important for the overall result as long the eigenstates under consideration have low angular momentum quantum numbers. If this could be confirmed, it will facilitate the SRG transformation because of the reduced memory consumption. Furthermore,

the results may be different for other nuclei. All these points cannot be discussed within this thesis and, will be addressed in future studies.

Since the situation for $\hbar\Omega = 28\,\text{MeV}$ is not problematic we use this frequency for our further investigations.

6.1.5 ^{4}He – contribution of the three-nucleon force on the ground-state energy

Finally, we study the impact of the different three-nucleon interactions on the results for the ground-state energy of ^{4}He. We start with the comparison of NN-only to NN+NNN-induced calculations, as shown in fig. 15. Firstly, we remark that the NN-only calculations (open symbols) are converged for all α parameters for $N_{\text{max}} \geq 14$ model spaces, though they converge to different energy values and the results are α dependent. This is caused by the loss of unitarity of the SRG transformation due to the omission of three- and four-body forces [34]. This should be improved when we solve the SRG flow equation in three-body space, since we then take the induced three-body force into account. This is exactly what we see from the results of NN+NNN-induced calculations (filled symbols). The results for $\alpha = 0.04\,\text{fm}^4$ and $\alpha = 0.08\,\text{fm}^4$ are already converged to -25.3 MeV which shows the repulsive character of the induced three-body forces compared to the NN-only results. The calculations with the two lower α parameters are not fully converged in the $N_{\text{max}} = 12$ model space but they seem to approach the same energy. Therefore, the results including the induced three-body forces are α independent for $\alpha \leq 0.08\,\text{fm}^4$ and induced four-body forces are negligible. However, for larger values of α the four-body forces start contributing as we have seen in section 6.1.3.

Next, we investigate the results of NN+NNN-induced vs. NN+NNN calculations, shown in fig. 16. The genuine three-body force generates more attraction compared to the induced three-body force. Therefore, the results converge to the lower energy of -28.43 MeV. As before, the results for $\alpha = 0.04\,\text{fm}^4$ and $\alpha = 0.08\,\text{fm}^4$ are already fully converged in the $N_{\text{max}} = 10$ model space, whereas the results for the smaller α seem to approach the same energy but need a larger model space than $N_{\text{max}} = 12$ for convergence. Moreover, the α-independence of the results is maintained. The comparison of the convergence properties is illustrated in fig. 17(b).

Finally, we compare the results of NN-only to NN+NNN calculations, as shown in fig. 17. Again, we see the convergence of the NN-only results to different energy values as discussed above. Moreover, we notice that the NN+NNN calculations converge to the same energy as the $\alpha = 0.08\,\text{fm}^4$ NN-only ones. This corresponds to the hitherto existing method of fine-tuning the α parameter to match experimental results [35]. Due to the α-independence of the results this is now no more

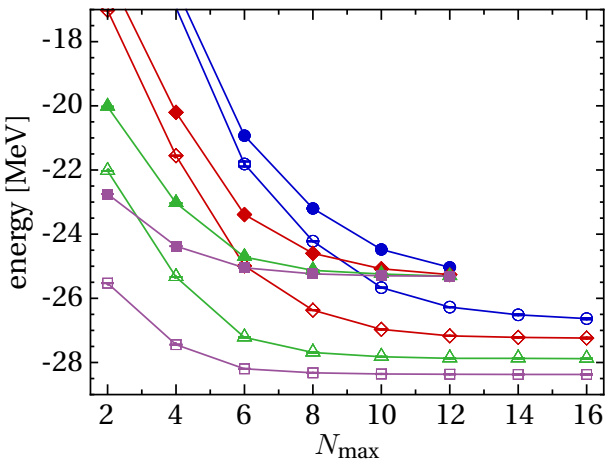

Figure 15 – *^{4}He ground-state energy calculations: NN-only (open symbols) vs. NN+NNN-induced (filled symbols). The SRG parameters are $\alpha = 0.01$ fm^4 (●,○); 0.02 fm^4 (◆,◇); 0.04 fm^4 (▲,△); 0.08 fm^4 (■,□). The harmonic-oscillator frequency is $\hbar\Omega = 28$ MeV.*

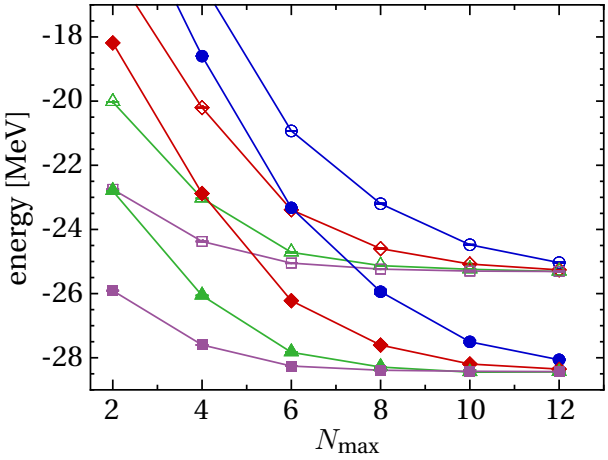

Figure 16 – *^{4}He ground-state energy calculations: NN+NNN-induced (open symbols) vs. NN+NNN (filled symbols). The SRG parameters are $\alpha = 0.01$ fm^4 (●,○); 0.02 fm^4 (◆,◇); 0.04 fm^4 (▲,△); 0.08 fm^4 (■,□). The harmonic-oscillator frequency is $\hbar\Omega = 28$ MeV.*

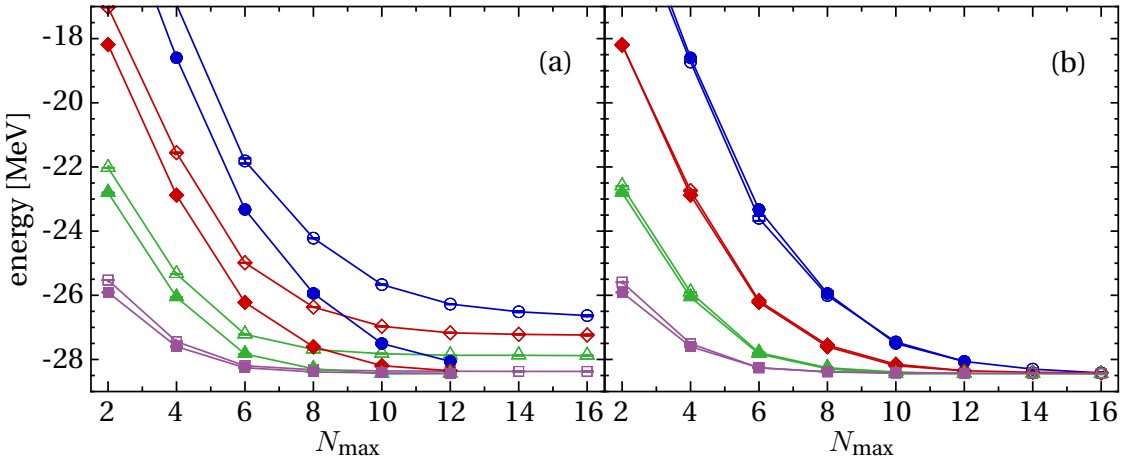

Figure 17 – *(a): ^{4}He ground-state energy calculations: NN-only (open symbols) vs. NN+NNN (filled symbols). The SRG parameters are $\alpha = 0.01$ fm^4 (●,○); 0.02 fm^4 (◆,◇); 0.04 fm^4 (▲,△); 0.08 fm^4 (■,□). The harmonic-oscillator frequency is $\hbar\Omega = 28$ MeV. (b): Same results as in (a) but we shifted the NN-only results such that they match the NN+NNN results at $N_{max} = 12$. Lines to guide the eye.*

necessary for ^{4}He and should be investigated for other nuclei, too.

Furthermore, we compare the rate of convergence of the NN-only calculations to the NN+NNN calculations with help of fig. 17(b). We shifted the NN-only results such that the results for $N_{\max} = 12$ match the NN+NNN results. Thereby, we observe that the rate of convergence is very similar for both calculations. If we look at the results for $N_{\max} = 6$ up to $N_{\max} = 10$ they are almost perfectly on top of each other, i.e., the convergence pattern is the same in both calculations. This is very helpful, since it means that the convergence properties do not change if we include genuine and induced three-body interactions to the NN-only calculations. Instead the three-body forces generate an energy shift only. Thus, we can identify this energy shift from the comparison of NN-only with NN+NNN results in the largest model space in which three-body forces can be handled. Then we can "extrapolate" the NN+NNN results using the NN-only convergence pattern to determine the ground-state energy. Unfortunately, this enables only the determination of eigenvalues of the Hamiltonian and not the eigenstates. However, this might be a hint that it is sufficient to employ three-body matrix elements only up to a lower $N_{\max}$ than the two-body matrix elements in the calculations. In this case, we would have access to the eigenstate of the Hamiltonian, too.

6.2 Three-body interactions and the Hartree-Fock method

As second kind of many-body calculation we deal with the Hartree-Fock method. Firstly, we briefly discuss the theoretical formalism in subsection 6.2.1. Secondly, we present first results of ground-state energy and charge radius systematics for the nuclei ^{4}He, ^{16}O, ^{40}Ca, ^{48}Ca and ^{90}Zr including chiral three-body forces in subsection 6.2.2.

6.2.1 Formalism

In the context of nuclear physics the Hartree-Fock method is the application of a variational calculation to the system of protons and neutrons. The variational principle [36, 37] implies that the solution of the Schrödinger equation is equivalent to finding the stationary points of the energy functional

$$E[|\Psi\rangle] = \frac{\langle\Psi|\boldsymbol{H}|\Psi\rangle}{\langle\Psi|\Psi\rangle} \,. \tag{6.7}$$

This method is helpful especially when one is interested in the ground state of a system, since in this case the corresponding stationary point is the absolute minimum of the functional. If the state $|\Psi\rangle$ resides in the complete Hilbert space, one finds the exact solutions of the eigenvalue problem of the Hamiltonian. When we, in contrast, parametrize the state $|\Psi\rangle$ only in a subset of the complete Hilbert space, the variation yields approximations of the eigenstates and eigenenergies. The fundamental constraint in the Hartree-Fock approximation is that the state $|\Psi\rangle$ is given as a single Slater determinant made up of A single-particle states

$$|\Psi\rangle = \prod_{i=1}^{A} \boldsymbol{a}_i^\dagger |0\rangle \,. \tag{6.8}$$

The operators $\boldsymbol{a}_i^\dagger$ are the creation operators corresponding to the single-particle state $|i\rangle$. These single-particle states are the variational parameters and have to be determined via the energy variation. For convenience, we expand the single-particle states $|i\rangle$ in terms of harmonic oscillator eigenstates

$$|i\rangle = \sum_k \langle\phi_k|i\rangle|\phi_k\rangle \,, \tag{6.9}$$

and use the expansion coefficients $c_k^i = \langle\phi_k|i\rangle$ as variational parameters. Therefore, the same three-body interaction matrix elements as in the NCSM approach are used. The variation itself leads to the well-known Hartree-Fock equations [36, 37].

They are given as coupled non-linear integro-differential equations and are solved iteratively. After their solution one takes the A single-particle states with the lowest single-particle energies to build up the ground-state Slater determinant.

From the Hartree-Fock equations one can identify the connection to the naive shell model, since the Hartree-Fock method belongs to the group of independent particle models, too. The extension, compared to the naive shell model, is the self-consistent derivation of the single-particle mean-field potential. However, the independent particle character implies by definition that correlations between the particles cannot be described. The quality of the description with the single Slater determinant can be compared to a $N_{\max} = 0$ model space in NCSM-type calculations. Therefore, we do not expect the Hartree-Fock results to have the same quality as converged NCSM results. Nevertheless, it is important to keep in mind that the Hartree-Fock results provide an upper bound for the exact ground-state energy of the system due to its variational origin. Additionally, their advantage is that the Hartree-Fock technique is applicable to the whole nuclear chart. Moreover, it has proven to describe nuclear charge radii quite well [38, 17].

In the following section, we investigate first results of Hartree-Fock calculations including the SRG transformed chiral N2LO three-body force.

6.2.2 Impact of N2LO three-body forces on the binding energy and charge radii systematics

In this section, we discuss our first results of the contributions of three-particle interactions to Hartree-Fock calculations. We investigate the binding energies and charge radii of ^{4}He, ^{16}O, ^{40}Ca, ^{48}Ca and ^{90}Zr. We again compare the contributions of the NN-only, NN+NNN-induced and NN+NNN calculations. All studies are performed using the harmonic-oscillator frequency $\hbar\Omega = 28\,\text{MeV}$ and SRG parameters $\alpha = 0.02\,\text{fm}^4, 0.04\,\text{fm}^4$ and $0.08\,\text{fm}^4$. Moreover, we truncated the sum in eq. (6.9) according to the maximum harmonic-oscillator single-particle energy $e_{\max} = 2n + l = 14$. This choice guarantees convergence for all Hartree-Fock states for all nuclei under consideration.

The binding energy results are shown in fig. 18. Firstly, we concentrate on the NN-only results and recognize that the binding energies in the $\alpha = 0.02\,\text{fm}^4$ calculations are underestimated for ^{4}He, ^{16}O, ^{40}Ca and ^{48}Ca compared with experiment, whereas we see overbinding for the heavier nucleus ^{90}Zr. While increasing the SRG parameter, all binding energies start to grow. Finally, for $\alpha = 0.08\,\text{fm}^4$, we see a dramatic overbinding of all nuclei except for ^{4}He. Since the SRG transformation only accounts for short-range correlations, one can think of further calculations starting from the Hartree-Fock basis to include the effects from long-range cor-

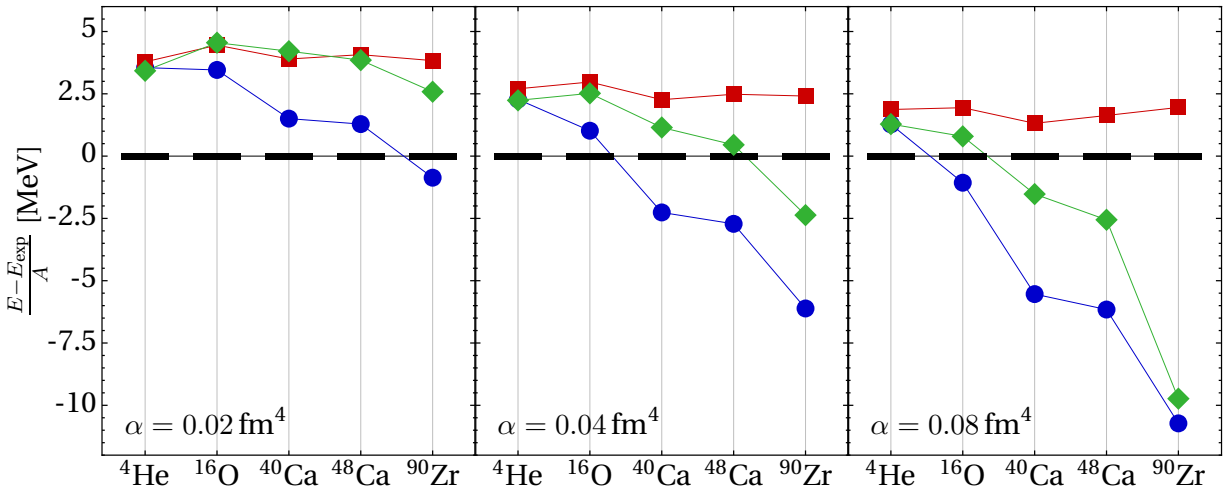

Figure 18 – *Difference of binding energy per nucleon from Hartree-Fock NN-only (●), NN+NNN-induced (■), NN+NNN (◆) calculations and experiment (▬) for different SRG flow parameters α. The harmonic-oscillator frequency is $\hbar\Omega = 28$ MeV and the experimental data is taken from [39].*

relations, e.g. by employing many-body perturbation theory. Now it is time to remember the variational character of the Hartree-Fock results and the fact that they provide an upper bound for the exact ground state energy. Therefore, many-body perturbation theory (or other more sophisticated calculations) can only increase the binding energies which leads to even worse results.

The hope is that three-body forces can "cure" the NN-only results. Actually, this is the case when we look at the NN+NNN-induced results in fig. 18. Here, the binding energy per nucleon is too small compared to experiment. This results from the repulsive character of the induced force that we already encountered in the NCSM calculations. Furthermore, the results are rather independent of the investigated nuclei. Also the behavior with increased α parameter is reasonable: The overall shape of the results is maintained while we gain a little binding energy as α increases. This gain is due to the fact that more information of high-energy properties of the interaction is shifted to the energy regime considered by Hartree-Fock. Since the binding energy is too small compared to experiment, many-body perturbation theory may improve it towards the experimental result.

Unfortunately, this picture is destroyed when we look at the results including the genuine three-body forces. For $\alpha = 0.02\,\text{fm}^4$, the results are still in agreement with the NN+NNN-induced results except for the slightly increased binding of ^{90}Zr. But if we increase the flow parameter all binding energies are increased and tend to overbinding. Especially for $\alpha = 0.08\,\text{fm}^4$, the overbinding for ^{48}Ca already reached -2.5 MeV per nucleon. For heavier nuclei the situation gets even worse, e.g. for

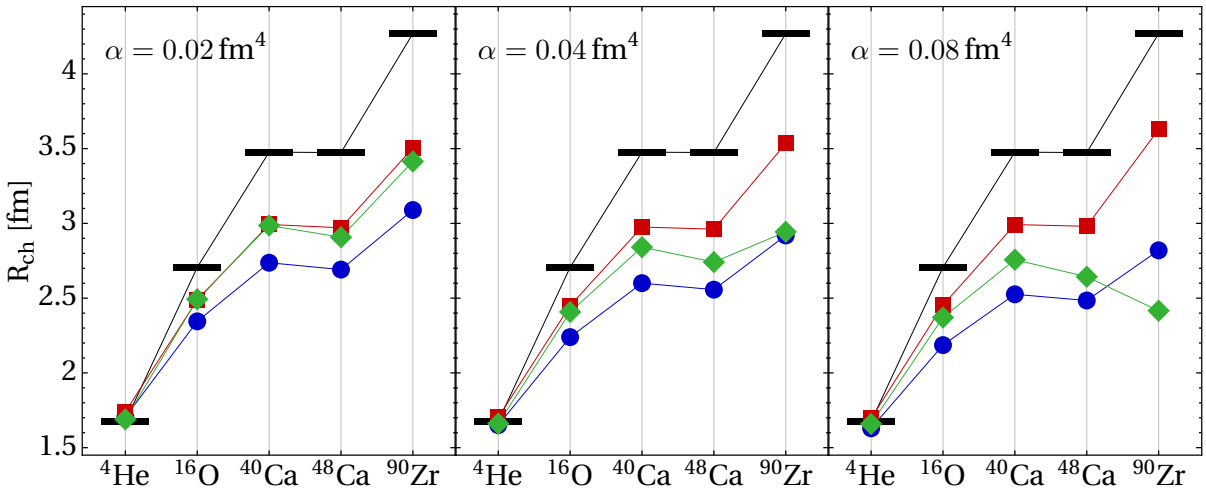

Figure 19 – *Charge radius systematics from Hartree-Fock NN-only (●), NN+NNN-induced (■), NN+NNN (◆) calculations with different SRG flow parameters α compared to experiment (—).The harmonic-oscillator frequency is $\hbar\Omega = 28$ MeV and the experimental data is taken from [40].*

^{90}Zr the overbinding is comparable to the one known from the NN-only calculations and many-body perturbation theory would increase the binding energy further.

Thus, the transformed N2LO three-body interaction does not help to improve the results obtained in NN-only calculations for heavier nuclei. If any, the results with $\alpha = 0.02\,\mathrm{fm}^4$ are the most reasonable ones. But even in this case one can expect overbinding for nuclei as heavy as ^{208}Pb. However, from these results it is not possible to decide whether the problems are due to the initial chiral interaction or due to the SRG transformation and the omission of the induced four-body forces. Since the inclusion of the induced three-body forces cured the NN-only results quite well, this might happen again if one includes the lost four-body forces from the genuine three-body forces. Though, if this were the case, the hierarchy of the many-body forces will not be maintained, since the induced four-body force then must provide a contribution comparable to the transformed genuine three-body force.

Additionally, we can investigate the charge radii of the nuclei, as shown in fig. 19. Here, the NN-only results basically reproduce the experimental trend but are systematically too small by 0.8 fm for ^{16}O and by 1.5 fm for ^{90}Zr. Higher values for the SRG parameter do not change the results significantly. The radii from NN+NNN-induced calculations are increased but still too small to reproduce the experimental trend. For ^{16}O the radius is 0.5 fm too small and for ^{90}Zr we lack 1 fm. Again, the results are rather insensitive to the increase of the SRG flow parameter. Finally, if

we carry out NN+NNN calculations the charge radii decrease again. Moreover, the decrease grows when we increase α. In particular for the heavier nuclei, this seems to be a problem, since the charge radius of ^{90}Zr is for $\alpha = 0.08\,\mathrm{fm}^4$ smaller than in NN-only calculations. Therefore, the genuine three-body force cannot help to reproduce the experimental charge radii, either.

It will be interesting to further study these systematics including many-body perturbation theory, e.g. to find out what happens to the NN+NNN-induced and NN+NNN results of the binding energy for $\alpha = 0.02\,\mathrm{fm}^4$. Another interesting point could be to use alternative generators in the SRG transformation. This will help to decide whether the problems arise from the SRG transformation itself or if they are caused by the initial chiral potential. Furthermore, one can try to fine-tune the low-energy constants c_D and c_E of the N2LO three-body interaction for a better reproduction of the binding energy and charge radii systematics. For that, the new parameters must provide a more repulsive three-body interaction. A similar procedure has already been applied with a three-nucleon contact interaction including one free parameter [38]. However, one has to be careful while tuning these parameters, because there exist few-body observables with strong dependence on their values as found in [3]. Finally, it would also be interesting to see what part of the three-body interactions has which effect on the systematics.

SECTION 7

Summary and outlook

The aim of this thesis is to develop the framework for studies of chiral three-nucleon forces in many-body methods like (IT-)NCSM and Hartree-Fock including the consistent similarity renormalization group transformation.

We start with the implementation of the transformation of antisymmetric Jacobi matrix elements of the chiral three-body interaction into m-scheme matrix elements, which are needed for the many-body calculations. The input are the antisymmetric harmonic-oscillator Jacobi matrix elements provided by P. Navrátil's MANYEFF-code. Our strategy was to transform these into $\mathcal{J}, T$-coupled matrix elements, which are decoupled on-the-fly during the many-body calculations. This coupled scheme is crucial, because it is the key to efficiently transform and employ matrix elements with three-particle energy beyond $E_{3\text{max}} = 8$, as we discuss extensively in section 4.4. Consequently, our transformation code can handle matrix elements up to $E_{3\text{max}} = 12$, which are included in many-body calculations for the first time. The codes will be developed further to deal with $E_{3\text{max}} = 14$ and 16 matrix elements in the near future.

Secondly, we implemented the SRG transformation of the three-nucleon interaction in antisymmetric Jacobi representation. The SRG provides a tool to soften the interaction by a continuous unitary transformation. This turns out to be necessary, because NCSM calculations with the bare interaction are not converged in the $N_{\text{max}} = 12$ model space even for ^{4}He. During this transformation higher-order many-body interactions are induced. Because we limit the transformation to two- or three-body space, we cannot account for all induced interactions. Therefore, we study the influence of these two limitation schemes on the many-body calculations. The IT-NCSM calculations of the ^{4}He ground-state energy with two-body transformed matrix elements yield different results depending on the SRG

flow parameter due to the omission of three- and four-body forces. This effect was used before for a fine-tuning of the SRG flow parameter such that the results match experimental data. Our converged results for the same calculations with three-body transformed matrix elements are independent of the flow parameter for $\alpha \leq 0.08\,\mathrm{fm}^4$. This means that effects of induced four-body forces are negligible in this domain of the flow parameter. In consequence, the parameter fine-tuning becomes dispensable. It will be interesting to study if this behavior is also maintained for heavier nuclei, where many-body interactions might have a stronger impact.

Furthermore, we are able to distinguish between effects of SRG-induced three-body interactions and effects of the transformed genuine chiral three-body force on our IT-NCSM results in case of ^{4}He. We find that the induced three-body forces are repulsive, which results in a reduced binding energy. In contrast, the genuine three-body force provides more attraction leading to a larger binding energy again. Furthermore, the convergence pattern with respect to model-space size is determined by the two-body forces, while the three-body contributions merely generate an energy shift. This might be a hint that it is sufficient to include three-body interactions only for a subspace of the full model space, which would facilitate computations. Further studies along these lines are planned.

Additionally, we investigate the dependence of the ground-state energies of ^{4}He and ^{6}Li on the model space used for performing the SRG transformation. We find that this convergence depends strongly on the harmonic-oscillator frequency. For low frequencies in the range of $16\,\mathrm{MeV}$ the ground-state energies show a large dependence on the SRG model space. For $\hbar\Omega = 28\,\mathrm{MeV}$ and $\alpha = 0.08\,\mathrm{fm}^4$, we found that the energies for ^{4}He and ^{6}Li are identical for the two truncations $E_{3\mathrm{SRG}} = 28$ and 32. This has to be further investigated for other nuclei. Moreover, studies of other truncation schemes will be interesting, e.g. an $E_{3\mathrm{SRG}}$ that depends on the angular momentum quantum number of the matrix elements.

Finally, we perform first studies of the impact of the SRG-transformed chiral interaction including the N2LO three-body force on the systematics of binding energies and charge radii in Hartree-Fock calculations. We observe that the SRG-transformed N2LO three-body interaction still generates a large overbinding for heavier nuclei. Also the charge radii are too small for all nuclei beyond ^{4}He. Here, it will be interesting to see whether a variation of the c_D and c_E parameters of the chiral three-body interactions can help to overcome these problems. Additionally, we plan to implement an alternative generator for the SRG transformation that might help to suppress induced interactions beyond the three-body level.

In conclusion, the study of three-body forces provides many exciting avenues

for further investigation. As an example it will be interesting to study B(E2) transition rates in isotopes of carbon, where experiments measured contradicting results [41, 42, 43].

APPENDICES

APPENDIX A

Implementation

In the following we give some remarks and comments on our implementation of the transformation discussed in section 4 and the SRG transformation in section 5. We start with an outline of the general structure and strategy of the code in appendix A.1. Then, we briefly discuss our implementation of the $\tilde{T}_{\mathcal{J}}$-coefficient in appendix A.2 and of the $\mathcal{J}, T$-coupled matrix elements in appendix A.3.

A.1 General remarks on the implementation

In this section, we discuss some basic properties of our C program that should simplify the overview of the code. Since the program is subdivided into many source files, we start with quoting the most important files. We list the files and give a short description of the contained routines for each in the following:

GLO_Base.c/h Inclusion of all used library header files, e.g.,the gnu scientific library (GSL) routines. Definition of various preprocessor constants, e.g. to determine the size of needed cache arrays during the calculations of the $\tilde{T}_{\mathcal{J}}$-coefficients.

PAR_Base.c/h Management of the command line parameters and generation of some file names.

JB_Base.c/h Contains the function for generation of the $|\alpha\rangle$ basis states given in eq. (3.90). The projection quantum numbers M_J and M_T do not appear in the code, since all quantities in which $|\alpha\rangle$ is included are independent of those. The basis generation is divided in different steps. Firstly, the states corresponding to the first Jacobi coordinate are generated, where the antisymmetry with respect to particle exchange $1 \leftrightarrow 2$ is taken into account by the con-

dition $(-1)^{(l_{12}+s_{ab}+t_{ab})} = -1$. Then, the states corresponding to the second Jacobi coordinate are generated and coupled with the states corresponding to the first Jacobi coordinate to end up with the $|\alpha\rangle$ states. The quantum numbers and additional book keeping quantities are stored in the JB_Struct. We stress that the used ordering of the basis states is indispensable. Because we extract the coefficients of fractional parentage (CFPs) from the MANYEFF-code, we have to stick to this ordering. Moreover, we use the JBA_Struct to store quantities that are relevant for each block with given energy E, total relative angular momentum J and total isospin T quantum number, e.g. the trace of the antisymmetrizer according to eq. (3.120) yielding the number of CFPs and three-body relative states $|EJTi\rangle$.

JB_AntiSym.c/h Here, the function to calculate matrix elements of the antisymmetrizer, essentially according to formula (3.119), is included. Besides, the file contains the function which computes the trace of the antisymmetrizer. In order to speed up this calculation we precalculate the necessary HOBs.

JME3B_Base.c/h All routines that are used to read CFP files or matrix element files from the MANYEFF-code are placed here. Thereby, we always assume that the matrix elements are given in the file as lower triangular matrix. Furthermore, the routine JME3B_MECenterCacheInit exists, which precomputes the results of the two inner loops during the calculation of the $\mathcal{J},T$-coupled matrix elements. We describe this technique in appendix A.3 in more detail.

ME2J_Base.c/h Contains the infrastructure to read, write and handle coupled two-body interaction matrix elements as given in eq. (5.28). Especially the routine ME2J_Init is crucial to reproduce the ordering of the matrix elements in the file. This is important since the gzipped file only includes their bare values without any information about the involved states.

ME3J_Base.c/h This is similar to ME2J_Base.c/h, but now for the $\mathcal{J},T$-coupled three-body matrix elements. Again, the ordering identifies the corresponding matrix elements and states. The routine that determines the ordering int this case is ME3J_Init.

ME2J_Conv3J.c/h Contains the routines that prepare the SRG-transformed matrix elements of the two-body interaction for the subtraction, as described in section 5.3. Because we use the matrix elements (5.30) as input for our code, we need only routines for the last three steps in the right path of the flow chart displayed in fig. 9.

ME3J_Calc.c/h Contains the functions that compute the $\mathcal{J},T$-coupled matrix elements according to eq. (4.79), but the loops are carried out implicitly. See appendix A.3.

TMC_Base.c/h Here, all routines that are necessary for precomputing and storing the 6j- and 9j-symbols as well as the HOBs are included. The 6j-symbols are calculated according to [20]. The 9j-symbols are computed as sums of products of three-6j-symbols. Finally, the HOBs are calculated via eq. (3.85). We precompute only the quantities that are relevant during the $\tilde{T}_{\mathcal{J}}$ calculation.

TTCJ_Base.c/h Contains the routines used for the calculation of the $\tilde{T}_{\mathcal{J}}$-coefficients. We discuss more details of this calculation in the following subsection.

SRG_ME3J All routines used for the SRG transformation are included here. The general strategy is to read one EJT-block of matrix elements into memory and solve the SRG-flow equation via a GSL Runge-Kutta routine. The matrix multiplications on the right-hand side of the flow equation (5.21) are accomplished with help of CBLAS routines.

SPB_Base.c/h Routines that initialize the underlying single-particle basis of the m-scheme states. This is necessary, e.g. for the decoupling of the two-body matrix elements during their preparation for proper subtraction.

CGC_Base.c/h Contains the routine to calculate the Clebsch-Gordan coefficients as well as a routine that precaches all Clebsch-Gordan coefficients up to a certain energy.

Typically, the identifier of the file names in front of the underscore is also the identifier of each contained routine.

Using the above discussed files, we compile two executable programs. One for the SRG transformation that uses the matrix elements of the MANYEFF-code as input and provides in three-body space SRG-transformed matrix elements as output. The second program uses these SRG transformed matrix elements as input and converts them into the $\mathcal{J},T$-coupled scheme. Then, it reads the two-body interaction matrix elements that were SRG transformed in two-body space, converts them into the $\mathcal{J},T$-coupled scheme, and subtracts them from the $\mathcal{J},T$-coupled two-plus-three-body interaction matrix elements. From subsequent execution of these two programs we obtain the matrix elements of the three-body induced interaction as well as the induced plus genuine SRG-transformed matrix elements, depending on the matrix elements that enter the SRG transformation.

We want to briefly discuss one possible program fetch for calculation of the $\mathcal{J},T$-coupled three-body interaction matrix elements. Therefore, we start with the program responsible for the SRG. As input it needs matrix elements of the Hamiltonian and of the intrinsic kinetic energy for the different EJT-blocks separately. An example command line of the SRG program reads

```
./transfjmesrg E3MaxIn=28 E3MaxOut=12 hwHO=28 alpha=0.08 E3MaxSRG=28
```

Thereby, `E3MaxIn` determines the maximum harmonic-oscillator energy quantum number of the interaction matrix elements that input the program. Accordingly, `E3MaxOut` defines the maximum harmonic-oscillator energy quantum number of the interaction matrix elements that are written into a file after the SRG transformation. The parameter `hwHO` identifies the used harmonic-oscillator frequency. Moreover, `alpha` determines the SRG flow parameter and, finally, `E3MaxSRG` corresponds to E_{3SRG} which determines the truncation of the summations. There are only three routines called in the main program: Firstly, TMC_BinomialInit initializes Binomial for the calculation of 6j-symbols. Secondly, we initialize the basis states $|\alpha\rangle$ and, finally, the routine SRGTransformMEHO_block does the SRG transformation of each block step by step. With the command line above the energy truncation in the summations via E_{3SRG} is the same for all matrix elements. The code can also handle different truncations depending on the total angular momentum quantum number J of the involved states.

Once we have the SRG transformed matrix elements we can run the program responsible for the conversion into $\mathcal{J},T$-coupled m-scheme matrix elements. A possible command line is given by

```
./convjme2me3j E3MaxIn=12 E3MaxOut=12 E3MaxSRG=32 eMax=12 hwHO=20
               alpha=0.08 EMax=12 MEID=n3lo_nocd ME3ID=chi2b3b
```

Here, `E3MaxIn` is again the maximum harmonic oscillator energy quantum number of the matrix elements that are read and `E3MaxOut` the one of the matrix elements that are converted into the $\mathcal{J},T$-coupled scheme. Moreover, `alpha` is the SRG parameter and `E3MaxSRG` is the energy used for the truncation of the summations during the SRG transformation. The `EMax` parameter determines the maximum harmonic oscillator energy quantum number of the two-body matrix elements that are read during the execution. Additionally, `hwHO` is again the harmonic oscillator frequency. The parameter `eMax` is the maximum single-particle energy. Finally, `MEID` and `ME3ID` determine the file names of the read and written files. Again, this command line is appropriate for a calculation with matrix ele-

ments that are truncated with the same $E_{3\mathrm{SRG}}$. The plan is that the code in future can handle different truncations for different J in order to study this dependence.

The illustration of the data flow during the program execution is shown in the flow chart in fig. A.1. The routines are shown in the ordering they are called in the main program including a short description of their role.

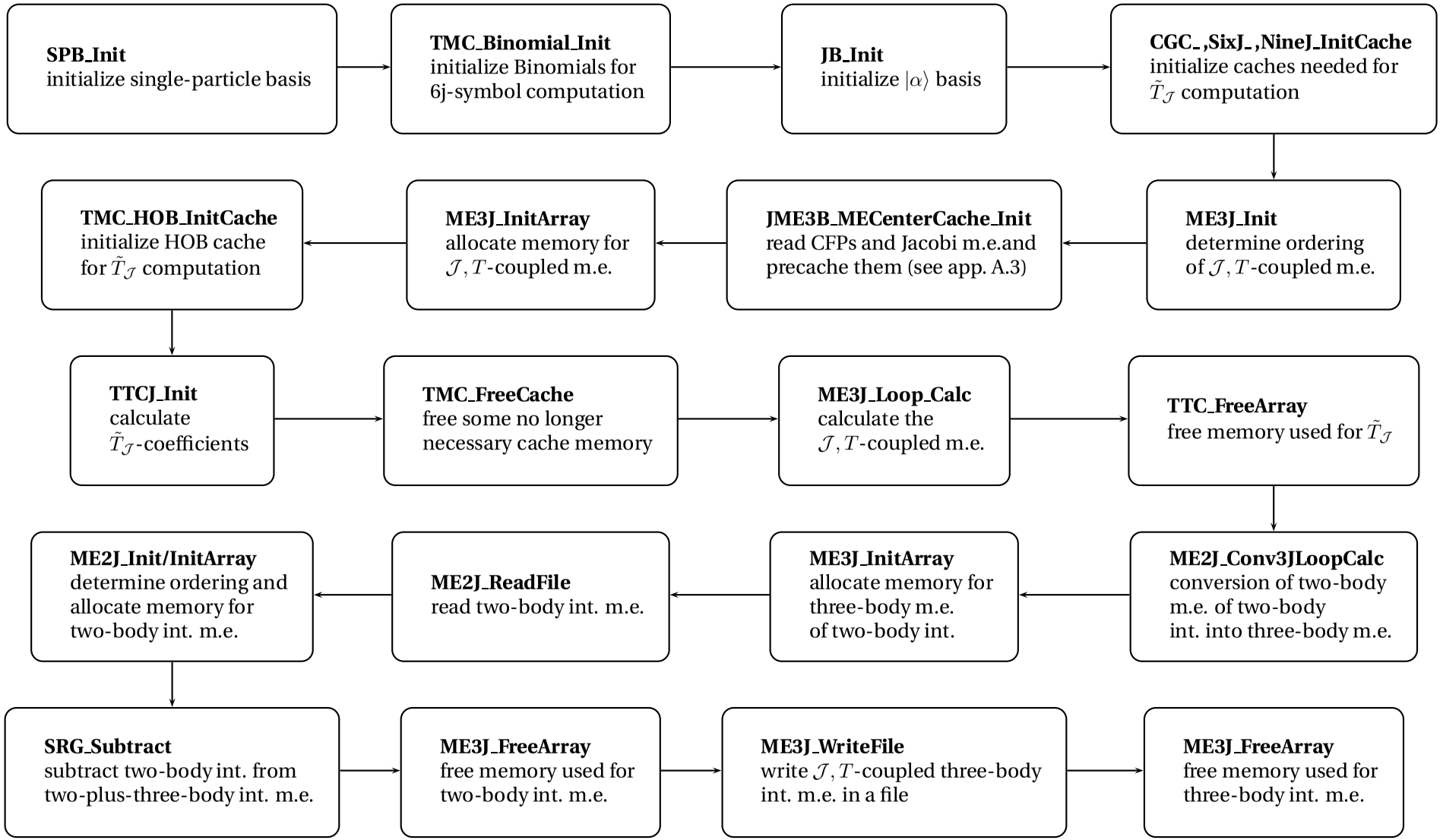

Figure 20 – *Used routines and their role during computation of $\mathcal{J},T$-coupled matrix elements ordered as called in the program. Abbreviations: int. – interaction, m.e. – matrix elements.*

A.2 Implementation of the $\tilde{T}_{\mathcal{J}}$-coefficient

In this section we discuss some technical details on the implementation of the $\tilde{T}_{\mathcal{J}}$-coefficients. The formula of the $\tilde{T}_{\mathcal{J}}$-coefficient is given in eq. (4.80). Now, we discuss the bounds of the sums in the $\tilde{T}_{\mathcal{J}}$-coefficient. There are many conditions that restrict the summation bounds but these conditions can only be used if all quantum numbers needed for the conditions are available. Obviously, this depends on the arrangement of the summations. The ordering we use in the implementation is given as

$$
\begin{aligned}
&\tilde{T}_{\mathcal{J}}\begin{pmatrix} a & b & c & J_{ab} & J & \mathcal{J} \\ n_{cm} & l_{cm} & n_{12} & l_{12} & n_3 & l_3 \\ s_{ab} & j_{12} & j_3 & & & \end{pmatrix} \\
&= (-1)^{l_c+l_{12}} \hat{j}_a \hat{j}_b \hat{j}_c \hat{s}_{ab} \hat{j}_3 \hat{j}_{12} \hat{J} \hat{J}_{ab}\, \delta_{2n_a+l_a+2n_b+l_b+2n_c+l_c-2n_{12}-l_{12},2n_{cm}+l_{cm}+2n_3+l_3} \\
&\quad \times \sum_{L_{12}} (-1)^{L_{ab}} \hat{L}_{ab}^2 \begin{Bmatrix} l_a & l_b & L_{ab} \\ s_a & s_b & s_{ab} \\ j_a & j_b & J_{ab} \end{Bmatrix} \\
&\quad \times \sum_{\mathcal{L}_{12}} \langle\langle \mathcal{N}_{12}\mathcal{L}_{12}, n_{12}l_{12}; L_{ab} | n_a l_a, n_b l_b \rangle\rangle_1 \\
&\quad \times \sum_{\Lambda} (-1)^{\Lambda} \hat{\Lambda}^2 \langle\langle n_{cm}l_{cm}, n_3 l_3; \Lambda | \mathcal{N}_{12}\mathcal{L}_{12}, n_c l_c \rangle\rangle_2 \\
&\quad \times \sum_{\mathcal{L}} (-1)^{\mathcal{L}} \hat{\mathcal{L}}^2 \begin{Bmatrix} l_c & \mathcal{L}_{12} & \Lambda \\ l_{12} & \mathcal{L} & L_{ab} \end{Bmatrix} \\
&\quad \times \sum_{S_3} (-1)^{\mathcal{J}+S_3} \hat{S}_3^2 \begin{Bmatrix} L_{ab} & l_c & \mathcal{L} \\ s_{ab} & s_c & S_3 \\ J_{ab} & j_c & \mathcal{J} \end{Bmatrix} \\
&\quad \times \sum_{L_3} \hat{L}_3^2 \begin{Bmatrix} l_{cm} & l_3 & \Lambda \\ l_{12} & \mathcal{L} & L_3 \end{Bmatrix} \begin{Bmatrix} l_{cm} & L_3 & \mathcal{L} \\ S_3 & \mathcal{J} & J \end{Bmatrix} \begin{Bmatrix} l_{12} & l_3 & L_3 \\ s_{ab} & s_c & S_3 \\ j_{12} & j_3 & J \end{Bmatrix} .
\end{aligned}
\tag{A.1}
$$

The summation bounds are essentially determined by the various triangle inequalities that have to be fulfilled for the 6j- and 9j-symbols. Thereby, it is useful to take their symmetry relations into account. If we have more than one condition for the lower bound, we can use the maximum value as lower summation bound and vice versa for the upper bound. In the following we present the summation bounds we use for the summation ordering above. We only give an additional explanation, if we used something different than the triangle conditions of the 6j- and 9j-symbols.

- $\sum_{L_{12}}$
  Lower Bound: Max($|J_{ab} - s_{ab}|, |l_a - l_b|$) ,
  Upper Bound: Min($J_{ab} + s_{ab}, l_a + l_b$) .

- $\sum_{\mathcal{L}_{12}}$
  Here, we can take advantage of the fact that we know the energy quantum number $\mathcal{E}_{12} = 2\mathcal{N}_{12} + \mathcal{L}_{12}$ from the HOB. Additionally we have a triangle inequality for L_{12} and l_{12}. Therefore the lower bound is given by $|L_{12} - l_{12}|$ if this value and $\mathcal{E}_{12}$ are both odd numbers. Else the lower bound is given by $|L_{12} - l_{12}| + 1$.
  Lower Bound: $|L_{12} - l_{12}|$ or $|L_{12} - l_{12}| + 1$,
  Upper Bound: Min($L_{12} + l_{12}, \mathcal{E}_{12} = 2n_a + l_a + 2n_b + l_b - 2n_{12} - l_{12}$) .

- $\sum_{\Lambda}$
  Lower Bound: Max($|\mathcal{L}_{12} - l_c|, |l_{cm} - l_3|$) ,
  Upper Bound: Min($\mathcal{L}_{12} + l_c, l_{cm} + l_3$) .

- $\sum_{\mathcal{L}}$
  Lower Bound: Max($|\Lambda - l_{12}|, |L_{12} - l_c|$) ,
  Upper Bound: Min($\Lambda + l_{12}, L_{12} + l_c$) .

- $\sum_{S_3}$
  Lower Bound: Max($|\mathcal{L} - \mathcal{J}|, |s_{ab} - s_c|$) ,
  Upper Bound: Min($\mathcal{L} + \mathcal{J}, s_{ab} + s_c$) .

- $\sum_{L_3}$
  Lower Bound: Max($|l_{12} - l_3|, |S_3 - J|, |\mathcal{L} - l_{cm}|$) ,
  Upper Bound: Min($l_{12} + l_3, S_3 + J, \mathcal{L} + l_{cm}$) .

In order to minimize the computation time for the $\tilde{T}_{\mathcal{J}}$-coefficients, we precalculate all 6j- and 9j-symbols as well as all HOBs that appear in eq. (A.1). Therefore, we employ as much static allocated arrays as possible, as we figured out that the access to these is faster compared with the access on dynamically allocated arrays.

Furthermore, the ordering of the loops during the computation of the $\tilde{T}_{\mathcal{J}}$ is important in our implementation. Our used loop ordering is inward-looking:

$$a, b, c, J_{ab}, l_{cm}, \mathcal{J}, T, J, E, k\,, \tag{A.2}$$

where k counts the $|\alpha\rangle$ states inside of the given EJT-block. We stress that the loop over the isospin quantum number T could be dropped, because $\tilde{T}_{\mathcal{J}}$ is independent of it. We still kept it for convenience, since otherwise we would have to initialize a second kind of $|\alpha\rangle$ basis without the isospin quantum number. However, this point should be improved in the future, since it will reduce the number of $\tilde{T}_{\mathcal{J}}$.

We save the nonzero $\tilde{T}_{\mathcal{J}}$ in an array of structures for the use in the matrix element computation later on. Besides the $\tilde{T}_{\mathcal{J}}$, we save the corresponding $l_{cm},\ \mathcal{J}$ and the number of the basis state $|\alpha\rangle$, which enables us the knowledge of J,T,E during the matrix element computation. Additionally, we save the number of nonzero $\tilde{T}_{\mathcal{J}}$-coefficients for each a,b,c,J_{ab} combination. All this is adapted to our implementation of the $\mathcal{J},T$-coupled matrix elements, as discussed in the following subsection.

A.3 Implementation of the $\mathcal{J},T$-coupled matrix element

The formula for the $\mathcal{J},T$-coupled matrix elements is given in eq. (4.79). However, for the implementation it lends itself for further simplifications. In addition, we can cache the inner sums over i and i' in a new quantity depending on α, E' and k'

$$CenterCache(\alpha,E',k') = \sum_i \sum_{i'} c_{\alpha,i}\, c^{k'}_{E'JT,i'} \langle EJM_JTM_Ti|\boldsymbol{V}_{NNN}|E'JM_JTM_Ti'\rangle\,, \tag{A.3}$$

where $c^{k'}_{E'JT,i'}$ is the CFP according to the k'th $|\alpha\rangle$ state in the $E'JT$ block. The J and T quantum numbers are already dictated by the α index. This $CenterCache$ appears one-to-one in our code as three-dimensional array which is called with the number of the $|\alpha\rangle$ states as first index, the energy quantum number of the ket as second index and with k' as third index. Then the final mathematical form for the matrix element that agrees most with the implemented form reads

$$\begin{aligned}
&{}_a\langle[(j_a,j_b)J_{ab},j_c]\mathcal{JM},[(t_a,t_b)t_{ab},t_c]T|\boldsymbol{V}_{NNN}|[(j'_a,j'_b)J'_{ab},j'_c]\mathcal{JM},[(t_a,t_b)t'_{ab},t_c]T\rangle_a \\
=&3!\sum_{l_{cm}} \\
&\times \sum_{\alpha} \tilde{T}_{\mathcal{J}}(a,b,c,J_{ab},\mathcal{J},l_{cm},\underbrace{J,T,k}_{\alpha}) \\
&\times \sum_{E',k'} \tilde{T}_{\mathcal{J}}(a',b',c',J'_{ab},\mathcal{J},l_{cm},J,T,k') \\
&\times CenterCache(\alpha,E',k')\,.
\end{aligned} \tag{A.4}$$

Here, $\sum_\alpha$ denotes a sum over $\{n_{12},l_{12},s_{ab},j_{12},n_3,l_3,j_3,J,t_{ab},T\}$ and $\sum_{k'}$ a sum over $\{n'_{12},l'_{12},s'_{ab},j'_{12},n'_3,l'_3,j'_3,t'_{ab}\}$. As mentioned in the last subsection the sums over T,t_{ab} and t'_{ab} could be avoided, which is more obvious here, since they are dictated by the left-hand side of the equation.

Finally, we stress that we do not explicitly carry out the summations in eq. (A.4). Instead, we employ a rather complicated way of summing up all necessary terms,

which can be found in the routine ME3J_Calc. We outline the principle idea as follows: From eq. (A.4) we know that we have to sum over all products of $\tilde{T}_{\mathcal{J}}$ with equal l_{cm} and $\mathcal{J}$, whereat additionally the a, b, c, J_{ab} and their primed counterpart is dictated by the left-hand side of the equation. Therefore, our modus operandi is to loop over all $\tilde{T}_{\mathcal{J}}$-coefficients that have the correct a, b, c, J_{ab} quantum numbers. Their location in the $\tilde{T}_{\mathcal{J}}$ array is known because we saved it during the $\tilde{T}_{\mathcal{J}}$ calculation. Next, we proceed through this block of $\tilde{T}_{\mathcal{J}}$ until we reach a coefficient with the correct $\mathcal{J}$. If we found one, we look for a compatible $\tilde{T}_{\mathcal{J}}$ in the a', b', c', J'_{ab} block, determined by the ket, via bisection. Compatible means here, that it must have the same l_{cm} and $\mathcal{J}$. For the bisection the mentioned loop ordering during the $\tilde{T}_{\mathcal{J}}$ calculation is crucial. When we found one, we check if it has the same J as the $\tilde{T}_{\mathcal{J}}$ from the bra. If so, we go through the array of these $\tilde{T}_{\mathcal{J}}$-coefficients, multiply each with the corresponding element of the $CenterCache$ and sum them up. We proceed until l_{cm} and $\mathcal{J}$ do not match anymore. Then, the intermediate sum is multiplied with the $\tilde{T}_{\mathcal{J}}$-coefficient according to the bra. Thereafter, we proceed through the $\tilde{T}_{\mathcal{J}}$ array that corresponds to the bra and the procedure for the ket part starts again. We organized the whole procedure in the way that the number of bisections is minimized.

APPENDIX B

Two-body Talmi Moshinsky transformation

In this section we present the formula for the transformation of harmonic oscillator two-body relative matrix elements into two-body m-scheme matrix elements. This is also referred to as "two-body Talmi-Moshinsky transformation" [17]. This transformation is necessary during the preparation of the SRG-transformed two-body matrix elements for the subtraction as it is indicated as second step in the flow chart in fig. 9.

Formally, the investigated transformation reads

$$\begin{aligned}&\langle (nl,S)JM_JTM_T|\boldsymbol{V}_{NN}|(n'l',S)JM_JTM_T\rangle \\ &\longrightarrow \\ &\langle [(n_al_a,s_a)j_a,(n_bl_b,s_b)j_b]\mathfrak{J}\mathfrak{M}_{\mathfrak{J}}TM_T|\boldsymbol{V}_{NN}|[(n'_al'_a,s_a)j'_a,(n'_bl'_b,s_b)j'_b]\mathfrak{J}\mathfrak{M}_{\mathfrak{J}}TM_T\rangle\ .\end{aligned} \tag{B.1}$$

The states $|(nl,S)JM_J,TM_T\rangle$ are the J-coupled harmonic oscillator two-body relative states introduced in eq. (5.28) and $|[(n_al_a,s_a)j_a,(n_bl_b,s_b)j_b]\mathfrak{J}\mathfrak{M}_{\mathfrak{J}}TM_T\rangle$ are the $\mathfrak{J}$-coupled two-body m-scheme matrix elements known from eq. (5.30). Obviously, the two kinds of states rely on different coordinate systems. Thus, we will make use of HOBs during the transformation. The operator $\boldsymbol{V}_{NN}$ is an arbitrary nucleon-nucleon interaction. Before we start with the transformation, we cast the $\mathfrak{J}$-coupled m-scheme matrix element in a more convenient form that will be our starting

point

$$
\begin{aligned}
&{}_a\langle[(n_a l_a,s_a)j_a,(n_b l_b,s_b)j_b]\mathfrak{JM}_\mathfrak{J}|\boldsymbol{V}_{NN}|[(n'_a l'_a,s_a)j'_a,(n'_b l'_b,s_b)j'_b]\mathfrak{JM}_\mathfrak{J}\rangle_a && \text{(B.2)}\\
&= {}_a\langle[(n_a l_a,s_a)j_a,(n_b l_b,s_b)j_b]\mathfrak{JM}_\mathfrak{J}|\boldsymbol{V}_{NN}\sqrt{2!}\mathcal{A}|[(n'_a l'_a,s_a)j'_a,(n'_b l'_b,s_b)j'_b]\mathfrak{JM}_\mathfrak{J}\rangle && \text{(B.3)}\\
&= {}_a\langle[(n_a l_a,s_a)j_a,(n_b l_b,s_b)j_b]\mathfrak{JM}_\mathfrak{J}|\mathcal{A}\boldsymbol{V}_{NN}\sqrt{2!}|[(n'_a l'_a,s_a)j'_a,(n'_b l'_b,s_b)j'_b]\mathfrak{JM}_\mathfrak{J}\rangle && \text{(B.4)}\\
&= {}_a\langle[(n_a l_a,s_a)j_a,(n_b l_b,s_b)j_b]\mathfrak{JM}_\mathfrak{J}|\boldsymbol{V}_{NN}\sqrt{2!}|[(n'_a l'_a,s_a)j'_a,(n'_b l'_b,s_b)j'_b]\mathfrak{JM}_\mathfrak{J}\rangle\,. && \text{(B.5)}
\end{aligned}
$$

Here we take advantage of the fact that $\boldsymbol{V}_{NN}$ commutates with the antisymmetrizer $\mathcal{A}$ in eq. (B.4) and of the idempotent property of $\mathcal{A}$ in eq. (B.5). Next, we explicitly carry out the antisymmetrization of the bra state, yielding

$$
\begin{aligned}
&{}_a\langle[(n_a l_a,s_a)j_a,(n_b l_b,s_b)j_b]\mathfrak{JM}_\mathfrak{J}TM_T|\\
=&\big(\langle[(n_a l_a,s_a)j_a,(n_b l_b,s_b)j_b]\mathfrak{JM}_\mathfrak{J}TM_T| - \langle[(n_a l_a,s_a)j_a,(n_b l_b,s_b)j_b]\mathfrak{JM}_\mathfrak{J}TM_T|\mathcal{T}_{12}\big)\frac{1}{\sqrt{2!}}\\
=&\big(\langle[(n_a l_a,s_a)j_a,(n_b l_b,s_b)j_b]\mathfrak{JM}_\mathfrak{J}TM_T|\\
&\qquad - (-1)^{j_a+j_b-J+T-1}\langle[(n_a l_a,s_a)j_a,(n_b l_b,s_b)j_b]\mathfrak{JM}_\mathfrak{J}TM_T|\big)\frac{1}{\sqrt{2!}}\,,
\end{aligned}
\qquad \text{(B.6)}
$$

where we use the symmetry of (jj)-coupled states under particle exchange, which introduces the phase factor [44].

Therefore, we have to concentrate on the following two terms of the matrix element

$$
\langle[(n_a l_a,s_a)j_a,(n_b l_b,s_b)j_b]\mathfrak{JM}_\mathfrak{J}|\boldsymbol{V}_{NN}|[(n'_a l'_a,s_a)j'_a,(n'_b l'_b,s_b)j'_b]\mathfrak{JM}_\mathfrak{J}\rangle\,, \qquad \text{(B.7)}
$$

$$
\langle[(n_b l_b,s_b)j_b,(n_a l_a,s_a)j_a]\mathfrak{JM}_\mathfrak{J}|\boldsymbol{V}_{NN}|[(n'_a l'_a,s_a)j'_a,(n'_b l'_b,s_b)j'_b]\mathfrak{JM}_\mathfrak{J}\rangle(-1)^{j_a+j_b-J+T-1}\,, \qquad \text{(B.8)}
$$

where we omit the isospin quantum numbers in the state.

Firstly, we concentrate on the matrix element (B.7). For the transformation, the strategy is to express the $\mathfrak{J}$-coupled state stepwise by the two-body relative states. We start with changing the $(j_a j_b)$-coupling into (LS)-coupling by inserting the ap-

propriate identity operator

$$
\begin{aligned}
&|[(n_a l_a, s_a) j_a, (n_b l_b, s_b) j_b] \mathfrak{J}\mathfrak{M}_\mathfrak{J}\rangle \\
&\quad = \sum_{\Lambda S} \langle [(n_a l_a, n_b l_b)\Lambda, (s_a, s_b) S] \mathfrak{J}\mathfrak{M}_\mathfrak{J} | [(n_a l_a, s_a) j_a, (n_b l_b, s_b) j_b] \mathfrak{J}\mathfrak{M}_\mathfrak{J}\rangle \\
&\qquad \times |[(n_a l_a, n_b l_b)\Lambda, (s_a, s_b) S] \mathfrak{J}\mathfrak{M}_\mathfrak{J}\rangle \\
&\quad = \sum_{\Lambda S} |[(n_a l_a, n_b l_b)\Lambda, (s_a, s_b) S] \mathfrak{J}\mathfrak{M}_\mathfrak{J}\rangle \begin{Bmatrix} l_a & l_b & \Lambda \\ s_a & s_b & S \\ j_a & j_b & J \end{Bmatrix} \hat{\Lambda}\hat{S}\hat{j}_a\hat{j}_b \,. \qquad \text{(B.9)}
\end{aligned}
$$

In the last line we replaced the overlap by a 9j-symbol using eq. (3.20). Next, we expand the state on the right-hand side in the basis $|[(NL, nl)\Lambda, S] J M_J\rangle$, where N, L denote the center-of-mass harmonic oscillator radial and orbital angular momentum quantum numbers and n, l the corresponding relative quantum numbers. We dropped the single-particle spins in the states for brevity. The expansion yields

$$
\begin{aligned}
&|[(n_a l_a, s_a) j_a, (n_b l_b, s_b) j_b] \mathfrak{J}\mathfrak{M}_\mathfrak{J}\rangle \\
&\quad = \sum_{\Lambda S} \sum_{NL,nl} \begin{Bmatrix} l_a & l_b & \Lambda \\ s_a & s_b & S \\ j_a & j_b & J \end{Bmatrix} \hat{\Lambda}\hat{S}\hat{j}_a\hat{j}_b \langle\langle NL, nl; \Lambda | n_a l_a, n_b l_b\rangle\rangle_1 |[(NL, nl)\Lambda, S] \mathfrak{J}\mathfrak{M}_\mathfrak{J}\rangle \,, \qquad \text{(B.10)}
\end{aligned}
$$

including the HOB according to the change of the coordinate system from Cartesian to relative and center-of-mass coordinates. In the next two steps we aim at the complete decoupling of the center-of-mass part of the state from the relative part. Firstly, we expand the state on the right-hand side in $|[NL, (nl, S) J] \mathfrak{J}\mathfrak{M}_\mathfrak{J}\rangle$ states, i.e.

$$
\begin{aligned}
&|[(n_a l_a, s_a) j_a, (n_b l_b, s_b) j_b] \mathfrak{J}\mathfrak{M}_\mathfrak{J}\rangle \\
&\quad = \sum_{\Lambda S} \sum_{NL,nl} \sum_{J} \begin{Bmatrix} l_a & l_b & \Lambda \\ s_a & s_b & S \\ j_a & j_b & J \end{Bmatrix} \hat{\Lambda}\hat{S}\hat{j}_a\hat{j}_b \langle\langle NL, nl; \Lambda | n_a l_a, n_b l_b\rangle\rangle_1 \\
&\qquad \times \langle [NL, (nl, S) J] \mathfrak{J}\mathfrak{M}_\mathfrak{J} | [(NL, nl)\Lambda, S] \mathfrak{J}\mathfrak{M}_\mathfrak{J}\rangle \; |[NL, (nl, S) J] \mathfrak{J}\mathfrak{M}_\mathfrak{J}\rangle \\
&\quad = \sum_{\Lambda S} \sum_{NL,nl} \sum_{J} \begin{Bmatrix} l_a & l_b & \Lambda \\ s_a & s_b & S \\ j_a & j_b & J \end{Bmatrix} \hat{\Lambda}\hat{S}\hat{j}_a\hat{j}_b \langle\langle NL, nl; \Lambda | n_a l_a, n_b l_b\rangle\rangle_1 (-1)^{L+l+S+\mathfrak{J}} \hat{\Lambda}\hat{J} \begin{Bmatrix} L & l & \Lambda \\ S & \mathfrak{J} & J \end{Bmatrix} \\
&\qquad \times |[NL, (nl, S) J] \mathfrak{J}\mathfrak{M}_\mathfrak{J}\rangle \,. \qquad \text{(B.11)}
\end{aligned}
$$

In the last line we replaced, the overlap by a the 6j-symbol with help of eq. (3.15). Secondly, we decouple the center-of-mass orbital angular momentum from the

relative angular momentum introducing Clebsch-Gordan coefficients

$$
\begin{aligned}
&|[(n_a l_a, s_a) j_a, (n_b l_b, s_b) j_b] \mathfrak{J} \mathfrak{M}_\mathfrak{J}\rangle \\
&\quad = \sum_{\Lambda S} \sum_{NL,nl} \sum_{J} \sum_{M_J M_L} \begin{Bmatrix} l_a & l_b & \Lambda \\ s_a & s_b & S \\ j_a & j_b & J \end{Bmatrix} \hat{\Lambda} \hat{S} \hat{j}_a \hat{j}_b \langle\langle NL, nl; \Lambda | n_a l_a, n_b l_b \rangle\rangle_1 \\
&\qquad \times (-1)^{L+l+S+\mathfrak{J}} \hat{\Lambda} \hat{J} \begin{Bmatrix} L & l & \Lambda \\ S & \mathfrak{J} & J \end{Bmatrix} \begin{pmatrix} L & J & \mathfrak{J} \\ M_L & M_J & \mathfrak{M}_\mathfrak{J} \end{pmatrix} |NLM_L, (nl, S) J M_J\rangle \,. \qquad \text{(B.12)}
\end{aligned}
$$

Now we are in the position to sandwich the two-body interaction with the expansion of the states given in eq. (B.12), which leads us to the final result for the first term. Thereby, we can make use of the following properties of the interaction

$$
\begin{aligned}
&\langle NLM_L, (nl, S) J M_J | \boldsymbol{V}_{NN} | N' L' M'_L, (n'l', S') J' M'_J\rangle \qquad \text{(B.13)} \\
&\quad = \delta_{S,S'} \, \delta_{N,N'} \, \delta_{L,L'} \, \delta_{M_L,M'_L} \, \delta_{J,J'} \, \delta_{M_J,M'_J} \, \langle (nl, S) J M_J | \boldsymbol{V}_{NN} | (n'l', S) J M_J\rangle \,,
\end{aligned}
$$

where we use in particular, that the interaction does not affect the center-of-mass part of the state. This fact, together with the orthogonality relation of the Clebsch-Gordan coefficients

$$
\sum_{M_L M_J} \begin{pmatrix} L & J & \mathfrak{J} \\ M_L & M_J & \mathfrak{M}_\mathfrak{J} \end{pmatrix} \begin{pmatrix} L & J & \mathfrak{J} \\ M_L & M_J & \mathfrak{M}_\mathfrak{J} \end{pmatrix} = \delta_{\mathfrak{J},\mathfrak{J}} \, \delta_{\mathfrak{M}_\mathfrak{J},\mathfrak{M}_\mathfrak{J}} = 1 \qquad \text{(B.14)}
$$

leads us to the final result for the transformation of the first term (B.7), denoted by

$$
\begin{aligned}
&\langle [(n_a l_a, s_a) j_a, (n_b l_b, s_b) j_b] \mathfrak{J} \mathfrak{M}_\mathfrak{J} T M_T | \boldsymbol{V}_{NN} | [(n'_a l'_a, s_a) j'_a, (n'_b l'_b, s_b) j'_b] \mathfrak{J} \mathfrak{M}_\mathfrak{J} T M_T\rangle \\
&\quad = \sum_{J} \sum_{NL,nl} \sum_{\Lambda} \sum_{S} \sum_{n',l'} \sum_{\Lambda'} \\
&\quad \times \begin{Bmatrix} l_a & l_b & \Lambda \\ s_a & s_b & S \\ j_a & j_b & J \end{Bmatrix} \begin{Bmatrix} l'_a & l'_b & \Lambda' \\ s_a & s_b & S \\ j'_a & j'_b & J \end{Bmatrix} \langle\langle NL, nl; \Lambda | n_a l_a, n_b l_b \rangle\rangle_1 \langle\langle NL, n'l'; \Lambda' | n'_a l'_a, n'_b l'_b \rangle\rangle_1 \\
&\quad \times \begin{Bmatrix} L & l & \Lambda \\ S & \mathfrak{J} & J \end{Bmatrix} \begin{Bmatrix} L & l' & \Lambda' \\ S & \mathfrak{J} & J \end{Bmatrix} \hat{\Lambda}^2 \hat{\Lambda}'^2 \hat{S}^2 \hat{j}_a \hat{j}'_a \hat{j}_b \hat{j}'_b \hat{J}^2 \underbrace{(-1)^{L+l+S+\mathfrak{J}} (-1)^{L+l'+S+\mathfrak{J}}}_{1} \\
&\quad \times \langle (nl, S) J M_J | \boldsymbol{V}_{NN} | (n'l', S) J M_J\rangle \,. \qquad \text{(B.15)}
\end{aligned}
$$

The factor with the underbrace is equal to one because L, S and J are all integer numbers and $l' = l \pm 2$, since the interaction does not connect states with other values for the relative orbital angular momenta l'.

Now, we derive the analogous formula for the matrix element in the second

term (B.8). Therefore, we concentrate on the bra state of the matrix element, since the transformation of the ket state is the same as presented above. Note the reversed order of the quantum numbers compared to the first term. We start with changing the $(j_b j_a)$-coupling into (LS)-coupling

$$\begin{aligned}&\langle[(n_b l_b, s_b) j_b, (n_a l_a, s_a) j_a] \mathfrak{J}\mathfrak{M}_\mathfrak{J}| \\ &\quad = \sum_{\Lambda S} \begin{Bmatrix} l_b & l_a & \Lambda \\ s_b & s_a & S \\ j_b & j_a & \mathfrak{J} \end{Bmatrix} \hat{j}_a \hat{j}_b \hat{\Lambda} \hat{S} \langle[(n_b l_b, n_a l_a)\Lambda, (s_b, s_a) S] \mathfrak{J}\mathfrak{M}_\mathfrak{J}| \,, \end{aligned} \tag{B.16}$$

where we introduced a 9j-symbol with help of eq. (3.20).

Next, we make the transition $s_a \leftrightarrow s_b$ to obtain the same ordering of the quantum numbers as in the first term. Since $s_1 = s_2 = \frac{1}{2}$ anyway, this makes no difference. We stress that we do not change the coupling order of the spins. It is not necessary because the first particle already couples with the second particle as in the first term (B.7).

$$\begin{aligned}&\langle[(n_b l_b, s_b) j_b, (n_a l_a, s_a) j_a] \mathfrak{J}\mathfrak{M}_\mathfrak{J}| \\ &\quad = \sum_{\Lambda S} \begin{Bmatrix} l_b & l_a & \Lambda \\ s_b & s_a & S \\ j_b & j_a & \mathfrak{J} \end{Bmatrix} \hat{j}_a \hat{j}_b \hat{\Lambda} \hat{S} \langle[(n_b l_b, n_a l_a)\Lambda, (s_a, s_b) S] \mathfrak{J}\mathfrak{M}_\mathfrak{J}| \,, \end{aligned} \tag{B.17}$$

The same applies for the isospin, which is omitted here.

Now, we insert the identity operator

$$\mathbb{1} = \sum_{NL,nl} |(NL, nl)\Lambda\rangle\langle(NL, nl)\Lambda| \tag{B.18}$$

which provides the transformation from Cartesian into center-of-mass and relative coordinates. Thus, we obtain

$$\begin{aligned}&\langle[(n_b l_b, s_b) j_b, (n_a l_a, s_a) j_a] \mathfrak{J}\mathfrak{M}_\mathfrak{J}| \\ &\quad = \sum_{\Lambda S} \sum_{NL,nl} \begin{Bmatrix} l_b & l_a & \Lambda \\ s_b & s_a & S \\ j_b & j_a & \mathfrak{J} \end{Bmatrix} \hat{j}_a \hat{j}_b \hat{\Lambda} \hat{S} \, \langle\langle n_b l_b, n_a l_a; \Lambda | NL, nl\rangle\rangle_1 \langle[(NL, nl)\Lambda, (s_a, s_b) S] \mathfrak{J}\mathfrak{M}_\mathfrak{J}| \,, \end{aligned} \tag{B.19}$$

with the HOB due to the coordinate transformation. In the following we again omit the single particle spins in the state.

In the next two steps we aim at the complete decoupling of the center-of-mass orbital angular momentum from the relative angular momentum. Therefore, we

carry out the same steps as in eqs. (B.11),(B.12) introducing a 6j-symbol and a Clebsch-Gordan coefficient resulting in

$$\begin{aligned}
&\langle[(n_b l_b, s_b) j_b, (n_a l_a, s_a) j_a] \mathfrak{J} \mathfrak{M}_\mathfrak{J}| \\
&\quad = \sum_{\Lambda S} \sum_{NL,nl} \sum_{J} \sum_{M_L M_J} \begin{Bmatrix} l_b & l_a & \Lambda \\ s_b & s_a & S \\ j_b & j_a & \mathfrak{J} \end{Bmatrix} \hat{j}_a \hat{j}_b \hat{\Lambda} \hat{S} \, \langle\langle n_b l_b, n_a l_a; \Lambda | NL, nl \rangle\rangle_1 \begin{Bmatrix} L & l & \Lambda \\ S & \mathfrak{J} & J \end{Bmatrix} \\
&\quad \times (-1)^{L+l+S+\mathfrak{J}} \hat{\Lambda} \hat{J} \begin{pmatrix} L & J \\ M_L & M_J \end{pmatrix} \begin{pmatrix} \mathfrak{J} \\ \mathfrak{M}_\mathfrak{J} \end{pmatrix} \langle N L M_L, [(nl)\Lambda, S] J M_J | \,, \qquad \text{(B.20)}
\end{aligned}$$

Next, we use the symmetry relation of the 9j-symbol

$$\begin{Bmatrix} l_b & l_a & \Lambda \\ s_b & s_a & S \\ j_b & j_a & \mathfrak{J} \end{Bmatrix} = \begin{Bmatrix} l_a & l_b & \Lambda \\ s_a & s_b & S \\ j_a & j_b & \mathfrak{J} \end{Bmatrix} (-1)^{l_a+l_b+\Lambda+s_a+s_b+S+j_a+j_b+\mathfrak{J}} \qquad \text{(B.21)}$$

and of the HOB

$$\begin{aligned}
\langle\langle n_b l_b, n_a l_a; \Lambda | NL, nl \rangle\rangle_1 &= (-1)^{\Lambda - L} \langle\langle n_a l_a, n_b l_b; \Lambda | NL, nl \rangle\rangle_1 \\
&= (-1)^{\Lambda - L} \langle\langle NL, nl; \Lambda | n_a l_a, n_b l_b \rangle\rangle_1 \qquad \text{(B.22)}
\end{aligned}$$

according to eqs. (3.62), because we want to cast this second term in the same form as the first one. Plugging the symmetry relations into eq. (B.20) yields

$$\begin{aligned}
&\langle[(n_b l_b, s_b) j_b, (n_a l_a, s_a) j_a] \mathfrak{J} \mathfrak{M}_\mathfrak{J}| \\
&\quad = \sum_{\Lambda S} \sum_{NL,nl} \sum_{J} \sum_{M_L M_J} (-1)^{l_a+l_b+\Lambda+s_a+s_b+S+j_a+j_b+\mathfrak{J}} (-1)^{\Lambda - L} (-1)^{L+l+S+\mathfrak{J}} \, \hat{j}_a \hat{j}_b \hat{\Lambda}^2 \hat{J} \hat{S} \\
&\quad \times \begin{Bmatrix} l_a & l_b & \Lambda \\ s_a & s_b & S \\ j_a & j_b & \mathfrak{J} \end{Bmatrix} \langle\langle NL, nl; \Lambda | n_a l_a, n_b l_b \rangle\rangle_1 \begin{Bmatrix} L & l & \Lambda \\ S & \mathfrak{J} & J \end{Bmatrix} \begin{pmatrix} L & J \\ M_L & M_J \end{pmatrix} \begin{pmatrix} \mathfrak{J} \\ \mathfrak{M}_\mathfrak{J} \end{pmatrix} \\
&\quad \times \langle N L M_L, [(nl)\Lambda, S] J M_J | \,. \qquad \text{(B.23)}
\end{aligned}$$

Now we use this bra state and the transformed ket state of eq. (B.12) to sandwich

$\boldsymbol{V}_{NN}$, yielding the final result of the second term

$$
\begin{aligned}
&(-1)^{j_a+j_b-\mathfrak{J}+T-1}\langle[(n_b l_b,s_b)j_b,(n_a l_a,s_a)j_a]\mathfrak{J}\mathfrak{M}_\mathfrak{J}|\boldsymbol{V}_{NN}|[(n'_a l'_a,s_a)j'_a,(n'_b l'_b,s_b)j'_b]\mathfrak{J}\mathfrak{M}_\mathfrak{J}\rangle \\
&\quad=\sum_{\Lambda S}\sum_{NL,nl}\sum_{J}\sum_{n'l'}\sum_{\Lambda'}\sum_{J} \\
&\quad\times(-1)^{j_a+j_b-J+T-1}(-1)^{l_a+l_b+\Lambda+s_a+s_b+S+j_a+j_b+\mathfrak{J}}(-1)^{\Lambda-L}(-1)^{L+l+S+\mathfrak{J}}(-1)^{L+l'+S+\mathfrak{J}} \\
&\quad\times\hat{j}_a\hat{j}_b\hat{j}'_a\hat{j}'_b\hat{\Lambda}^2\hat{\Lambda}'^2\hat{S}^2\hat{J}^2 \\
&\quad\times\begin{Bmatrix} l_a & l_b & \Lambda \\ s_a & s_b & S \\ j_a & j_b & \mathfrak{J}\end{Bmatrix}\begin{Bmatrix} l'_a & l'_b & \Lambda' \\ s_a & s_b & S \\ j'_a & j'_b & \mathfrak{J}\end{Bmatrix}\begin{Bmatrix} L & l & \Lambda \\ S & \mathfrak{J} & J\end{Bmatrix}\begin{Bmatrix} L & l' & \Lambda' \\ S & \mathfrak{J} & J\end{Bmatrix} \\
&\quad\times\langle\langle NL,nl;\Lambda|n_a l_a,n_b l_b\rangle\rangle_1\langle\langle NL,n'l';\Lambda'|n'_a l'_a,n'_b l'_b\rangle\rangle_1 \\
&\quad\times\langle[(nl)\Lambda,S]JM_J|\boldsymbol{V}_{NN}|[(n'l')\Lambda,S]JM_J\rangle\,. \qquad \text{(B.24)}
\end{aligned}
$$

The last thing to do is to simplify the phase factor, which is the only difference between the results for the first term, given in eq. (B.15), and the according result for the second term, i.e.

$$
\begin{aligned}
&(-1)^{j_a+j_b-\mathfrak{J}+T-1}(-1)^{l_a+l_b+\Lambda+s_a+s_b+S+j_a+j_b+\mathfrak{J}}(-1)^{\Lambda-L}(-1)^{L+l+S+\mathfrak{J}}(-1)^{L+l'+S+\mathfrak{J}} \\
&=(-1)^{2j_a+2j_b}(-1)^{s_a+s_b-1}(-1)^{2\Lambda+2S+2\mathfrak{J}}(-1)^{l+l'}(-1)^{l_a+l_b-L}(-1)^{T+S} \qquad \text{(B.25)}
\end{aligned}
$$

Now we discuss the factors step by step:

$(-1)^{2j_a+2j_b}$:	Since j_a and j_b are half-integral numbers $2j_i$ are odd numbers and so $2j_a+2j_b$ is even and the factor is equal to one.
$(-1)^{s_a+s_b-1}$:	Because $s_a=s_b=\frac{1}{2}$, this factor is equal to one.
$(-1)^{2\Lambda+2S+2\mathfrak{J}}$:	Here, Λ, S and $\mathfrak{J}$ are integers and the factor is equal to one.
$(-1)^{l_a+l_b-L}$:	The interaction matrix elements are only nonzero for $l'=l\pm2$ and, therefore, this factor is also equal to one.

Altogether the phase factor is given by $(-1)^{l+S+T}$. Both transformed terms together yield the final result of the transformation of J-coupled two-body relative

matrix elements into $\mathfrak{J}$-coupled m-scheme matrix elements

$$
\begin{aligned}
&{}_a\langle[(n_a l_a, s_a) j_a, (n_b l_b, s_b) j_b]\mathfrak{J}\mathfrak{M}_\mathfrak{J} T M_T | \boldsymbol{V}_{NN} | [(n'_a l'_a, s_a) j'_a, (n'_b l'_b, s_b) j'_b]\mathfrak{J}\mathfrak{M}_\mathfrak{J} T M_T\rangle_a \\
&\quad = \hat{j}_a \hat{j}_b \hat{j}'_a \hat{j}'_b \sum_{\Lambda,S} \sum_{NL,nl} \sum_{J} \sum_{n'l'} \sum_{\Lambda'} \hat{\Lambda}^2 \hat{\Lambda}'^2 \hat{J}^2 \hat{S}^2 \\
&\quad \times \begin{Bmatrix} l_a & l_b & \Lambda \\ s_a & s_b & S \\ j_a & j_b & \mathfrak{J} \end{Bmatrix} \begin{Bmatrix} l'_a & l'_b & \Lambda' \\ s_a & s_b & S \\ j'_a & j'_b & \mathfrak{J} \end{Bmatrix} \begin{Bmatrix} L & l & \Lambda \\ S & \mathfrak{J} & J \end{Bmatrix} \begin{Bmatrix} L & l' & \Lambda' \\ S & \mathfrak{J} & J \end{Bmatrix} \\
&\quad \times \langle\langle NL, nl; \Lambda | n_a l_a, n_b l_b\rangle\rangle_1 \langle\langle NL, n'l'; \Lambda' | n'_a l'_a, n'_b l'_b\rangle\rangle_1 \\
&\quad \times \left(1 - (-1)^{l+S+T}\right) \langle [(nl)\Lambda, S] J M_J T M_T | \boldsymbol{V}_{NN} | [(n'l')\Lambda, S] J M_J T M_T\rangle \,. \qquad \text{(B.26)}
\end{aligned}
$$

REFERENCES

[1] Steven C. Pieper; *Quantum Monte Carlo Calculations of Light Nuclei*; Nuclear Physics A **751** (2005) 516 .

[2] Steven Weinberg; *Nuclear forces from chiral Lagrangians*; Phys. Lett. B **251** (1990) 288.

[3] P. Navrátil, V. G. Gueorguiev, J. P. Vary, *et al.*; *Structure of $A = 10 - 13$ Nuclei with Two- Plus Three-Nucleon Interactions from Chiral Effective Field Theory*; Phys. Rev. Lett. **99** (2007) 042501.

[4] P. Navrátil; *Local three-nucleon interaction from chiral effective field theory*; Few Body Syst. **41** (2007) 117.

[5] A. Nogga, P. Navratil, B. R. Barrett, J. P. Vary; *Spectra and binding energy predictions of chiral interactions for 7Li*; Phys. Rev. C **73** (2006) 064002.

[6] Robert Roth; *Importance Truncation for Large-Scale Configuration Interaction Approaches*; Phys. Rev. C **79** (2009) 064324.

[7] Steven Weinberg; *Three-body interactions among nucleons and pions*; Phys. Lett. B **295** (1992) 114.

[8] Steven Weinberg; *Effective chiral Lagrangians for nucleon-pion interactions and nuclear forces*; Nucl. Phys. B **363** (1991) 3.

[9] Evgeny Epelbaum; *Few-nucleon forces and systems in chiral effective field theory*; Few-Body Systems **43** (2008) 57.

[10] D. R. Entem, R. Machleidt; *Accurate Charge-Dependent Nucleon-Nucleon Potential at Fourth Order of Chiral Perturbation Theory*; Phys. Rev. C **68** (2003) 041001(R).

[11] E. Epelbaum, A. Nogga, W. Glöckle, *et al.*; *Three-nucleon forces from chiral effective field theory*; Phys. Rev. C **66** (2002) 064001.

[12] E. Epelbaum; *Four-nucleon force in chiral effective field theory*; Physics Letters B **639** (2006) 456 .

[13] P. Navratil, G. P. Kamuntavicius, B. R. Barrett; *Few-nucleon systems in translationally invariant harmonic oscillator basis*; Phys. Rev. C **61** (2000) 044001.

[14] Doron Gazit, Sofia Quaglioni, Petr Navrátil; *Three-Nucleon Low-Energy Constants from the Consistency of Interactions and Currents in Chiral Effective Field Theory*; Phys. Rev. Lett. **103** (2009) 102502.

[15] Sven Binder; *Angular momentum projection and three-body forces in the no-core shell model*; Master's thesis; TU Darmstadt (2010).

[16] D.A. Varshalovich, A.N. Moskalev, V.K. Khersonskii; *Quantum Theory of Angular Momentum*; World Scientific Publishing Co. Pte Ltd. (1988).

[17] R. Roth, P. Papakonstantinou, N. Paar, *et al.*; *Hartree-Fock and many body perturbation theory with correlated realistic NN interactions*; Phys. Rev. C **73** (2006) 044312.

[18] I. Talmi; Helv. Phys. Acta **25** (1952) 185.

[19] M. Moshinsky; *Transformation brackets for harmonic oscillator functions*; Nuclear Physics **13** (1959) 104.

[20] G. P. Kamuntavicius, R. K. Kalinauskas, B. R. Barrett, *et al.*; *The general harmonic-oscillator brackets: compact expression, symmetries, sums and Fortran code*; Nuclear Physics A **695** (2001) 191 .

[21] L. Trlifaj; *Simple Formula for the General Oscillator Brackets*; Phys. Rev. C **5** (1972) 1534.

[22] T.A. Brody, M. Moshinsky; *Tablas de Parentesis de Transformation*; Universidad nacional autonoma de Mexico (1960).

[23] Stanislaw D. Glazek, Kenneth G. Wilson; *Perturbative renormalization group for Hamiltonians*; Phys. Rev. D **49** (1994) 4214.

[24] F. Wegner; *Flow-equations for Hamiltonians*; Annalen der Physik **506** (1994) 77–91.

[25] F. J. Wegner; *Flow equations for Hamiltonians*; Nucl. Phys. Proc. Suppl. **90** (2000) 141.

[26] S. Szpigel, R. J. Perry; *Quantum Field Theory. A 20th Century Profile*; Hindustan Publishing Co., New Delhi (2000).

[27] S. K. Bogner, R. J. Furnstahl, R. J. Perry; *Similarity renormalization group for nucleon-nucleon interactions*; Phys. Rev. C **75** (2007) 061001.

[28] N. Paar, P. Papakonstantinou, H. Hergert, R. Roth; *Collective multipole excitations based on correlated realistic nucleon-nucleon interactions*; Phys. Rev. C **74** (2006) 014318.

[29] Yousef Saad; *Numerical Methods for Large Eigenvalue Problems*; Manchester University Press (1992).

[30] Beresford N. Partlett; *The Symmetric Eigenvalue Problem*; Prentice-Hall Series in Computational Mathematics (1980).

[31] Zoltán Rolik, Agnes Szabados, Péter R. Surján; *On the perturbation of multiconfiguration wave functions*; J. Chem. Phys. **119** (2003) 1922.

[32] P. Surján, Z. Rolik, Szabados A., D. Köhalmi; *Partitioning in multiconfiguration perturbation theory*; Annalen der Physik **13** (2004) 223.

[33] R. Roth, P. Navrátil; *Ab Initio Study of ^{40}Ca with an Importance-Truncated No-Core Shell Model*; Phys. Rev. Lett. **99** (2007) 092501.

[34] E. D. Jurgenson, P. Navrátil, R. J. Furnstahl; *Evolution of Nuclear Many-Body Forces with the Similarity Renormalization Group*; Phys. Rev. Lett. **103** (2009) 082501.

[35] R. Roth, S. Reinhardt, H. Hergert; *Unitary correlation operator method and similarity renormalization group: Connections and differences*; Phys. Rev. C **77** (2008) 064003.

[36] P. Ring, P.Schuck; *The nuclear many-body problem*; Springer Verlag (2004).

[37] Robert Roth; *Vorlesungsskript "Theoretische Kernphysik"* (WS 2007/08).

[38] A. Günther, R. Roth, H. Hergert, S. Reinhardt; *Systematics of binding energies and radii based on realistic two-nucleon plus phenomenological three-nucleon interactions*; Phys. Rev. C **82** (2010) 024319.

[39] A. H. Wapstra, G. Audi, C. Thibault; *The 2003 atomic mass evaluation: (I). Evaluation of input data, adjustment procedures*; Nuclear Physics A **729** (2003) 129 .

[40] H. De Vries, C. W. De Jager, C. De Vries; *Nuclear charge-density-distribution parameters from elastic electron scattering*; Atomic Data and Nuclear Data Tables **36** (1987) 495 .

[41] N. Imai, H. J. Ong, N. Aoi, *et al.*; *Anomalously Hindered $E2$ Strength $B(E2;2_1^+ \rightarrow 0^+)$ in ^{16}C*; Phys. Rev. Lett. **92** (2004) 062501.

[42] M. Wiedeking, P. Fallon, A. O. Macchiavelli, *et al.*; *Lifetime Measurement of the First Excited 2^+ State in ^{16}C*; Phys. Rev. Lett. **100** (2008) 152501.

[43] H. Ong, N. Imai, D. Suzuki, *et al.*; *Observation/confirmation of hindered E2 strength in $^{18}C/^{16}C$*; The European Physical Journal A - Hadrons and Nuclei **42** (2009) 393.

[44] Hans Feldmeier; *Vorlesungsskript "Einführung in die theoretische Kernphysik"* (WS 2009/10).

DANKSAGUNG

Zuerst möchte ich *Prof. Dr. Robert Roth* für die Möglichkeit danken, dieses spannende Thema zu bearbeiten und diese Arbeit anzufertigen. Sein offenes Ohr für physikalische Fragen aller Art sowie diverse Tipps bei der Implementierung haben maßgeblich zum Gelingen dieser Arbeit beigetragen.

Außerdem bedanke ich mich bei *Petr Navrátil* für das Bereitstellen seines MANYEFF-Codes sowie für die Hinweise, die die Orientierung im Programm erleichtert haben.

Desweiteren danke ich *Angelo Calci* und *Sven Binder* für die fruchtbaren physikalischen Diskussionen sowie für die außerphysikalischen Abwechslungen.

Außerdem bedanke ich mich bei *Markus Hild* und *Felix Schmitt* für die Hilfe bei lästigen Computer Problemen.

Bei dem Rest der *TNP++ Arbeitsgruppe* bedanke ich mich für die gute und angenehme Arbeitsatmosphäre.

Ein besonderes Dankeschön geht an *Jacqueline Bonnet* für das Korrekturlesen dieser Arbeit und die Geduld mit mir.

Schließlich bedanke ich mich bei meinen Eltern *Elke und Johannes Langhammer* sowie meinem Bruder *Ralph Langhammer* für die Unterstützung während des gesamten Studiums. Ohne diese wäre all das nicht möglich gewesen.

Erklärung zur Eigenständigkeit

Hiermit versichere ich, dass ich die vorliegende Arbeit ohne die Hilfe Dritter und nur mit den angegebenen Quellen als Hilfsmittel angefertigt habe. Alle Stellen, die aus Quellen entnommen sind, wurden als solche kenntlich gemacht. Diese Arbeit hat in gleicher oder ähnlicher Form noch in keiner Prüfungsbehörde vorgelegen.

Ort	Datum	Unterschrift